THREE-DIMENSIONAL NUMERICAL ANALYSIS OF SLOPES CONSIDERING EFFECTS OF SURCHARGE LOADS

by

Muhammed Eyüp Polat

B.S., Civil Engineering, Maltepe University, 2019

Submitted to the Institute for Graduate Studies in
Science and Engineering in partial fulfillment of
the requirements for the degree of
Master of Science

Graduate Program in Civil Engineering

Boğaziçi University

2024

ACKNOWLEDGEMENTS

I would like to thank Assist. Prof. İrem Zeynep YILDIRIM, my advisor, for all of her patience, knowledge, and guidance during the research. Her knowledge of geotechnical engineering has greatly benefited our research. I also would like to thank my thesis committee members: Prof. Özer Çinicioğlu and Assist. Prof. Berrak Teymür for their feedback.

My deepest gratitude goes to my well-beloved family, my sister, my brother in law and my niece Azra.

At last, there are a lot of people I am unable to name here, but I am incredibly grateful for their friendship, support, and existence.

Finally, I would like to acknowledge the financial support provided by Boğaziçi University Scientific Research Projects (BAP Project Code: 16961) for this study.

ABSTRACT

THREE-DIMENSIONAL NUMERICAL ANALYSIS OF SLOPES CONSIDERING EFFECTS OF SURCHARGE LOADS

Slope stability analysis and slope stabilization techniques have been a subject of research study for civil engineers for decades. The factor of safety (F_S) of a slope is very sensitive to various factors related to slope geometry, soil parameters and surcharge loads. The required F_S values for slopes are generally lowered than those required for the stability of foundations. Accordingly, slope failures are more frequently observed than failures in other geotechnical structures. Surcharge loads can easily lead to slope failures. When surcharge loads with limited dimensions are present near the crest of a slope, a two-dimensional (2D) analysis may not suffice and a three-dimensional (3D) analysis may be required. Both limit equilibrium methods (LEM) and finite element methods (FEM) combined with the strength reduction (SR) techniques are employed for slope stability analysis. With the advanced computational power, 3D FEM has become a reliable tool to analyze slopes with geometric conditions that cannot be reliably modeled in two dimensions. FEM analysis of slopes may be advantageous as it can also provide deformations. Numerical analysis based on both LEM and FEM are employed in practice, however, these two methods use completely different approaches in calculating F_S, and the results are rarely identical. Additionally, in most scenarios, the engineers prefer 2D analysis over 3D analysis which generally leads to uneconomical designs for slopes under the effects of surcharge loads with limited areas. This study investigated the short-term stability of clayey slopes under the effects of surcharge loads by performing numerical analysis using 2D LEM, 3D LEM, 2D FEM and 3D FEM. In the 3D analysis, the effects of surcharge magnitude and surcharge shape on the short-term stability of clayey slopes were investigated for a wide range of slope geometries and soil undrained shear strengths. The results of this study showcase the differences in the analysis performed using LEM and FEM. The results also indicated that performing 3D analysis for slopes under surcharge loads with limited dimensions can lead to F_S values notably higher than those obtained from 2D analysis.

ÖZET

SÜRŞARJ YÜKLERİ ETKİSİNDEKİ ŞEVLERİN ÜÇ BOYUTLU NÜMERİK ANALİZLERİ

Şev stabilite analizi ve şev stabilizasyon teknikleri inşaat mühendisleri için onlarca yıldır süregelen önemli bir araştırma konusudur. Bir şevin güvenlik katsayısı (F_s), şevin geometrisi, zemin parametreleri ve sürşarj yükleriyle ilgili çok sayıda parametreye bağlıdır. Şevler için gerekli olan F_s değerleri genellikle temellerin stabilitesi için gerekli olan değerlerden daha düşüktür. Bu sebeple şev göçmelerine de diğer geoteknik yapılarda gözlenen toptan göçmelere kıyasla daha sık rastlanmaktadır. Sürşarj yükleri kolaylıkla şev göçmelerine sebep olabilir. Şev tepesi yakınında sınırlı boyutlara sahip sürşarj yükleri mevcut olduğunda, iki boyutlu (2D) analiz yeterli olmayabilir ve üç boyutlu (3D) analiz gerekebilir. Şev stabilite analizleri için limit denge yöntemleri (LEM) ve dayanım azaltma (SR) teknikleriyle birleştirilerek sonlu elemanlar yöntemleri (FEM) kullanılır. Gelişmiş hesaplama gücü ile 3D FEM, iki boyutlu olarak gerçekçi modellememesi zor olan şevlerin analizi için güvenilir bir araç haline gelmiştir. FEM analizi şevlerde deformasyonları değerlerini de vermesi açısından avantajlı olabilir. Pratikte LEM ve FEM'e dayanan analizler yaygın olarak kullanılmaktadır. Ancak, bu iki yöntem F_s değerlerinin hesaplanmasında tamamen farklı yaklaşımlar kullanır ve bu yüzden sonuçlar da nadiren birebir aynıdır. Ek olarak, çoğu senaryoda mühendisler 2D analizi 3D analize tercih ederler; bu da genellikle sınırlı alanlı ek yüklerin etkisi altındaki şevler için ekonomik olmayan tasarımlara yol açar. Bu çalışmada, killi şevlerin sürşarj yüklerinin etkisi altındaki kısa süreli stabilitesi, analizlerde 2D LEM, 3D LEM, 2D FEM ve 3D FEM kullanılarak araştırılmıştır. 3 boyutlu analizlerde, sürşarj büyüklüğü ve sürşarj şeklinin killi şevlerin kısa süreli stabilitesi üzerindeki etkiler çeşitli şev geometrileri ve drenajsız kayma mukavemeti değerleri için araştırılmıştır. Bu çalışma LEM ve FEM kullanılarak yapılan analiz sonuçlarındaki farklılıkları ortaya koymaktadır. Sonuçlar ayrıca, özellikle sınırlı boyutlara sahip sürşarj yükleri etkisinde olan şevlerin 3D analizlerinin sonucunda, 2D analizlerin sonucunda elde edilenden oldukça yüksek F_s değerleri elde edilebileceğini de göstermektedir.

TABLE OF CONTENTS

ACKNOWLEDGEMENTS iii
ABSTRACT iv
ÖZET v
TABLE OF CONTENTS vi
LIST OF FIGURES viii
LIST OF TABLES xiii
LIST OF SYMBOLS xiv
LIST OF ACRONYMS/ ABBREVIATONS xvi
1. INTRODUCTION 1
1.1. Aims of the Study 2
1.2. Thesis Outline 3
2. LITERATURE REVIEW 4
2.1. Slope Stability Analysis 4
2.1.1. Why 3D Slope Stability Analysis is Required? 5
2.2. Slope Stability Analysis Using Limit Equilibrium Method (LEM) 6
2.2.1. Bishop's Simplified Method 10
2.2.2. Janbu's Simplified Method 11
2.2.3. Spencer's Method 14
2.2.4. Morgenstern and Price's (GLE) Method 15
2.2.5. Failure Surface Searching Methods 16
2.2.6. 3D Extension of LEM 18
2.3. Slope Stability Using Finite Element Method (FEM) 22
2.4. Slope Stability Analysis Under Surcharge 25
3. METHODOLOGY 27
3.1. Analysis Performed Using 2D and 3D LEM 27
3.1.1. Calibration Study 27
3.2. Analysis Performed Using 3D FEM 31
3.3. Cases Analyzed 33
4. RESULTS 36
4.1. Effect of Slope Geometry, Soil Strength & Surcharge Magnitude on F_s 36

4.2. Effect of Slope Geometry, Surcharge Magnitude and Shape on 3D Failure Surfaces 44
4.3. Effect of Surcharge Shape on 3D Slope Stability 49
4.4. Comparison of the Results of the Analyses Performed Using 3D LEM and 3D FEM 55
4.5. Comparison of 2D and 3D Analysis 61
5. CONCLUSIONS 67
5.1. Recommendations for further research 68
REFERENCES 69

LIST OF FIGURES

Figure 2.1. Basic of method of slices (modified after Duncan 2014)..... 9

Figure 2.2. Generic forces acting on a single slice (modified after Abramson, 2002). 12

Figure 2.3. Janbu correction factor (modified after Duncan 2014). 14

Figure 2.4. Possible functions that describe variation of interslice force inclinations: (a) user specified; (b) constant (equivalent to Spencer's method) (modified after Abramson 2002)..... 16

Figure 3.1. Effect of extrusion depth on F_s in Slide3 for the stability of clayey slope. 30

Figure 3.2. Critical slip surface for a 3D slope with 400 m extrusion depth..... 31

Figure 3.3. Total displacements for different constitutive models in deformation analysis: (a) MC; (b) HS; (c) HSS. 32

Figure 3.4. Generic cross-section of the loaded slopes..... 33

Figure 3.5. Typical loading scheme: (a) L/B=1; (b) L/B=6..... 34

Figure 4.1. Effect of surcharge magnitude and slope height on Fs of slopes (L/B ratio=1; B≠H) using 3D FEM. 37

Figure 4.2. Effect of surcharge shape and magnitude on F_s of slopes (L/B ratio= 2; B≠H) using 3D FEM. 38

Figure 4.3. Effect of surcharge magnitude and slope height on F_s of slopes (L/B ratio=6; B≠H) using 3D FEM. 39

Figure 4.4. F_s for slope height (H) = 10 m and surcharge (q) = 100 kPa in: (a) 3D LEM, (b) 3D FEM..... 40

Figure 4.5. F_s for slope height (H) = 40 m and surcharge (q) = 100 kPa in: (a) 3D LEM, (b) 3D FEM..... 41

Figure 4.6. Decrease in factor of safety of different slope angles due to the change in H for q= 50 kPa in 3D FEM B≠H β= 33.69°. 42

Figure 4.7. Decrease in factor of safety of different slope angles due to the change in H for q= 50 kPa in 3D FEM B≠H cases: (a) β= 45°; (b) β=63.43°..... 43

Figure 4.8. Failure surfaces obtained from 3D LEM analysis of slopes of β= 33.7° slopes loaded with q=200 kPa and L/B = 1: (a) H=20 m (b) H=30 m..... 44

Figure 4.9. Failure surfaces obtained from 3D LEM analysis of slopes of β= 33.7° slopes loaded with q=200 kPa and L/B = 1 for H=40 m..... 45

Figure 4.10. Failure surfaces obtained from 3D FEM analysis of slopes of β= 33.7°, loaded with q=100 kPa and L/B=1: (a) H=10 m; (b) H=20 m..... 45

Figure 4.11. Failure surfaces obtained from 3D FEM analysis of slopes of β= 33.7°, loaded with q=100 kPa and L/B=1: (a) H=30 m; (b) H=40 m..... 46

Figure 4.12. Failure surfaces obtained from 3D FEM analysis of slopes of H=30 m loaded with q=100 kPa and L/B=6: (a) β=33.7°, (b) β=45°..... 46

Figure 4.13. Failure surfaces obtained from 3D FEM analysis of slopes of H=30 m loaded with q=100 kPa and L/B=6 for β=63.4°. 47

Figure 4.14. Failure surfaces obtained from 3D FEM analysis of 33.7° slopes with H=10 m, loaded with a surcharge L/B=6: (a) q=50 kPa, (b) q=100 kPa. 47

Figure 4.15. Failure surfaces obtained from 3D FEM analysis of 33.7° slopes with H=10 m, loaded with a surcharge L/B=6 for q=200 kPa. 48

Figure 4.16. Failure surfaces obtained from 3D FEM analysis with H=30 m, β=33.7° and load with surcharge load of q=100 kPa cases: (a) L/B=1, (b) L/B=2. 48

Figure 4.17. Failure surfaces obtained from 3D FEM analysis with H=30 m, β=33.7° and load with surcharge load of q=100 kPa for L/B=6. 49

Figure 4.18. Surcharge load L/B ratio versus F_s obtained from 3D FEM analysis of slopes loaded with q=100 kPa: (a) S_u= 75 kPa; (b) S_u=100 kPa. 50

Figure 4.19. Surcharge load L/B ratio versus F_s obtained from 3D FEM analysis of slopes loaded with q=100 kPa: (a) S_u=150 kPa; (b) S_u =200 kPa. 51

Figure 4.20. Surcharge load L/B ratio versus F_s obtained from 3D FEM analysis of slopes loaded with q=200 kPa: (a) S_u= 75 kPa; (b) S_u=100 kPa. 52

Figure 4.21. Surcharge load L/B ratio versus F_s obtained from 3D FEM analysis of slopes loaded with q=200 kPa: (a) S_u=150 kPa; (b) S_u =200 kPa. 53

Figure 4.22. Deformation contours of slope with β=45° and q=100 kPa and S_u=150 kPa. 54

Figure 4.23. Surcharge L/B versus ratio of F_s obtained from the analyses performed using 3D FEM to 3D LEM for slopes with H =5 m, 10m, 20 m and 40m and β=33.7° and S_u =75 kPa. 55

Figure 4.24. Surcharge L/B versus ratio of F_s obtained from the analyses performed using 3D FEM to 3D LEM for slopes with H =5 m, 10 m, 20 m and 40m and β=33.7° and S_u =100 kPa. 56

Figure 4.25. Surcharge L/B versus ratio of F_s obtained from the analyses performed using 3D FEM to 3D LEM for slopes with H =5 m, 10 m, 20 m and 40 m and β=33.7^o and S_u =200 kPa..... 57

Figure 4.26. Surcharge L/B versus ratio of F_s obtained from the analyses performed using 3D FEM to 3D LEM for slopes with H =5 m, 10 m, 20 m, and 40 m and β=45^o and S_u =75 kPa..... 58

Figure 4.27. Surcharge L/B versus ratio of F_s obtained from the analyses performed using 3D FEM to 3D LEM for slopes with H =5 m, 10 m, 20 m, and 40 m and β=45^o and S_u =100 kPa..... 58

Figure 4.28. Surcharge L/B versus ratio of F_s obtained from the analyses performed using 3D FEM to 3D LEM for slopes with H =5 m, 10 m, 20 m and 40 m and β=45^o and S_u =200 kPa..... 59

Figure 4.29. Surcharge L/B versus ratio of F_s obtained from the analyses performed using 3D FEM to 3D LEM for slopes H =5 m, 10 m, 20 m and 40 m and β=63.4^o and S_u =75 kPa..... 60

Figure 4.30. Surcharge L/B versus ratio of F_s obtained from the analyses performed using 3D FEM to 3D LEM for slopes with H =5 m, 10 m, 20 m and 40 m and β=63.4^o and S_u =100 kPa..... 60

Figure 4.31. Surcharge L/B versus ratio of F_s obtained from the analyses performed using 3D FEM to 3D LEM for slopes with H =5 m, 10 m, 20 m and 40 m and β=63.4^o and S_u =200 kPa..... 61

Figure 4.32. Slope height versus $F_{s,3DLEM}/F_{s,2DLEM}$ obtained from the analyses performed using 2D and 3D LEM for S_u=200 kPa, q=100 kPa: (a) L/B=1; (b) L/B=2. 62

Figure 4.33. Slope height versus $F_{s,3DLEM}/F_{s,2DLEM}$ obtained from the analyses performed using 2D and 3D LEM for S_u=200 kPa, q=100 kPa and L/B=6. 63

Figure 4.34. Slope height versus $F_{s,3DFEM}/F_{s,2DFEM}$ obtained from the analyses performed using 2D and 3D FEM for S_u=200 kPa, q=100 kPa and L/B=1. 63

Figure 4.35. Slope height versus $F_{s,3DFEM}/F_{s,2DFEM}$ obtained from the analyses performed using 2D and 3D FEM for S_u=200 kPa, q=100 kPa: (a) L/B=2; (b) L/B=6. 64

Figure 4.36. Slope height versus $F_{s,3DFEM}/F_{s,2DFEM}$ obtained from the analyses performed using 2D and 3D FEM for S_u=150 kPa, q =100 kPa, β=33.69^o for surcharge widths B = 20 m & B = 30 m. 65

Figure 4.37. Slope height versus $F_{s,3DFEM}/F_{s,2DFEM}$ obtained from the analyses performed using 2D and 3D FEM for S_u=200 kPa, q =100 kPa, β=45^o for surcharge widths B = 20 m & B = 30 m. 66

LIST OF TABLES

Table 2.1. Summary of definition of F_S (modified after Abramson *et al.*, 1996). 8

Table 2.2. General definitions for the generic forces acting on slice and their locations together with the corresponding abbreviations used in (modified after Abramson, 2002). 13

Table 2.3. Common LEM-based Slope Stability Methods. 16

Table 3.1. Slide2 limit equilibrium methods. 28

Table 3.2. Slide3 limit equilibrium methods. 29

Table 3.3. Effect of iteration and nest number for cuckoo search in 3D LEM..... 30

Table 3.4. Analyses results for different constitutive soil models..... 32

Table 3.5. The parameter range analyzed in 3D stability of slopes loaded with surcharge. 34

Table 3.6. Range of strength and stiffness parameters for undrained clays used in the analysis. 35

Table 3.7. Slope geometries used in the analysis. 35

Table 4.1. Total Crest and Toe Displacements for S_u=150 kPa & q=100 kPa & β=45^o in FEM. 54

LIST OF SYMBOLS

B	Surcharge width
c	Cohesion intercept
B	Young's Modulus
B_{50}	Triaxial loading stiffness
B_{50}^{ref}	Secant stiffness in standard drained triaxial test
B_{oed}^{ref}	Tangent stiffness for primary oedometer loading
B_{ur}^{ref}	Unloading/ reloading stiffness
B_s	Factor of safety
G	Shear modulus
G_0^{ref}	Reference shear modulus at very small strains
H	Slope height
K_0	Coefficient of earth pressure at rest
L	Surcharge Length
m	Power for stress-level dependency of stiffness
p^{ref}	Reference stress for stiffnesses
q	Surcharge load magnitude
R_f	Failure ratio
R_{inter}	Interface strength reduction factor
s	Shear strength
S_u	Undrained shear strength
u	Pore water pressure

β	Slope angle
γ	Unit weight of soil
$\gamma^{0.7}$	Threshold shear strain
ν	Poisson's ratio
ν_{ur}	Poisson's ratio for unloading-reloading
σ_h	Horizontal stress

σ	Normal stress
σ_v'	Vertical effective stress
τ	Shear stress
ϕ	Friction angle
ψ	Dilatancy angle

LIST OF ACRONYMS/ ABBREVIATONS

2D	Two-dimensional
3D	Three-dimensional
FE	Finite Element
FEM	Finite Element Method
GI	Gravity Increase
HS	Hardening Soil Model
HSS	Hardening Soil Model with Small Strain Stiffness
I	Iteration Number for Cuckoo Search
L/B	Surcharge Length to Surcharge Width Ratio
LEM	Limit Equilibrium Method
MC	Mohr-Coulomb
N	Nest Number for Cuckoo Search
NURBS	Non-uniform Rational B-Spline
SR	Strength Reduction
SRF	Strength Reduction Factor
SRM	Strength Reduction Method

1. INTRODUCTION

The foundation works require excavations leading to slopes, foundations are often placed on sloping ground, the existing natural slopes threaten the living spaces and the constructions for embankment fills also generate slopes. Civil engineers often encounter slopes in various construction projects, and they address the issues related to slope stability. Due to its geographic location and geologic nature, Turkey generally has a rugged nature consisting of various mountains surrounded by three main shore lines. Both natural and man-made slopes are common in this geography, and hence slope stability is a significant part of most construction projects.

The main purpose of performing slope stability analyses is to ensure the slope is safe, in both long-term and short-term conditions. If safety of the slope is deemed inadequate, then the engineers plan for one of the slope stabilization techniques. Proper slope stability analysis can prevent human and property losses and ensure the continuation of important public services, because the failure of slopes can result disruption of important services such as vehicular traffic flow, railways and electricity distribution. In order to produce an effective solution to this problem, engineers must first analyze the geometric and loading conditions of the existing or a planned slope, perform stability of the slope in both long-term and short-term conditions. Additionally, engineers may also need to comprehend the factors that may cause the slopes to fail in the future as well. For this reason, slope stability problems are complex problems and it is necessary to know the triggering factor that lead to failure the slope. Abramson et al. (2002) indicated that once changes occur in topography, seismicity, groundwater level, water flow conditions, strength, stress, loading conditions and weathering conditions, even natural slopes that have been stable for years may go through failures. One of the most common situations is the change of loading conditions on the slope. This can happen due to a construction near the crest of the slope in urban areas or maybe be due to a temporary crane loading in industrial plants. These types of surcharge loads can cause slope instabilities depending on their magnitude, dimensions and its location on the slope (*i.e.* its distance to the crest).

To analyze a given natural slope or a designed man-made slope, the selection of the most suitable slope stability analysis method is important to achieve reliable results. The selected stability method should be able to describe the slope geometry and the loading condition correctly, to produce a rigorous and economical solution. At the same time, cost of computation is another important factor in numerical analysis. The various studies presented in the literature and the common engineering practice show that slope stability analysis are generally performed using either Limit Equilibrium Method (LEM) or Finite Element Method (FEM), combined with the strength reduction (SR) technique to calculate the factor of safety (F_S) values. These two methods employ different approaches in stability calculations, and hence, they generally yield different F_S values. The main advantage of FEM analysis is the fact that when crest or toe movements are critical, the deformation analysis can provide these displacements. This is typically not possible with LEM-based analysis.

In cases of surcharge loads, when a continuous load is present, it is reasonable to assume plane strain conditions. However, the studies in the literature and the practicing engineers indicate that even when surcharge loads of limited size are present near the crest of a slope, a conservative approach is common and two-dimensional (2D) analysis is performed. In these type of scenarios, a three-dimensional (3D) analysis may be advantageous to achieve economical designs.

1.1. Aims of the Study

With the advancements in computers, three-dimensional slope stability analysis have become common in the recent years. Yet, the 3D effects are not very well understood in slope stability analysis. One of the sources of these 3D effects on the slopes is the presence of a non-continuous, surcharge load with limited dimensions located near the crest of the slope. This numerical study focuses on the effects of surcharge magnitude and dimensions on the short-term stability of clayey slopes. Both 2D and 3D analysis were performed using both FEM and LEM. The parametric study investigated a range of slope heights, slope angles and undrained shear strength values. The dimensions and magnitude of the surcharge load was varied.

The main objectives of this thesis can be listed as follow:

a. Determining the differences in F_s values obtained for loaded slopes (*i.e.*, slopes under surcharge effects) from the slope stability analysis performed using LEM and FEM coupled with the SR technique.
b. Comparing the results of 2D and 3D stability analysis of loaded slopes.
c. Investigating the effect of geometry and soil strength parameters on the F_s and the failure shapes of slopes under surcharge loads.
d. Investigating the effect of surcharge dimensions and magnitude on the F_s and the failure shapes of slopes.

1.2. Thesis Outline

This thesis is comprised of five primary chapters. Chapter 1, presents the topic, main objectives and outline of this thesis. Chapter 2 provides a general review of slope stability problem, focusing on 3D effects and a literature review. Chapter 3 presents the general methodology used in this study providing detailed information about the analysis performed using LEM and FEM, as well as the parametric study. Chapter 4 presents the results and discussions derived from the numerical analyses. Chapter 5 provides the main conclusions obtained from the study.

2. LITERATURE REVIEW

2.1. Slope Stability Analysis

Civil engineering is undoubtedly one of the most important engineering branches that lead to the today's modern world. Buildings for the people's need for shelter, all underground structures, such as the water and sewer systems of cities, pipelines, offshore structures, nearshore structures, transportation systems and surface structures built for various purposes have all been designed by civil engineers. Civil engineers have come to this day with a cumulative knowledge of many sub-disciplines dealing with these problems to produce solutions to today's problems. One of these sub-disciplines is geotechnical engineering. Geotechnical engineering is a branch of engineering that deals with soil related problems. Geotechnical engineers are involved with the analysis and the design of any structure that is in contact with soil or made-up of soil such as dams, slopes, tunnels and foundations. One of the problems that geotechnical engineers generally encounter is slope stability problems. When the delicate balance of a natural soil slope has been disturbed by human activity or by the forces of nature, slope stability issues have occurred throughout history (Abramson et al., 2002). Problems associated with failures of natural and man-made slopes often pose a great challenge in geotechnical engineering (Huang, 2014). It is the responsibility of geotechnical engineers to design slopes properly to prevent collapses that may cause loss of life and property. Any loading, especially near the edge of the slope, has the potential to create stability issues. Forensic examination of failed slopes indicates the need to have a better and comprehensive understanding of all relevant parameters. It is important to note that time dependent change of soil behavior also has to be accounted for in stability analysis. For this purpose, detailed laboratory and field tests are required to attain short-term and long-term soil strength parameters. Additionally, an understanding of the mechanics of the slope stability problem, led to the development of advanced analytical and numerical analysis and the utilization of computers to perform these types of analyses. Especially with the use of computers, it is possible to prepare detailed models that can reflect the field conditions. Today, using computer programs that utilize the limit equilibrium method (LEM) and the finite element method (FEM) engineers can easily perform numerical analysis of slopes with various soil strength and loading conditions, accurately and quickly. In the past, stability of

slopes was evaluated mainly by 2-dimensional (2D) analyses. Nowadays, it is possible to model slopes with complex geometric conditions in three-dimensions (3D) and to perform 3D slope stability analysis.

2.1.1. Why 3D Slope Stability Analysis is Required?

Slope stability studies are generally carried out in 2D with the assumption of plane strain conditions. In plane strain conditions the value of the strain component perpendicular to the plane of interest is zero. If one dimension of a structure is particularly large in comparison to the other two, the plane strain assumption is generally valid. Additionally, plane strain conditions also require that the failure surface should be the same in all cross sections as such the failure shape does not include curvature in the direction perpendicular to the plane of interest (Azizian and Popescu, 2006). However, assuming plane strain conditions is not always feasible. The 3D slope-stability analysis becomes essential especially in the presence of highly non-homogenous and anisotropic soils properties and when local surcharge loads are present, in essence when a 3D, a bowl-like shaped slip surface is anticipated. 3D analysis becomes also very useful in complex slope geometries in excavations when it is required to back calculate the shear strength of a failed slope (Chakraborty, 2016). Additionally, 3D slope stability analysis is also required in cases of slopes stabilized with piles that are placed with spacing in the perpendicular/longitudinal direction of the slope.

For typical slope stability issues 2D slope stability analysis has traditionally been used. Some prior research (Chen & Morgenstern, 1983; Cheng, 2003; Zheng et al., 2005; Griffiths and Lane, 1999) solely employ the Finite Element (FE) approach in 2D. The 3D analysis has recently become more widespread thanks to technological advancements and the associated decrease in computation time. Especially, when the slopes are loaded with surcharge the stability problem becomes 3D and the results may differ significantly with a 2D problem. The limited surcharge shape is modeled with an infinite length in 2D may result in a significant overdesign. Defining the differences between the results of 2D and 3D analysis of slopes can significantly help with optimization of design especially in geotechnical problems that involve slow draining soils with static loading situations – as seen in the case of loading of shallow foundations on clays – could be especially critical in short-term

undrained loading conditions in which soil strength characterized by the undrained shear strength parameter (S_u).

Until now, some researchers have contributed to the literature on 3D LEM, including Anagnosti (1969), Hovland (1977), Chen and Chameau (1982), Leshchinsky et al. (1985, 1986, and 1992), Cavounidis (1987), Hungr (1987, 1989), Lam and Fredlund (1993), Yamagami (1997), Huang et al. (2000 and 2002), Jiang et al. (2004), Cheng et al. (2005), Cheng and Yip (2007), Sun et al. (2012), and Ahmed et al. (2012). All of these authors have essentially expanded 2D LEM approaches to 3D analysis in their works. Some of these investigations, like those presented by Agnosti (1969), Hovland (1977), Hungr (1987), Hungr et al. (1989), and Lam (1993), were founded on straightforward assumptions which were: failure surface is symmetrical, the sliding direction is known and an asymmetric slope failure cannot be modeled. In models with a complex soil model and under localized surcharge loading, these assumptions were not particularly useful. But, in their research, Cheng and Yip (2007) created an original asymmetric 3D analytical formula. With the help of this formula, it became possible to conduct a 3D analysis by identifying a single sliding direction for an entire failure mass. Although they attempted to include all equilibrium circumstances (equilibrium in three directions for forces along coordinate axes and moments around three coordinate axes), they were unable to do so in their study. In the 3D analyses, in z axis, they were unable to reach moment equilibrium. Additionally, several other researchers have used the FE method to conduct various investigations (Nian et al., 2012; Ho, 2014; Kelesoglu, 2016). In their 3D studies, some researchers compared LEM and FEM (Ugai and Leshchinsky, 1995; Duncan, 1996; Wei et al., 2009; Chakraborty and Goswami, 2016).

Even though numerous slope stability methods are available in the literature (*e.g.*, limit analysis), analysis based on LEM and FEM are the most commonly employed two. These are detailed in the next Chapters.

2.2. Slope Stability Analysis Using Limit Equilibrium Method (LEM)

Limit equilibrium Method (LEM) is very widely used for slope stability analysis. LEM relies on the assumption of a pre-determined failure surface. Even though, various

different calculation approaches perform calculations over a single free body (*e.g.*, planar surface analysis, Swedish circle method) to perform slope stability analysis using LEM, the vast majority of LEM-based approaches are performed using the method of slices technique. The method of slices technique allows the incorporation of forces at unique locations in the geometry and allow for an accurate determination of F_S. In the past, LEM-based calculations were manually performed, based on the assumptions of several pre-determined failure surfaces. The critical slip surface refers to the surface yielding the F_S, among the number of different slip surfaces analyzed and this minimum value is reported as the F_S of a slope with certain geometry and soil conditions (Duncan, 2014). Nowadays the advancement of computers and the new software allow the execution of LEM-based numerical analyses of thousands of surfaces within minutes.

The results of the LEM-based slope stability analysis provide how safe the state of the slope is and how the failure mechanism will be in case of slope failure, as the calculations are based on assuming several pre-determined failure surfaces and calculating the factor of safety (F_S) for the most critical failure surface. In LEM, the very general form of F_S can be defined as the ratio of shear strength to the mobilized shear stress required to maintain balance at the incipient of failure

$$F_S = \frac{S}{\tau}. \tag{2.1}$$

In other words, the equilibrium shear stress is the shear stress required for the slope to maintain its current state without collapse. It is the mobilized portion of the strength divided by the F_S expressed as follows

$$\tau = \frac{S}{F_S}. \tag{2.2}$$

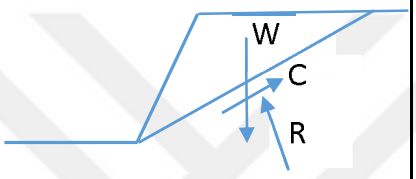
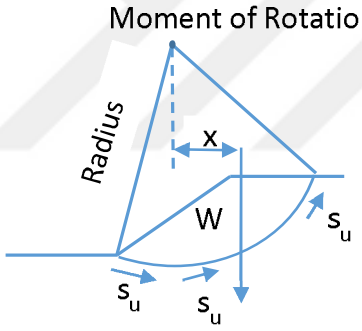
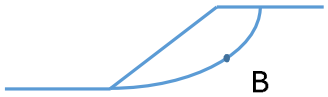
The is the main concept behind LEM analysis and once the shear strength is expressed in terms of Mohr-Coulomb failure criterion, mobilized shear can be express as follows in terms of total and effective stresses

$$\tau = \frac{c+\sigma \tan\varphi}{F_S}, and \tag{2.3}$$

$$\tau = \frac{c\prime+\sigma\prime \tan\varphi\prime}{F_S} = \frac{c\prime+(\sigma-u)\tan\varphi\prime}{F_S}. \tag{2.4}$$

In these equations, c and c' represent total and effective cohesion intercepts, φ and φ' represent total and effective internal friction angle values, σ and σ' denotes the total and effective normal stress on the shear plane and u is the pore water pressure. Table 2.1 summarizes the basic definitions of F_s. F_s can also be represented by the ratio of resisting forces to mobilized forces or ratio of resisting moments over overturning moments, these definitions are used in combination with the basic LEM definition in slope stability methods.

Table 2.1. Summary of definition of F_s (modified after Abramson *et al.*, 1996).

Main Concept	F_s Definition
	$F_s = \frac{Summation\ of\ resisting\ force}{Summation\ of\ mobilized\ force}$
	$F_s = \frac{Resisting\ moment}{Overturning\ moment}$
	$F_s = \frac{s_u}{\tau_{required}}\ (Total\ stress)$ $F_s = \frac{c' + \sigma' tan\theta'}{\tau_{required}}\ (Total\ stress)$

Various different calculation approaches (*e.g.*, planar surface analysis, Swedish circle method) use a single free body diagram to define the force and moment equilibrium equations to perform slope stability analysis using LEM. However, the vast majority of LEM-based approaches are performed nowadays dividing the slope into slices. These slope stability approaches are grouped under the general heading of method of slices. Separating the sliding body into discrete slices, allow the incorporation of forces at unique locations in the geometry and allow for an accurate determination of F_s. In these group of methods, a

combination of horizontal, vertical and moment equilibrium of individual slices and the overall moment or force equilibrium system are considered. Each method satisfies a different set of equilibrium equations, in other words, not all equilibrium equations are satisfied in each method. Figure 2.1 shows the basic representation of a slope geometry and the forces on one of the individual slices of this discretized slope for the most basic slice method: Ordinary method of slices also known as Fellenius method of slices, in which the inter-slice forces are neglected.

The base of each slice is part of the slip surface, so that the immovable portion of the soil mass below the slip surface exerts normal and shear forces on the slice bases. The shear forces exerted on the slice bases by the fixed mass are the stabilizing forces (resistance forces) that depend on the mobilized portion of the shear strength of the soil. Additionally, each slice is affected by any surface force directly applied to it, its own weight, and the forces exerted by the two slices on either side. These forces can be resistances or driving forces, depending on the geometry of the slice and its position within the sliding mass.

The slope stability problem is statically indeterminate, in which number of equations is lower than number of unknown. Therefore, it is essential to make some assumptions (*e.g*, location of the effective normal stress acting at the bottom of each slide) to reduce the number of unknowns. This in turn necessitates further assumptions relating to interstice forces: their presence, directions and application locations, with consequent implications for equilibrium. The assumptions relating to interslice forces differ from one LEM-based analysis to another.

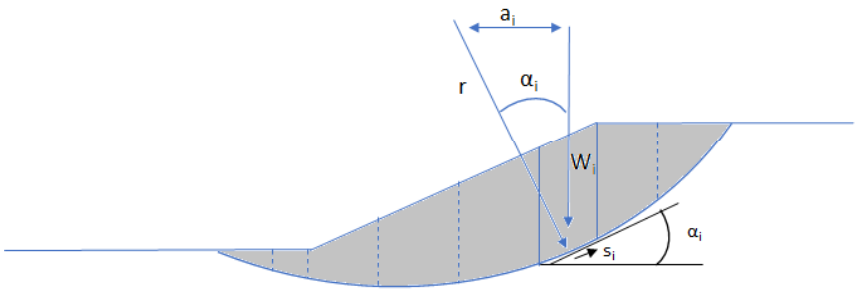


Figure 2.1. Basic of method of slices (modified after Duncan 2014).

The most well-known LEM methods are Bishop (1955), Janbu (1957), Morgenstern and Price (1965), Spencer (1967) and Janbu (1973). All these methods emerged on the basis of 2D analyzes, and later on, it became possible to perform 3D analyzes with the studies that extended these methods. These methods are classified by their assumptions for solving the equilibrium equations generated. It is not difficult for an engineer to perform these analyses with the help of a computer once slope geometry is established, soil parameters are determined. However, the results of the analysis should be thoroughly examined, comments should be made on how meaningful the results are, and the analysis should be re-performed again with different assumptions when needed. At that point, it is up to the engineer's judgment to adopt the proper assumptions and to decide which of the above-mentioned methods may be more suitable for the problem or what type of slip surface will be likely. Some of these methods are applicable to circular slip surfaces whereas others are applicable to both circular and non-circular slip surfaces. For this reason, the theoretical background of these methods should be known and the selection should be made accordingly.

2.2.1. Bishop's Simplified Method

The Bishop's Simplified Method is a widely used method in slope stability analysis. One of the reasons for this is its ease of application, but it is not the only reason. It is also generally known to provide similar results to more complex and advanced methods used for circular failure surfaces. The interslice shear forces are assumed zero, only horizontal interslice forces are taken into account (Bishop, 1955). In this method, vertical force balance and overall moment balance around the center of the circular slip surfaces are established for each slice. Several assumptions are made to perform the analysis. The first of these assumptions is that the sliding surface has a circular shape. That is, normal forces on the base of the slip surface pass through the center of rotation. The second assumption is that the resultant force is horizontal at the edges of the slices. Finally, the total normal forces are located at the center of the base of each slice. To summarize, moment equilibrium is established, a vertical force equilibrium is established and interslice normal forces are taken into account in this method for a circular failure surface. Normal force (N) is calculated by the following formula

$$N = \frac{[W - \frac{1}{F_S} \times (c' \times l \times sin\alpha - u \times l \times tan\varphi' \times sin\alpha]}{m_\alpha} \quad (2.5)$$

where, W= is weight of the slice, l = length of slice base, α= angle of the base of the slice with the horizontal and m_α equals to

$$m_\alpha = cos\alpha + \frac{(sin\alpha \times tan\varphi')}{F_s}. \quad (2.6)$$

F_s can be expressed by the ratio of the resisting and overturning moments about the center of the circle as expressed by the equation below

$$F_s = \frac{\sum[\frac{c' \times l \times cos\alpha + (W - u \times l \times cos\alpha) \times tan\varphi'}{cos\alpha + \frac{(sin\alpha \times tan\varphi')}{F_s}}}{\sum W \times sin\alpha}. \quad (2.7)$$

Since both sides of the above equation contain F_s, this method requires an iterative solution. Even though this analysis is usually performed for the circular failure surface assumption, it is worthwhile to note that Fredlund and Kahn (1977) performed a study to extend this method to non-circular slip surface cases.

2.2.2. Janbu's Simplified Method

The Janbu's Simplified Method is also based on the assumption that the interslice forces are horizontal and there is no shear stress between the slices. According to the Janbu's Simplified Method, the vertical force equilibrium for each slice and the overall horizontal force equilibrium for the entire shear surface are satisfied. This method generally tends to provide lower F_s values compared to those obtained from more comprehensive methods. Results can be obtained for both circular and non-circular failure surfaces. Assuming the interslice shear forces to be zero results in incomplete moment equilibrium conditions. Figure 2.2 shows forces acting on a slice, in a generic scenario considering all possible forces acting on a slice including the external loads, surface water forces, and seismic loads. For the very generic case shown in Figure 2.2, the vertical force equilibrium in each slide provides

$$\sum F_v = (N' + U_\alpha) \times cos\alpha + S_m \times sin\alpha - W \times (1 - k_v) - U_\beta \times cos\beta - Q \times cos\delta = 0, \quad (2.8)$$

$$N' = \frac{1}{m_\alpha} \times \left[W \times (1 - k_v) - \frac{c\, sin\alpha}{F_S} - U_\alpha cos\alpha + U_\beta \times cos\beta + Q \times cos\delta \right] \quad (2.9)$$

where $S_m = \tau.l = \frac{c+\sigma \tan\varphi}{F_s}$, in which l = length of slice base. According to this method, the base normal force (N) is calculated in a similar manner as explained in the Bishop's Simplified Method.

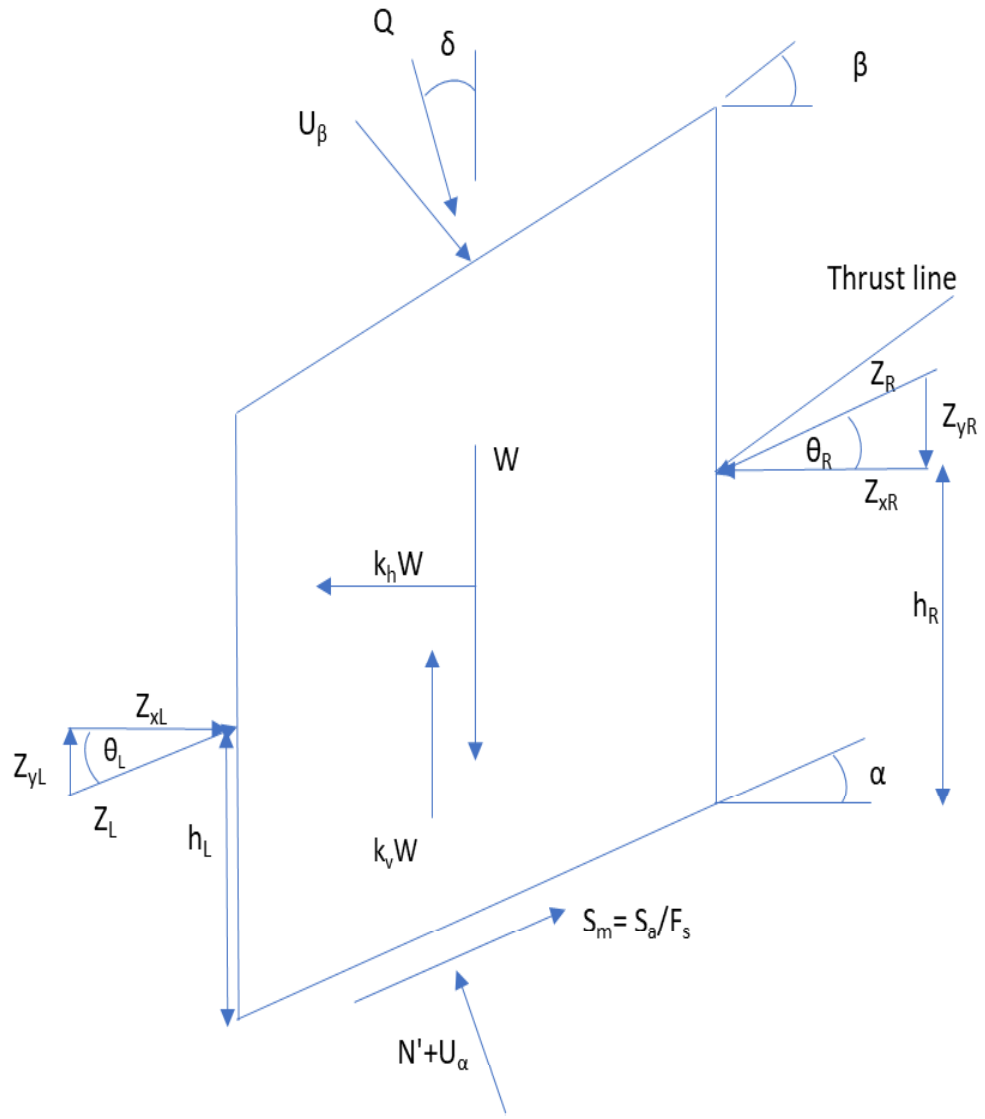


Figure 2.2. Generic forces acting on a single slice (modified after Abramson, 2002).

Table 2.2. General definitions for the generic forces acting on slice and their locations together with the corresponding abbreviations used in (modified after Abramson, 2002).

Abbrev.	Definition	Abbrev.	Definition
F_s	Factor of safety	Z_{yR}	Right interslice force y axis
S_a	Available strength	Z_{xR}	Right interslice force x axis
S_m	Mobilized strength	θ_L	Left interslice force angle
U_α	Pore water force	θ_R	Right interslice force angle
U_β	Surface water surface	h_L	Height of application of force Z_L
W	Weight of slice	h_R	Height of application to force Z_R
N'	Effective normal force	α	Inclination of slope base
Q	External surcharge	β	Inclination of slice top
k_v	Vertical seismic coefficient	θ	Inclination of surcharge
k_h	Horizontal seismic coefficient	b	Width of slice
Z_{yL}	Left interslice force y axis	h	Average height of slice
Z_{xL}	Left interslice force x axis	h_c	Height to centroid of slice

The overall horizontal equilibrium of the system leads to the following equation

$$\sum_{i=1}^{n}[F_H]_i = \sum_{i=1}^{n}\left[(N' + U_\alpha)sin\alpha + Wk_h - U_\beta \times cos\beta\right] - \sum_{i=1}^{n}\left[Q\ \sin\delta + \frac{c'.l + N'}{F_s}cos\alpha\right] = 0. \quad (2.10)$$

Then the $F_{s,calculated}$ can be formulated as the ratio of the shear strength over the driving force expressed equation below

$$F_{s,calculated} = \frac{\sum_{i=1}^{n}[c'l + N'\tan\varphi']\cos\alpha}{\sum_{i=1}^{n}(U_\alpha sin\alpha + Wk_h - U_\beta \times \sin\beta - Q\ \sin\delta) + \sum_{i=1}^{n}N'\sin\alpha}. \quad (2.11)$$

Janbu presented a correction factor (f_0) accounting for the depth to length ratio of the sliding mass and the type of soil. Figure 2.3 shows the variation of this correction factor depending on the soil parameter and slope geometry. F_s obtained from the Janbu's Simplified Method is calculated after applying this correction factor as expressed by the following formula

$$F_s = f_0 \times F_{s,calculated}. \tag{2.12}$$

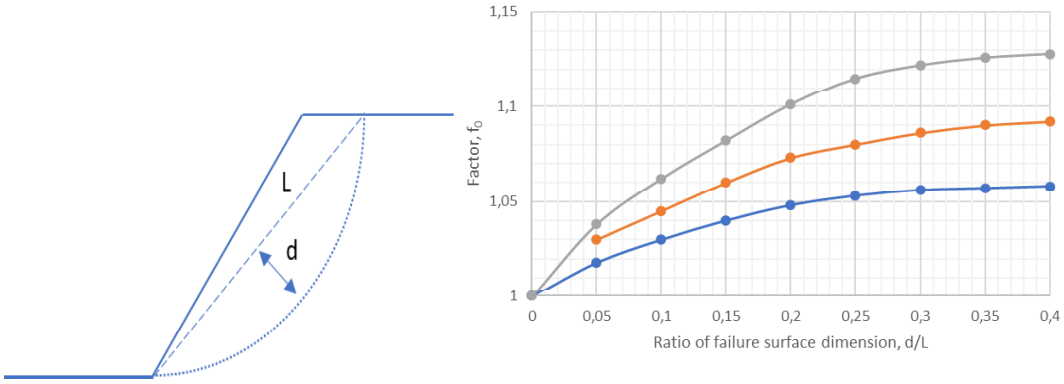


Figure 2.3. Janbu correction factor (modified after Duncan 2014).

2.2.3. Spencer's Method

Spencer's Method is among the rigorous slope stability methods in which both horizontal force equilibrium, vertical force equilibrium and moment equilibrium equations are satisfied. This method is applicable to both circular and non-circular failure surfaces. Spencer method is based on the assumption that the interslice forces are always parallel to each other in each slice, thus all interslice forces have the same inclination θ as expressed by the equation below

$$\theta = \tan^{-1}\left(\frac{Z_{yR}}{Z_{xR}}\right) \tag{2.13}$$

where, Z_{yR} and F_{xR} are the vertical and horizontal interslice forces, respectively. The normal forces act at the center of the base of each slice, and can be written as

$$N = \frac{[W-(Z_{xR})-(Z_{xL}))\times tan\theta - \frac{1}{F_s}\times(c'\times l\times sin\alpha - u\times l\times tan\varphi'\times sin\alpha]}{m_\alpha} \tag{2.14}$$

where, Z_{xR} is the horizontal interslice force on the right of the slice, and Z_{xL} is the horizontal interslice force on the left side of the slice. The calculations are performed for a range of inclination angles. The F_s considering the force equilibrium $(F_s)_f$ can be written as

$$(F_s)_f = \frac{\sum[c'\times l + (N - u\times l)\times tan\varphi']\times sec\alpha}{\sum[W - ((Z_{yR}) - (Z_{yL}))]\times tan\alpha} \tag{2.15}$$

where, Z_{yR} is the vertical interslice force on the right of the slice, and Z_{yL} is the vertical interslice force on the left side of the slice. The F_s considering the moment equilibrium $(Z_s)_m$ can be written as

$$(F)_m = \frac{\sum[cr \times l + (N - u \times l) \times tan\varphi r]}{\sum(W \times sin\alpha)}. \quad (2.16)$$

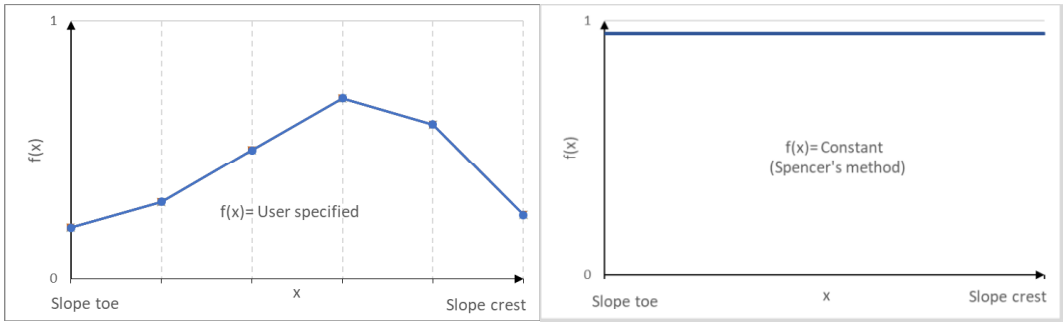
When the inclination angle that yields the same F_s from force equilibrium and moment equilibrium equations are determined, this is reported as the F_s of the slope per Spencer's Method. In order to evaluate a range of interslice force inclination angle (θ) values, performing hand calculations is not feasible, this method requires computational effort. It is important to note that in Spencer's Method, θ angle is assumed to be constant same for all slices of the single surface analysis.

2.2.4. Morgenstern and Price's (GLE) Method

The Morgenstern and Price's Method, also known as Generalized Limit Equilibrium Method, is a more advanced and generalized form of Spencer's method. Unlike, Spencer's method, Morgenstern and Price's Method allows the chance of the interslice force inclination angle using an arbitrary function f(x) along the failure line, changing from toe to crest in which x is the position of the slice center. Accordingly, θ can be expressed as below

$$\theta = \lambda \times f(x). \quad (2.17)$$

Each slice has its own value of f(x), ranging between 0 and 1. At this point, the Spencer's Method can be obtained by substituting 1 for f(x) in the above formula. Figure 2.4 shows some examples of the variation of f(x): in essence, it shows how f(x) can change in for each slice, from crest to toe. Morgenstern and Price (1956) proposed some reasonable conditions for the accuracy of the analyses. The first of these is that the normal stress on the shear surface is compressive and the F_s value on any slice does not exceed the global F_s value. All equilibrium conditions are satisfied in this method.



(a) (b)

Figure 2.4. Possible functions that describe variation of interslice force inclinations: (a) user specified; (b) constant (equivalent to Spencer's method) (modified after Abramson 2002).

2.2.5. Failure Surface Searching Methods

There are numerous LEM-based slope stability methods. Only a few of the most widely used methods are explained herein. The equilibrium equations satisfied by LEM-based methods introduced in the previous section is summarized in Table 2.2 together with their assumptions of failure surfaces and the information indicating if computer calculations are required.

Table 2.3. Common LEM-based Slope Stability Methods.

Method	Overall Moment Equilibrium	Slice Moment	Vertical Force	Horizontal Force	Slip Surface	Hand Calculation	Computer Calculation
Bishop S.	Yes	No	Yes	No	Circular	Yes	Yes
Janbu S.	No	No	Yes	Yes	Any	Yes	Yes
Spencer	Yes	Yes	Yes	Yes	Any	No	Yes
GLE	Yes	Yes	Yes	Yes	Any	No	Yes

There are several slip surface search approaches in LEM. The most preferred technique employed in LEM-based software is performing a grid search, especially when circular slip surfaces are considered. When performing stability analysis using the grid search technique, a grid area is located in the geometry, in which each point in the grid corresponds to the center of each sliding surface considered. The grid size, the grid location in the geometry

and the spacing of the grid affects the results. Eventually, the F_s values for all of the failure surfaces corresponding to circles with centers in the grid are determined. The lowest F_s corresponds to the most critical slip surface. For clayey slopes, as circular failures are common, this failure surface searching technique performs well. However, if non-circular slip surfaces needed to be investigated, this method cannot be used.

In addition to the grid search technique, there is another technique called Cuckoo Search, which has recently become more popular. Cuckoo Search is inspired by the nature and it is a metaheuristic algorithm introduced to the literature by Yang and Deb (2009). These researchers were inspired by the cuckoo bird while designing this algorithm. The breeding behaviors and habits of the cuckoo birds were utilized. These birds can lay their eggs in a nest that they choose randomly. The one with the best quality eggs from the nests where they lay their eggs will ensure the continuity of the bird species, that is, the solution produced. Since the number of nests where the eggs are laid is known, if a better solution is found for the same nest in a new iteration, this solution replaces the old one. This is the principal idea of the cuckoo search algorithm in which various locations in the slope geometry is targeted and with each iteration, there is an optimization to find the critical failure surface. Typically, two parameters are requested to perform and refine the slope stability analysis using cuckoo search, these are the: *(i)* nest number and the *(ii)* iteration number. With each iteration, an optimization is carried out to find the lowest factor of safety. The most distinct advantage of the Cuckoo search algorithm is that it allows the user to search non-circular slip surfaces as well.

Grid search is popular and easy to use in analyses performed with the assumption of circular slip surface type, so it is frequently used in 2D analyses. However, the situation is slightly different for 3D analyses. It is quite difficult to find the grid area where we can find the center of the critical slip surfaces in 3D slope geometry. In 3D analyses, the grid area turns into a grid volume. It is necessary to determine the size in the x, y and z planes including the grid spacing (i.e., exact the number of points in the grid volume) in order to increase the accuracy of the result obtained. Locating the center of the grid volume is also challenging in 3D analysis, and hence, it is difficult for the user to generate and locate the critical grid volume that can yield the most critical slip surface. Additionally, as discussed in analysis performed with 2D LEM, one of the most important disadvantages of grid search in 3D LEM

is that only simple circular-shaped slip surface searches can be performed (Cheng et al., 2005; Wei et al., 2009). For these reasons, in 2D analysis where non-circular slip surfaces are anticipated or when a 3D analysis is performed, Cuckoo search technique provides a more comprehensive search.

2.2.6. 3D Extension of LEM

All of the LEM-based slope stability analysis described in the previous chapters are developed initially for 2D analyses. Designing 3D problems in two dimensions, and performing 2D analysis with the use of these previously introduced methods is very common. One of the main reasons for this is the ease of analysis and the fact that the results obtained from 2D analyses tend to remain on the safe side (Sun, 2012). However, actual slope stability failures are 3D, and 2D idealization is not always suitable in all cases. Same LEM-based slope stability approaches developed for 2D analysis, can be utilized to perform 3D analyses. In the recent years, 3D slope stability analyses have become popular. Software that allows 3D modeling and analysis, have become more accessible to engineers due to the exponential growth of computer technologies. 3D analyses allow the evaluation the individual or combined effects of various factors in complex geometries encountered in geotechnical engineering. Generally, slices used in 2D analyses can be converted to columns with depth in the third direction in 3D analyses. The importance of 3D slope stability analyses is mostly seen in cases where the slope geometry and sliding surface change in the lateral direction, soil material properties vary widely within the slope and are anisotropic, and the slope model is loaded with a local surcharge. Situations where 2D idealization is not suitable can be summarized as follows:

1) Soil separations of the model should not differ in the 3rd axis. In other words, layer change should not be inclined on the 3rd axis. Layer separation should continue perpendicular to the 3rd axis. If there is non-homogeneity or anisotropy, it is not appropriate to perform the analysis by making a 2D assumption.

2) There are 3 different types of assumptions when making 2D assumptions. These are plane strain, plane stress and axi-symmetry. However, 2D analyses are generally based on the plane strain assumption. According to this assumption, the strain

component in the 3rd axis is taken as zero. However, this assumption is a logical and realistic approach if there is no discontinuity in the 3rd axis and the length in the 3rd axis is quite large. In other words, there should not be a concave-convex situation, there should not be a horizontal boundary that prevents slope deformations (for example, a dam structure located near a narrow rock wall valley).

3) It is not correct to work in 2D especially under earthquake loads. When designing, the largest of the 3-component earthquake accelerations is taken into account. Therefore, the vertical component and the lower horizontal component are neglected. In 2D slope stability analyses, the earthquake load is usually applied in the direction along the slope plane. Therefore, any instability out of the plane, i.e. in the 3rd axis, is not taken into account (Azizian and Popescu, 2006).

3D slope stability analysis is still evolving today and there are drawbacks as well as advantages of 3D analysis. Most of the existing slope stability formulations do not consider the sliding direction, so for those methods that are extended to 3D, the sliding direction should also be selected. The location of the non-spherical critical 3D failure surface is a difficult global optimization problem that has not been effectively solved. The fact that there are significantly more redundant equations in 3D limit equilibrium analyses than in the corresponding 2D analysis is one of the other challenges (Cheng et al. 2007). A 3D slope stability analysis requires more effort to enter the data and to visualize the results. However, recent advancements in computation and visualization make this possible in relatively short-time periods (Leong and Rahardjo 2012). Several researchers have contributed to the literature on 3D LEM.

Anagnosti (1969) studied the method of Morgenstern and Price and extended it to a 3D model. As a result of his work, the F_S values he obtained were about 50% higher compared to those obtained from 2D analysis. He also stated that the effect of his assumptions on internal forces on F_S is very low.

Chen and Chameau (1982) extended the Spencer method to 3D. Accordingly, the sliding surface was assumed to be symmetrical and the sliding surface was divided into columns. In some of the 3D analysis performed on sandy soils, the F_S values lower than those

obtained in 2D were attained. Cavounidis (1987) showed that the F_S value obtained from 3D analysis is higher than those obtained from 2D analysis.

Hungr (1987) extended the Bishop's Simplified Method to 3D. According to this study where symmetrical failure surface analysis can be performed, the following assumption was made: vertical inter-column shear forces were neglected. Another assumption is that horizontal force equilibrium conditions are neglected. At the end of the study, it was found that the F_S values obtained from 3D analysis was notably greater than the F_S values obtained from 2D.

Hungr (1989) proposed the extensions of the Bishop's Simplified Method and the Janbu's Simplified Method to 3D. He stated that the F_S values obtained with the Bishop's Simplified Method were found to be more conservative, in other words lower F_S values were especially in the case of non-rotational and asymmetric sliding surfaces. He stated that the reason for this is the due to neglecting vertical internal shear stresses according to the Bishop's Simplified method.

Leshchinsky (1992) worked on 3D slope stability analysis for symmetric slip surface assumption. Following up with his previous studies, he worked on the layered slope model. All global LEM equations are satisfied and the result shows that the F_S value obtained from 3D analysis is greater than the one obtained from 2D analysis.

Lam (1993) carried out a study based on the method of columns in which the 2D GLE method was extended to 3D. He stated that the F_S values obtained from the analysis with the GLE method is relatively insensitive to intercolumn force functions. However, he showed that the use of the half-sine function gives a more reasonable result. While the Bishop's Simplified Method provided realistic results for the analyses that involve circular slip surfaces, for noncircular failure surfaces this method gives very different results compared to more rigorous methods such as GLE. The results indicated that Janbu's Simplified Method significantly underestimates the F_S, when compared with those obtained from 3D analysis employed by GLE.

Yamagami (1997) performed 3D slope analysis using Janbu's Simplified Method developed by Ugai (1988). With this study, he was able to obtain the F_s value by dividing a sliding surface of any shape into columns. With this approach, not only can a failure surface of any shape be obtained, but also inhomogeneous and non-symmetrical failure plane cases could be analyzed.

Huang and Tsai (2000) performed the first 3D asymmetrical slope stability analysis. In their analysis the sliding direction affects the determination of F_s and the sliding direction of each column can be different. Bishop's Simplified Method, which was previously extended to three-dimensional analysis by Hungr (1987) and Ugai (1988), was modified to include an extra moment balance equation. Possible errors related to plane of symmetry were eliminated. However, the analyses were made with the assumption of circular failure surface, so the most critical failure surface that can be a noncircular surface may not have been obtained.

Huang (2002) extended the Janbu's Method to 3D with some simplifications on transverse shear forces so that failure surface of any shape can be analyzed. In order to examine the stability of a potential failure mass, this new method develops a force and moment limit equilibrium in two orthogonal directions. Thus, the slip direction becomes part of the solution instead of being an assumption. The direction of movement of the columns differs from each other. The shear direction of the columns is obtained by secant method.

Jiang et al. (2004) performed a study extending the Spencer's method to 3D for slope stability analysis. This study was also compared with the Janbu's Method and the variational approach of Baker and Leschinsky (1987). The analysis showed a significant difference between the 3D extension of the Janbu's method and the variational approach. The variational approach gives almost the same F_s value and the same critical sliding surface for vertical cut as the FEM. Since the 3D extension of the Spencer's Method provides almost the same result as the variational approach and the FEM, it should be preferred in 3D analysis performed using LEM.

Cheng et al., (2005) suggested using 3D non-uniform rational B-spline (NURBS) surface and simulated annealing method to obtain the most critical failure surface in 3D

LEM. In previous studies, the location of the critical failure surface was generally limited to a spherical shape. In this study, ellipsoidal surfaces were also considered. According to their method, the location of the critical sliding surface is determined by 3D NURBS surface and simulated annealing method. In their case study, they were able to obtain lower F_S values compared to the spherical surface search. The authors recommend the use of ellipsoidal failure surface, especially in the cases of presence of weak zones and in cases of asymmetric slopes.

Cheng et al. (2007) developed a 3D asymmetrical slope stability formulation using Bishop's Simplified Method, Janbu's Simplified and Morgenstern Price's Methods. According to this study, the slip direction is determined by 3D force/moment balance equations. The F_S results obtained with this new formula are close to the results of previous similar studies. In addition to the work done by Huang (2000), this new formula provides reliable results under transverse loads.

Sun (2012) proposed a method extending the Morgenstern Price's method to 3D. According to this method, no assumption is made about the internal forces, but all equilibrium conditions are met. The results clearly indicated the F_S value obtained from 3D analysis is greater than the F_S value obtained from 2D analysis.

Ahmed et. al. (2012) compared the work of Hovland (1977) with the results of the analysis performed with 3D extension of Janbu's Simplified Method. As a result of this comparison that included several different scenarios, Hovland's Method provided lower F_S values for soils with low cohesion and high friction angle values, especially in cases with narrower slip surface width and high-water pressure along the slip surface. In addition, the F_S value obtained from the 3D analyses of the Hovland's Method was lower than the 2D analyses.

2.3. Slope Stability Using Finite Element Method (FEM)

The use of FEM in geotechnical engineering has increased especially in recent years. In addition to F_S, soil stresses and soil can also be obtained when the analysis is performed using FEM. This is the most important difference that distinguishes FEM from LEM. The

stresses in the slope are strongly influenced by the initial stress condition. Nowadays, advanced computer programs are used to perform FEM analyses. In these analyses user-defined conditions such as initial stress condition and soil constitutive model are important criteria that directly affect the result of the analysis. The K_0 value, which is the ratio of horizontal normal effective stresses to vertical effective stresses, is not considered in LEM analyses but is used in FEM analyses. Griffiths and Lane (1999) listed the important differences that distinguish the FEM from LEM as follows:

1) Analysis performed using FEM does not require any assumptions about failure surface shape and failure surface location.
2) In the analysis performed with LEM, each method requires several assumptions including those relevant to slices. These assumptions affect the results. Since there is no concept of discrete slices in FEM analysis, there is no need to make any assumptions about these slices.
3) If the compressibility values of the soil are chosen appropriately, it is possible to perform deformation analysis to obtain a realistic value of deformations.
4) With FEM analyses, the stress condition in the slope can be observed gradually as staged construction can simulate the construction progress.

In FEM analysis, the most common technique used to determine F_s of a slope is the strength reduction (SR) technique. Another technique to analyze slope stability using FEM is the gravity increase (GI) technique. In this research study SR was employed accordingly the details of this technique is explained herein.

In order to obtain F_s using FEM, a safety phase is defined to apply SR technique. In the safety phase, repeated analyses are performed by reducing the strength of the soil by a factor, increased each time until the failure condition occurs. The factor specified here is referred to as strength reduction factor (SRF). At the end of the analysis, the SRF value yields the F_s value. By dividing the shear strength parameters by SRF, F_s is obtained in the equilibrium. This process is also known as c-φ reduction technique. The c and φ of soils are reduced as shown in below

$$c_f = \frac{c\prime}{SRF}, \tag{2.18}$$

$$\varphi_f = \arctan\left(\frac{tan\varphi r}{SRF}\right). \quad (2.19)$$

The F_S value corresponds to the SRF value that leads to the failure. The primary advantage of the SR technique is that the critical slip surface is found automatically from the shear strains, which increases as the shear strength decreases. However, one of the limitations of SR is that it cannot locate other ''slip'' possibly critical surfaces (Liu et al., 2015).

The most important disadvantage of FEM compared with LEM is the time required to perform the analysis. This required time is quite long compared to that of LEM, especially when 3D analysis is preferred. The results of the analyses performed using FEM, can also provide stresses, deformations and pore water pressures besides the F_s analysis. The soil body is divided into smaller elements that is called meshing. Each element is connected to each other and to the model boundaries by nodes. Displacement, stresses, and strains at each node are calculated based on compatibility equations. Using 3D FEM analysis coupled with SR technique can simultaneously provide the F_s and the critical slip surface (shape and location), together with the stress, deformation, and progressive shear failure of the slope. Moreover, using 3D modeling can help with reflecting the accurate slope dimensions and boundary conditions, as such a complex geometric configuration in all three (*i.e.*, x–y–z) directions can be represented realistically. In this way, the computational accuracy can be greatly improved, and the fundamental nature of slope failure mechanisms can be fully revealed.

Liu et al. (2015) evaluated the results of FEM and LEM analysis on F_s and critical slip surfaces. FEM analyses performed by defining a constitutive model with an associated flow rule, gave slightly higher F_s values compared with the results of the analysis performed with LEM. Nian et al. (2012) highlighted the importance of geometric effects in 3D slope stability analysis by performing FEM analysis.

Griffiths and Marquez (2007) conducted an analysis using 3D FEM. The results of the study performed on a homogeneous slope model indicated that the F_s obtained in the 3D analysis merges closer to the F_s obtained from 2D FEM as the length in third-dimension is extended. Additionally, in FEM analysis, a finer mesh presents a lower F_S value compared

to a coarse mesh with a very small difference (not exceeding 2%). The 3D analyses are more realistic and not only the accuracy of the result is improved but also the collapse mechanism of the slopes can be better understood.

2.4. Slope Stability Analysis Under Surcharge

One of the factors that trigger the movement that will lead to the collapse of natural or man-made slopes is the surcharge loads. Slopes that are stable in their natural state may lose their stability due to the effects of surcharge load. At this point, factors such as the magnitude of the surcharge load and the location of the surcharge can affect the results drastically.

Wei et al. (2009) carried out a 3D slope stability analysis using both the LE method and finite difference method coupled with SR considering various cases. This study showed that convergence criteria, model boundary conditions, and mesh optimization significantly affect the performance of 3D slope stability analysis coupled with SR. The magnitude of the applied load determines the shape and dimensions of the critical failure surface (*i.e.*, 2D or 3D) of a slope under surcharge loads.

Zhang et al. (2011) studied the effects of shear strength parameters, boundary conditions, and surcharge loads on the slope failure mechanisms using both 2D and 3D finite difference method coupled with SR technique. The Authors found that when the ratio of the failure length to slope height is greater than or equal to ten (10), this failure mode can be regarded as plane strain conditions. When the surcharge is applied near the crest, a 3D failure can be obtained. When the ratio of loading length to slope height reduces below six (6), a 3D failure shape occurs.

Moni et al. (2015) investigated the effect of surcharge load performing analyses using LEM and FEM. In his study of homogeneous and layered slope models, slope failures can be observed with the increase in plastic strains triggered by the surcharge load. As the location of the surcharge load is moved away from the crest of the slope, F_S increases. After a certain distance from the crest, no change in F_S is observed.

Kelesoglu (2015) investigated the effects of local surcharge loading, pile stabilization, and slope curvature on the F_s and failure mechanism of slopes, Keleşoğlu (2015) used finite difference coupled with SR in his study. According to his findings, 3D failure is anticipated when the local surcharge loading is close to the slope's crest. If not, 2D failure results because the slopes' own weight has a greater influence on the failure surface's shape.

The shape of failure and F_s of a slope under surcharge loads are affected by the slope geometry, soil strength, surcharge magnitude, surcharge location and surcharge shape. Additionally, the results may vary based on the analysis performed, in other words analysis of the same slope using 2D LEM, 2D FEM, 3D LEM and 3D FEM will reveal different results. The 3D effects on the analysis of loaded slopes have not been investigated thoroughly using both LEM and FEM comparatively.

3. METHODOLOGY

This research study focused on determining the short-term slope stability analysis of loaded clayey slopes based on 3D LEM and 3D FEM coupled with the SR technique. The results of 2D and 3D stability analysis of loaded slopes were compared in context of the evaluation of surcharge characteristics. For this purpose, both LEM-based and FEM-based 2D and 3D analyses were performed in this study. This chapter explains the problem investigated, the details of the 3D LEM and 3D FEM software program, analysis steps, and the calibration process.

3.1. Analysis Performed Using 2D and 3D LEM

LEM-based stability analysis is frequently preferred in evaluating stability of slopes. In the studies conducted within the scope of this thesis, a series of analyses were performed using LEM. Slide2 and Slide3 software programs (Rocscience Inc., 2023) were used to perform these analyses. Initially, calibration studies were carried out to refine the model dimensions and analysis methods. Later, the models prepared for the parametric studies were structured based on the results of the calibration studies.

3.1.1. Calibration Study

The Slide2 program is frequently preferred by engineers mainly because it does not require extensive input and the solution can be obtained quickly. When using Slide2, project settings are arranged, including the selection of measurement units and the failure direction in the model created. Then, one or more of the preferred LEM-based slope stability analysis (e.g., Spencer's Method, Bishop's Simplified Method) are selected for the analysis. The LEM-based analysis that can be preferred in Slide2 software and the failure surface search methods available for each are given in Table 3.1 The same are presented for Slide3 in Table 3.2

Once the model is established, the type of slip surface and the search methods are determined from Table 3.1 and Table 3.2 before performing the analysis in 2D and 3D,

respectively. For homogenous clayey or sandy slopes circular slip surfaces are observed. However, non-circular slip surfaces are more common in heterogeneous slopes and slopes with the presence of weak layers. The first studies on Slide2 examined non-circular failure surfaces. Furthermore, additional analyses were also carried assuming circular slip surfaces in 2D. As a result of these studies, for the actual parametric study, circular failure surface assumption was selected in Slide2. For Slide3 the ellipsoid (non-circular) slip surface type were the primary choices in the analysis, considering that the non-circular surface type is more likely to occur. It is also recommended to use an ellipsoid (non-circular) surface especially when using the Cuckoo search.

Table 3.1. Slide2 limit equilibrium methods.

LEM Options	Surface Selection	Search Type Selection
Bishop's Simplified, Corps of Engineers #1, Corps of Engineers 2, GLE/Morgenstern Price, Janbu's Simplified, Janbu's Corrected, Lowe-Karafiath, Ordinary/Fellenius, Spencer's, Sarma	Circular	Auto refine, Grid, Slope
	Non-circular	Cuckoo, Simulated Annealing, Particle Swarm, Auto Refine, Block, Path

Among many search methods, grid search is one of the most popular techniques used to identify circular failure shapes. According to this search method, the center of the slip surface is located in the grid area. However, in order to obtain accurate results, selection of the size and location of the grid area are important. In preliminary studies, grid search was used. In 2D analyses, the use of grid search is practical, but as explained previously, creating and locating the grid volume that gives the most critical F_S value is challenging in 3D. Additionally, using grid search in both Slide2 and Slide3, the analysis can only be performed for the circular failure surface assumption. Besides, the analysis using grid search takes longer time compared to Cuckoo search. For these reasons, Cuckoo search technique was preferred especially for the analysis performed in 3D. This method is presented in both Slide2 and Slide3. This method was introduced by Yang and Deb (2009), and developed

using cuckoo bird breeding behavior and habits, it is a metaheuristic optimizing algorithm. With each iteration, an optimization is carried out to find the lowest factor of safety. The Cuckoo search is based on this sampling principle, which is the algorithm's central notion. In cuckoo search the selection of: *(i)* nest number (N) and the *(ii)* iteration number (I) are required to perform the analysis.

Table 3.2. Slide3 limit equilibrium methods.

LEM Options	Surface Selection	Search Type Selection
Bishop's Simplified, GLE/Morgenstern Price, Janbu's Simplified, Spencer's	Sphere	Cuckoo, Grid, Particle Swarm, Auto Refine
	Ellipsoid	Cuckoo, Particle Swarm
	Multi-Planar	Cuckoo, Particle Swarm
	Wedge	Cuckoo, Grid, Particle Swarm, Auto Refine

Among the LEM options in Table 3.1 and Table 3.2, Spencer, GLE, Bishop's Simplified Method and Janbu's Simplified are the methods that can be used in both Slide2 and Slide3. These methods seem appropriate for comparing 2D analysis with 3D analysis. Among them, Spencer's Method was preferred for the analysis since it satisfies all equilibrium equations.

A calibration study was conducted to decide on the iteration and nest numbers required for the analysis performed using Cuckoo search technique. Table 3.3 shows the result of this study.

Table 3.3. Effect of iteration and nest number for cuckoo search in 3D LEM.

Program	Iteration (I); Nest number (N)	Slip Surface Type	Search Type	Factor of Safety (F_s)	
				Search Methods	
				Spencer's	GLE
Slide3	I=40 ; N=20	Ellipsoid	Cuckoo	2.997	2.965
Slide3	I=80 ; N=40	Ellipsoid	Cuckoo	2.674	2.858

Based on the results obtained in Table 3.3 and the required computation time, optimum iteration number and nest numbers were selected as 40 and 20 using Cuckoo Search. Another important point to be considered in 3D analysis is the extrusion depth. A study was carried out to obtain an adequate extrusion depth value. Figure 3.1 shows the results of this study. According to this, no significant change was observed in F_s values for extrusion depth greater than 400 m depth. As a result of this study, selecting an extrusion depth of about 400m was deemed sufficient. Figure 3.2 shows a critical slip surface obtained using the extrusion depth of 400 m.

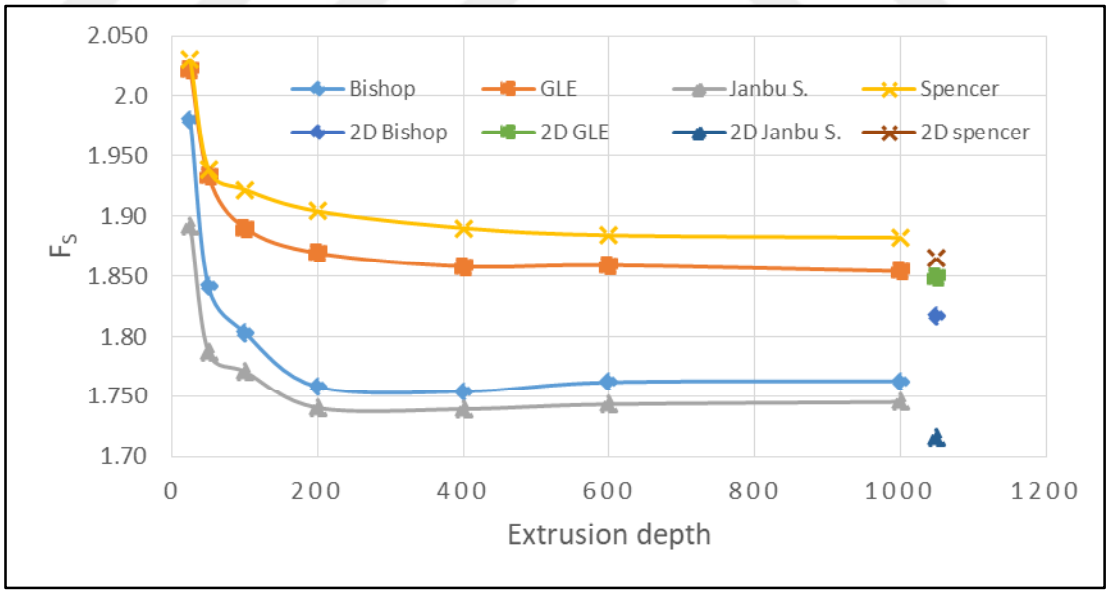


Figure 3.1. Effect of extrusion depth on F_s in Slide3 for the stability of clayey slope.

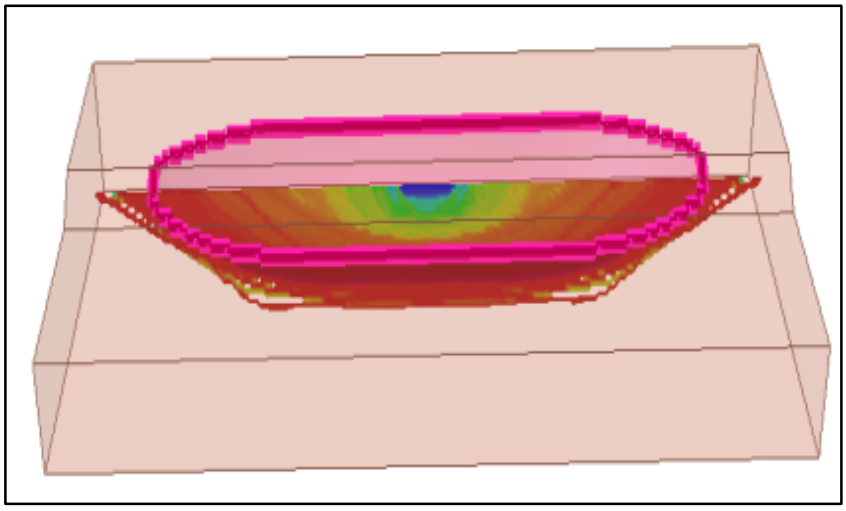


Figure 3.2. Critical slip surface for a 3D slope with 400 m extrusion depth.

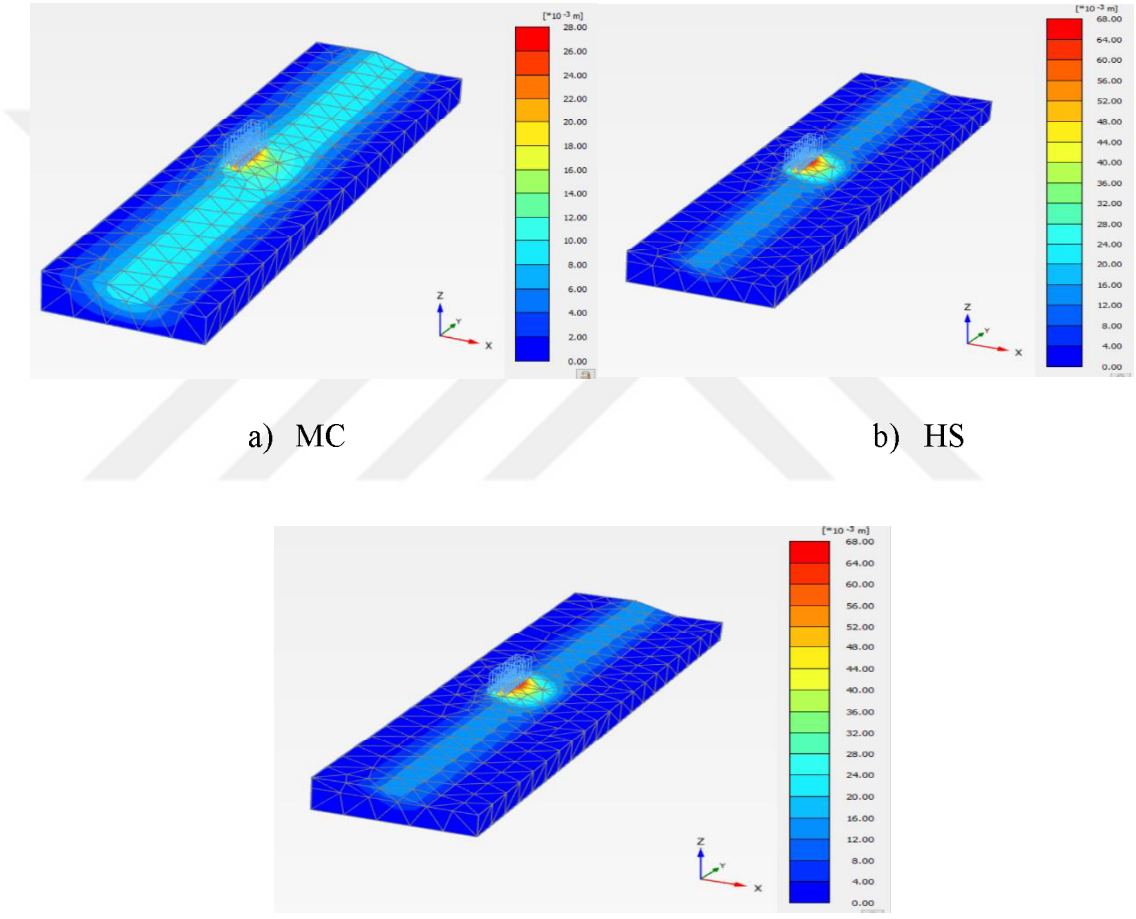
3.2. Analysis Performed Using 3D FEM

As described in previous chapters finite element method (FEM) is a numerical modeling tool in which the problem's geometry is partitioned into a finite number of elements connected by corresponding boundary conditions. Every domain consists of a set of nodes that form a mesh and an area. Displacements are determined using the mesh and the established stress-strain relationships. The rigorousness of the selected constitutive model and the quality of the mesh directly affect the model's accuracy. Slope models were prepared and analyzed using the 2D FEM and 3D FEM software: PLAXIS 2D and PLAXIS 3D, respectively (Brinkgreve *et al.*, 2021). PLAXIS coupled with (SR) technique was utilized to determine the F_S of the slopes analyzed.

Soil strength and unit weight are adequate in analysis performed using LEM to characterize the soil. This is not the case with FEM, and another significant factor influencing the deformations is the choice of soil constitutive model. Hardening small strain model (HSS model) is recommended in PLAXIS for slope stability study (Brinkgreve et al. 2021). HSS model was utilized in this study since it better represents stress-dependent stiffness behavior of soil. Table 3.4 shows the results of the comparative study conducted using Mohr-Coulomb (MC), Hardening Soil (HS) and Hardening Small Strain (HSS) constitutive models. Figure 3.3 shows the deformation analysis results in 3D models presented in Table 3.4.

Table 3.4. Analyses results for different constitutive soil models.

Model	Fs	Node	Crest deformation(m)			Cal. Time (min)
			x	y	z	
MC	1.24	2474	0.013	0.000172	-0.0174	2
HS		2474	0.109196	0.001791	-0.10277	3
HSS		2474	0.048845	0.000852	-0.04325	3



a) MC b) HS

c) HSS

Figure 3.3. Total displacements for different constitutive models in deformation analysis: (a) MC; (b) HS; (c) HSS.

As all methods use SR technique, at the safety stage of the analysis, all three (3) constitutive models provide the same F_S values. However once crest deformations are compared significant differences can be observed at the same node in deformation analysis.

In this study, deformations were also recorded after the application of surcharge load, before the safety analysis. Accordingly, HSS model was utilized.

In the analysis performed with FEM, mesh characteristics play a key role on the results. Mesh coarseness was adjusted, in essence a finer mesh option was used in the vicinity of the loaded area and in the region where possible failure is expected. Figure 3.4 shows area that is has a refined mesh in the models.

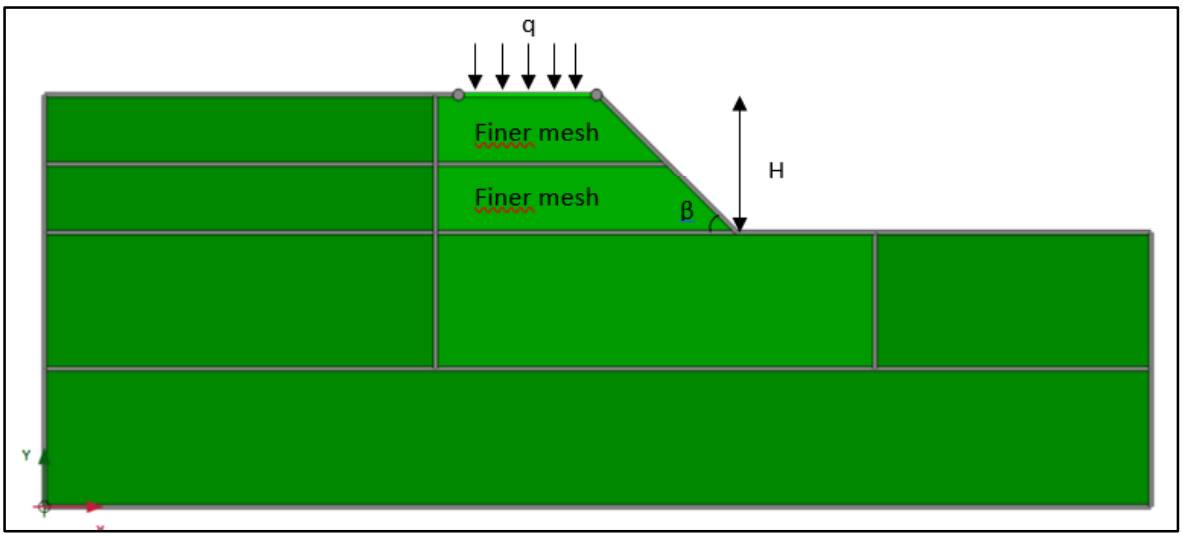
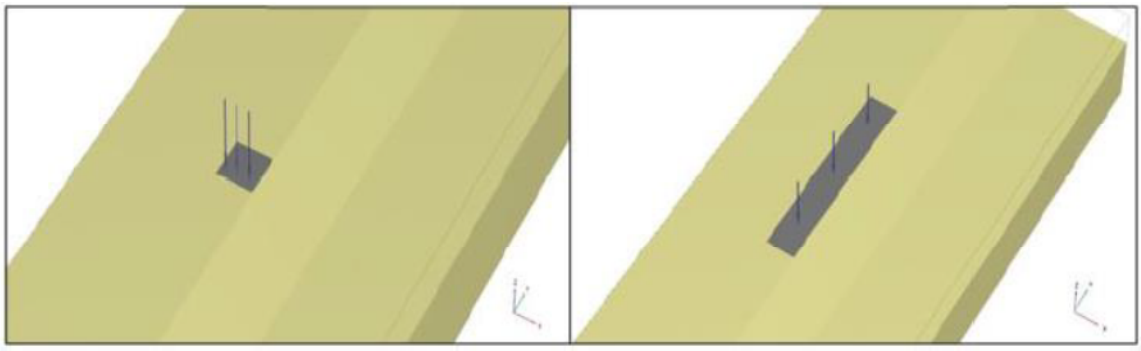


Figure 3.4. Generic cross-section of the loaded slopes.

3.3.Cases Analyzed

The aim of this study is to investigate the short-term stability of clayey slopes under the effect of surcharge loads. Investigation was carried out by changing the surcharge length (L), width (B), and the surcharge magnitude (q). Surcharge length (L) is the long side of the surcharge area that is along the extrusion depth in this case. The length of the short side is denoted by B and it is perpendicular to L. Various L/B ratios were considered. Figure 3.5 shows the surcharge cases of L/B = 1 and L/B = 6, respectively.



(a) L/B=1 (b) L/B=6

Figure 3.5. Typical loading scheme: (a) L/B=1; (b) L/B=6.

For all loaded clayey slopes, LEM analysis was carried out considering short-term conditions and undrained shear strength (S_u). The slope heights of 5, 10, 20, 30, and 40 m; slope angles of 33.7^0,45^0, and 63.4^0; surcharge loads of 100 and 200 kPa and surcharge width-to-length ratios (L/B) of 1, 2, and 6 were analyzed. A total of 180 cases were examined using 2D LEM software, while 540 cases were processed through 3D LEM software. Due to the unreliability of the F_s values derived from the safety analysis, which are less than 1, S_u=25 and S_u=50 kPa cases were not analyzed using FEM. As a result, approximately 120 cases of 2D FEM and 360 cases of 3D FEM analyses were performed. The range of values used in the parametric study of the slopes loaded with surcharge are compiled in Table 3.5.

Table 3.5. The parameter range analyzed in 3D stability of slopes loaded with surcharge.

Surcharge (kPa)	Angle (Deg.)	Height (m)	Surcharge Dimension (L/B Ratio)	S_u (kPa)
100-200	33.7^0,45^0,63.4^0	5,10,20,30,40	1,2,6	25-200

Based on the study by Kelesoglu (2015), the distance of the surcharge loading from the crest point of the slope was taken as 0.5 m. Table 3.6 shows the range of parameters use for the clayey soils and Table 3.7 shows the geometries of the slope models analyzed.

Table 3.6. Range of strength and stiffness parameters for undrained clays used in the analysis.

Material Properties					
S_u (kPa)	E_{50}^{ref} (kN/m^2)	E_{oed}^{ref} (kN/m^2)	E_{ur}^{ref} (kN/m^2)	$\gamma_{0.7}$	G_o (kN/m^2)
25 - 200	6000-48000	6000-48000	18000-144000	0.0003	35000-125000

Table 3.7. Slope geometries used in the analysis.

Model Geometry					
Slope Angle	Slope Height	Slope Angle	Slope Height	Slope Angle	Slope Height
33.7^0	5	45^0	5	63.4^0	5
33.7^0	10	45^0	10	63.4^0	10
33.7^0	20	45^0	20	63.4^0	20
33.7^0	30	45^0	30	63.4^0	30
33.7^0	40	45^0	40	63.4^0	40

4. RESULTS

This chapter presents the results of the parametric slope stability analyses conducted using 3D LEM and 3D FEM within the scope of this thesis. The parametric study included soil slopes with various angles, heights and undrained shear strength parameters. Initially, the cases were analyzed considering the width of the surcharge B is equal to slope height H (i.e., B=H). The length of the surcharge was varied in these analyses using L/B =1, 2 and 6. Additional cases were also analyzed assuming fixed surcharge widths of B = 20 m and B = 30 m, in essence considering B≠H. The results of these analyses were also presented. For these cases, a note indicating that B≠H was placed within the graphs and in the figure captions. The cases presented correspond to B=H unless noted otherwise as B≠H.

The effects of surcharge magnitude and surcharge size were also investigated. The critical failure surfaces and the corresponding F_S values were reported and discussed.

4.1. Effect of Slope Geometry, Soil Strength & Surcharge Magnitude on F_S

Effect of slope model parameters: the slope height (H) and slope angle (β) values on the slope stability analysis results were examined using 3D FEM analyses. Accordingly, slope heights of 5 m, 10 m, 20 m, 30 m, and 40 m and slope angles of 26.57°, 33.69°, 45°, 63.43° degrees were selected for the analysis. These ranges of the two slope model parameters were used together with various strength- and surcharge-related parameters in all combinations. Two approaches were followed for surcharge dimensions. In the first set of analyses, the width of the surcharge load was equal to the height of the slope model (i.e., B = H). A second set of analyses was also performed considering the cases in which the width of the surcharge was not equal to the height of the slope. Accordingly, the analyses were also carried out considering surcharge loads with the fixed widths of B=20 m and B=30 m. In these analyses, the effect of the shape of the surcharge load on the results were also investigated. For this purpose, three different width to length ratios were considered for the surcharge load (L/B=1, B/L=2 and L/B=3).

Figure 4.1, Figure 4.2, and Figure 4.3, present the results (i.e., F_s) of the analysis of the slope models prepared with a fixed surcharge width (B=20 m and B=30 m), using two surcharge magnitudes of 50 kPa and 100 kPa, using three different slope angles (β = 33.69º, 45º, 33.69º), one undrained shear strength value (S_u = 150 kPa), and four different slope heights (H= 10 m, H= 20 m, H = 30 m, and H= 40m), for L/B= 1, L/B=2 and L/B=6, respectively.

As seen in Figure 4.1, when the L/B value is 1, the effect of the surcharge load on the F_s decreases almost diminishes when H≥20 m for 33.69º and 45º slope angles, the data series expressing different surcharge magnitudes and widths, all merge, come close to each other. However, in the case of 63.43º degree slope angle, a slight effect of surcharge is visible when H= 20 m, it disappears when the slope height reaches 30 m. This allows the conclusion that with an increase in the slope angle and a decrease in slope height the effect of the surcharge load on the F_s becomes more noticeable on the slope.

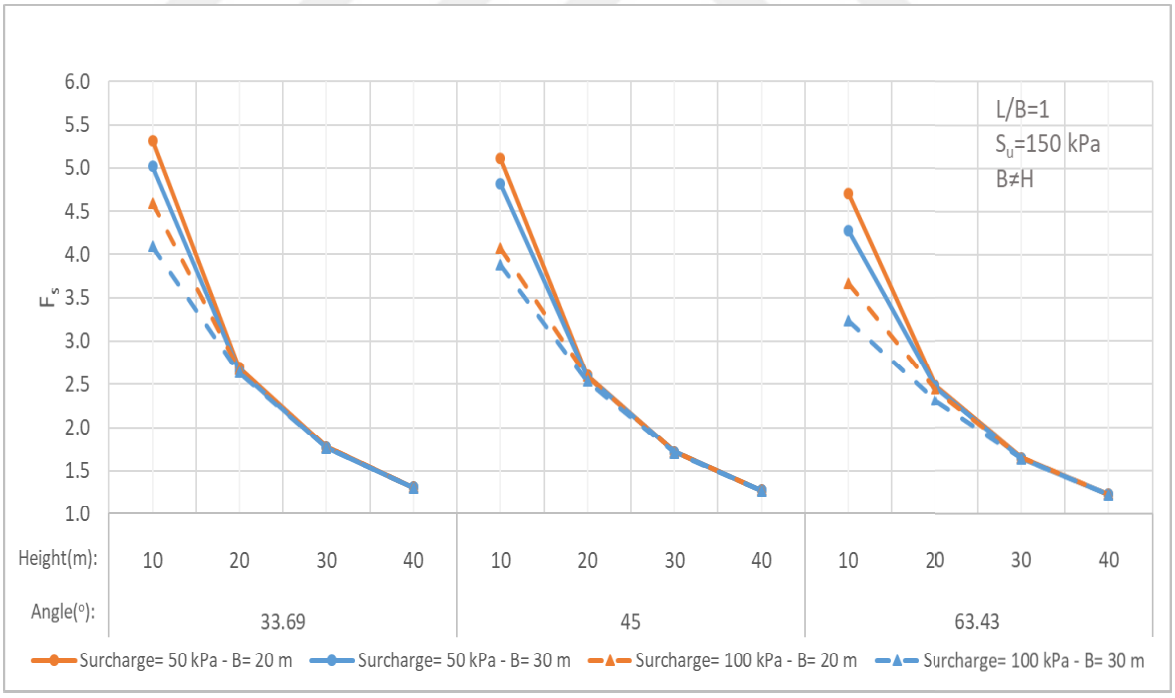


Figure 4.1. Effect of surcharge magnitude and slope height on F_s of slopes (L/B ratio =1; B≠H) using 3D FEM.

Figure 4.2 and Figure 4.3 shows the results of surcharge cases of L/B = 2 and L/B = 6, respectively. In Figure 4.2 (unlike the trend seen in Figure 4.1), surcharge effect is still visible when H= 20 m. Effects of the surcharge load almost disappears when the slope height reaches 30 m for L/B = 2. In the case with β = 63.43° degrees and with the surcharge load of 100 kPa, the effect of the surcharge almost diminishes when H reaches 40 m. However, when the surcharge load is 50 kPa, it is observed that this effect disappears again when the slope height is 20 m. In the case analyzed with the largest surcharge area (i.e., L/B=6) seen in Figure 4.3, when q = is 100 kPa, the surcharge effect disappears at H ≥ 30 m for β = 33.69° and at H ≥ 40 m for β = 45°. For the case of the lower surcharge (i.e., q = 50 kPa), the effect of L/B disappears completely as such, same F_s values were obtained Figure 4.1 and Figure 4.2.

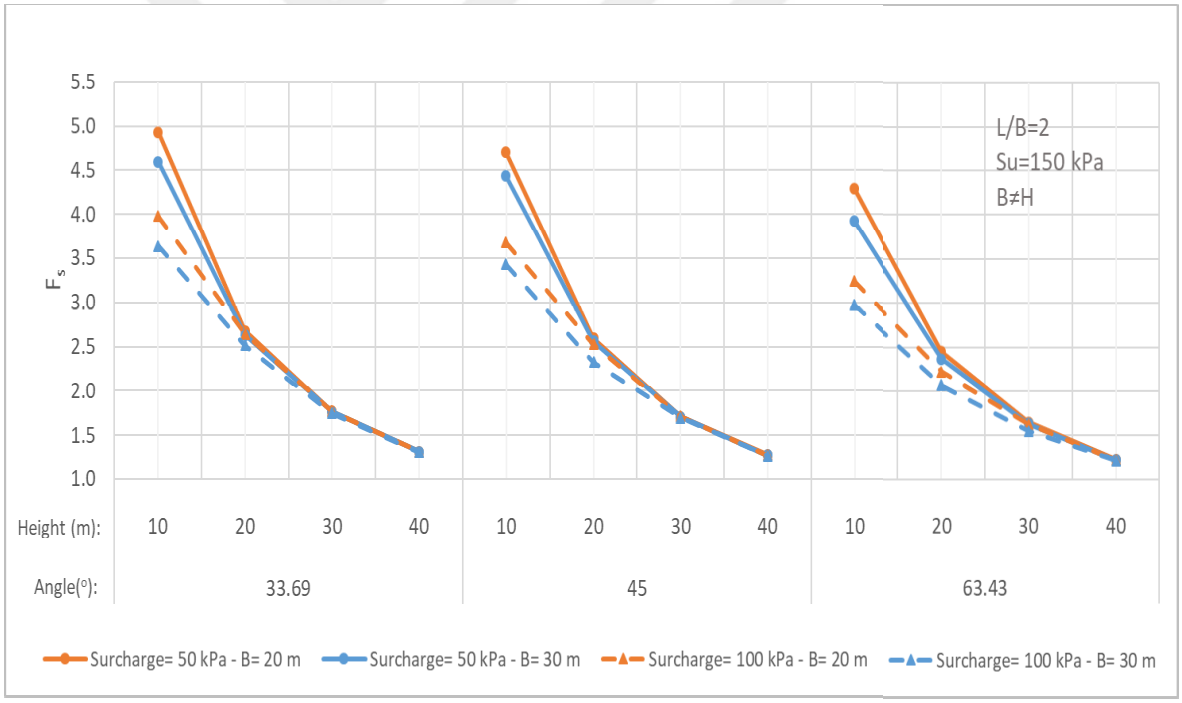


Figure 4.2. Effect of surcharge shape and magnitude on F_s of slopes (L/B ratio= 2; B≠H) using 3D FEM.

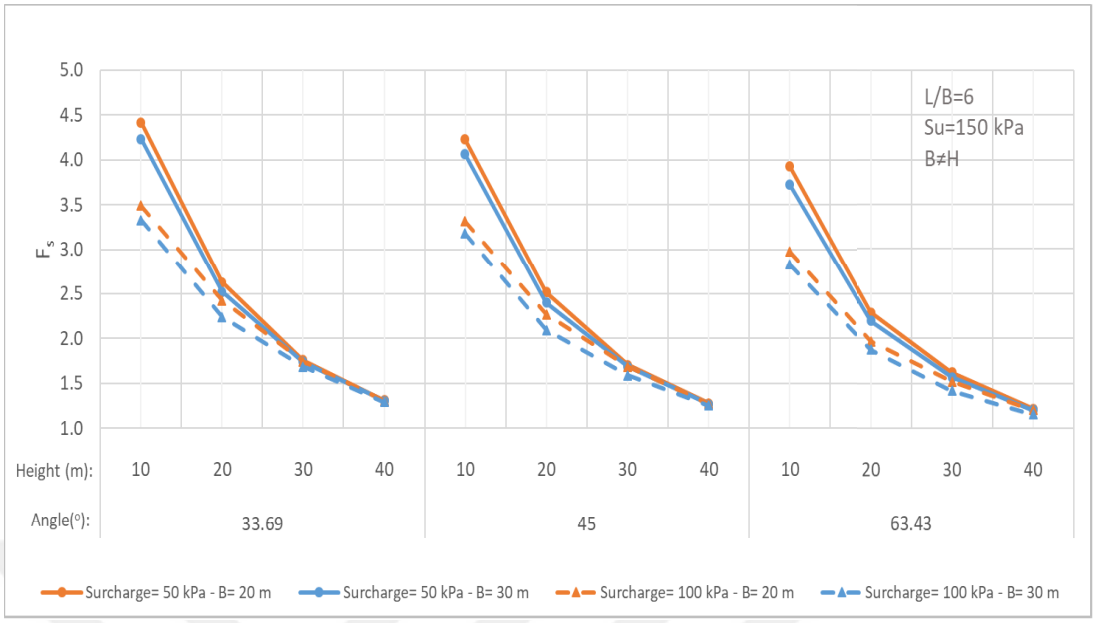


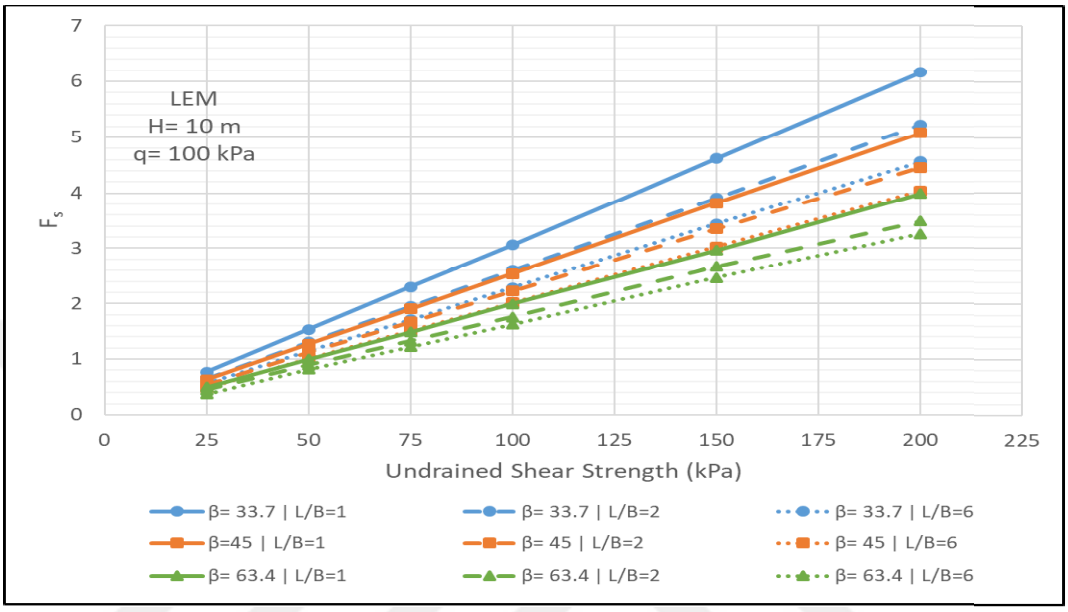
Figure 4.3. Effect of surcharge magnitude and slope height on F_s of slopes (L/B ratio=6; B≠H) using 3D FEM.

These results show that with an increase in L/B ratio, the effect of surcharge on the F_s become more noticeable. Additionally, the effect of L/B ratio is more prevalent in the case of q = 100 kPa compared with the case of q = 50 kPa.

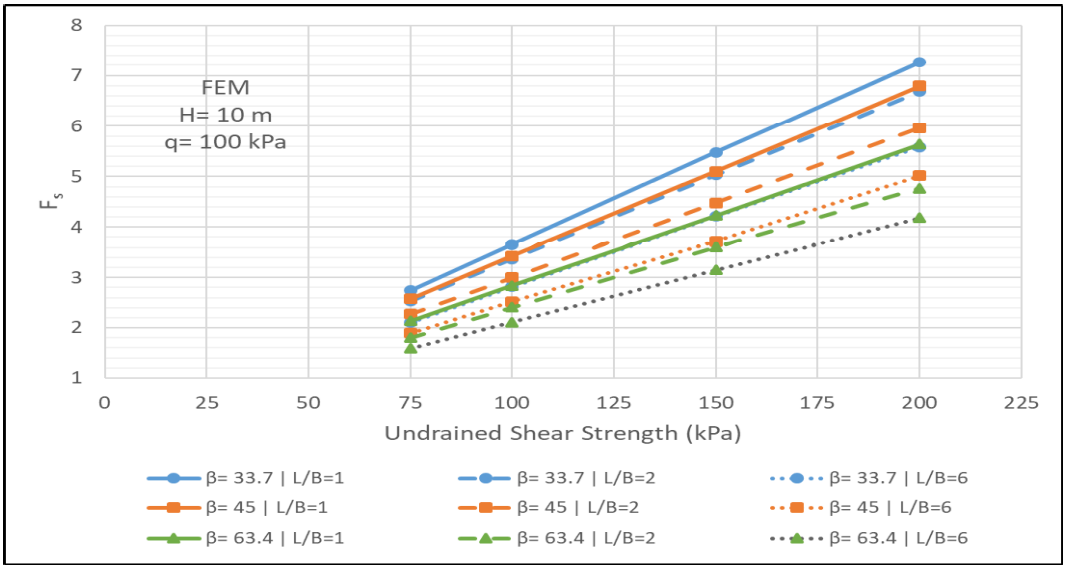
Figures 4.4 and 4.5 present the results (i.e., F_s) of the analysis of the slope models prepared with a surcharge load width equal to the height of the slope model (B=H). S_u versus F_s obtained from 3D LEM and 3D FEM analysis for the slopes with H=10 m & q=100 kPa, and with H=40 m & q=100 for L/B= 1, L/B=2 and L/B=6 and for $\beta = 33.69^o$, 45^o, 63.43^o are shown in Figures 4.4 and 4.5, respectively. As expected, F_s of the slopes increase with an increase in S_u. This increase is almost linear in both 3D LEM and 3D FEM results. The models prepared with the lowest angle: $\beta = 33.7^o$ produced the highest F_s values, and those prepared with the highest angle: $\beta = 63.4^o$ produced the lowest F_s values. Additionally, a decrease in F_s values was observed with an increase in the L/B ratio.

Once the cases with the same parameters are compared in Figures 4.4 and 4.5, it can be seen that the F_s values obtained from the analysis utilizing 3D FEM are larger than those obtained from the analysis performed using 3D LEM. With an increase in slope height, F_s decreases noticeably in both LEM and FEM analysis. As H increases, the effect of both

surcharge magnitude and dimensions also decreases. The F_s of the slope model decline with increasing H, but this decrease is accompanied by an ongoing decrease of the effects of surcharge (q).

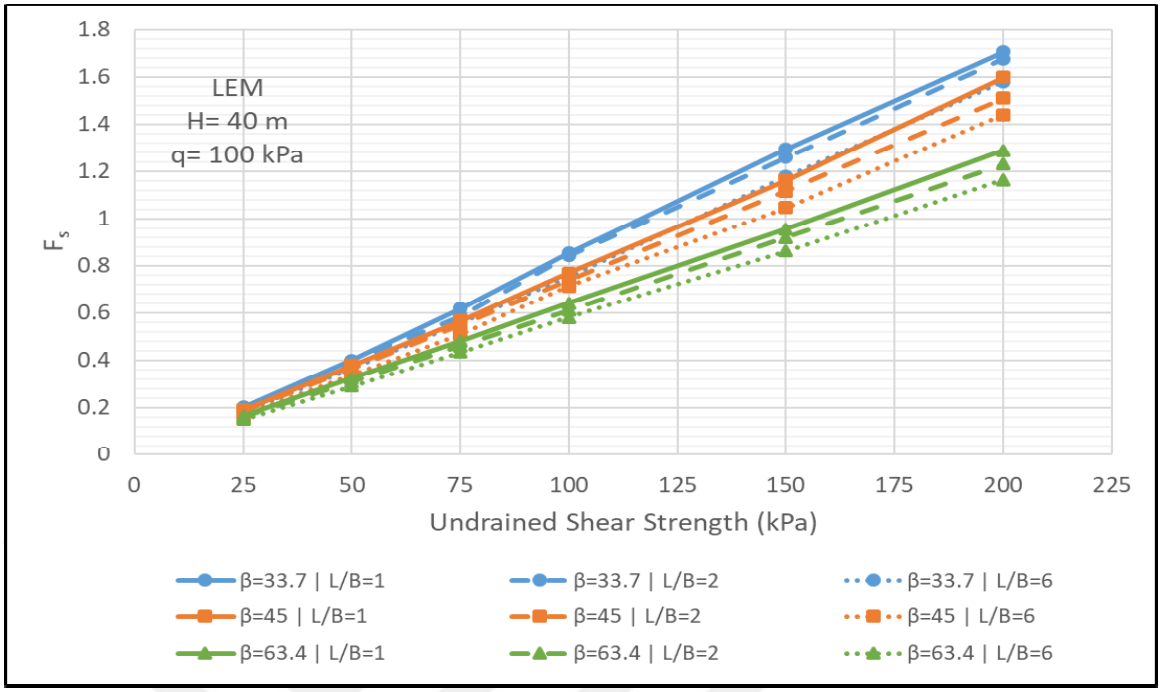


(a) 3D LEM

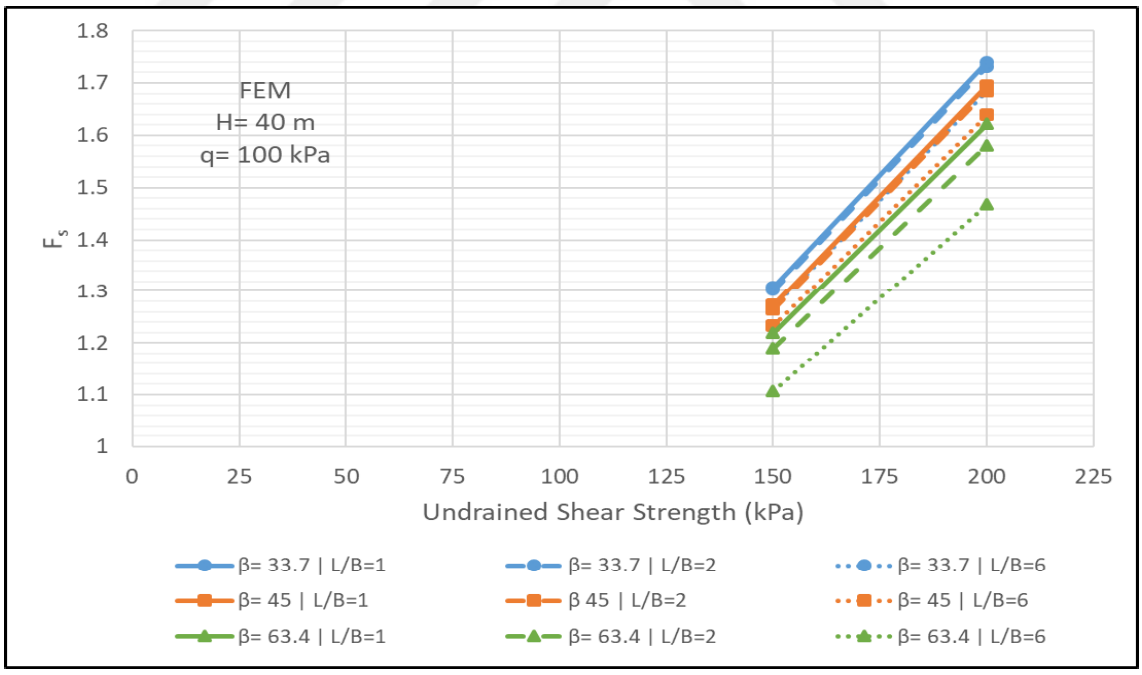


(a) 3D FEM

Figure 4.4. F_s for slope height (H) = 10 m and surcharge (q) = 100 kPa in: (a) 3D LEM, (b) 3D FEM.



(a) 3D LEM



(b) 3D FEM

Figure 4.5. F_s for slope height (H) = 40 m and surcharge (q) = 100 kPa in: (a) 3D LEM, (b) 3D FEM.

Figure 4.6 and Figure 4.7 show the change in H versus % decrease in F_s values for the models with surcharge widths B= 20 m and 30 m, with q= 50 kPa and with L/B =1, 2 and 6, and β= 33.69º, 45º, and 63.39º, respectively. The results show that the highest % reduction in F_s values were observed in the case of L/B=1. The reason for this the case of L/B=1 and q= 50 kPa, the surcharge loading does not have a significant presence on the slope. In other words, since this surcharge magnitude and surcharge area are both low in this case, this loading condition did not have a significant effect on the stability of the slope. Accordingly, higher F_s values were obtained, and therefore the % changes in the F_s were dominated by the self-weight of the slope, rather than the surcharge itself. However, as the L/B ratio increases to 2 and 6, the effect of the surcharge becomes more pronounced on the stability, and hence the surcharge effects on F_s is greater for the larger surcharge area cases. A similar trend is also observed for all.

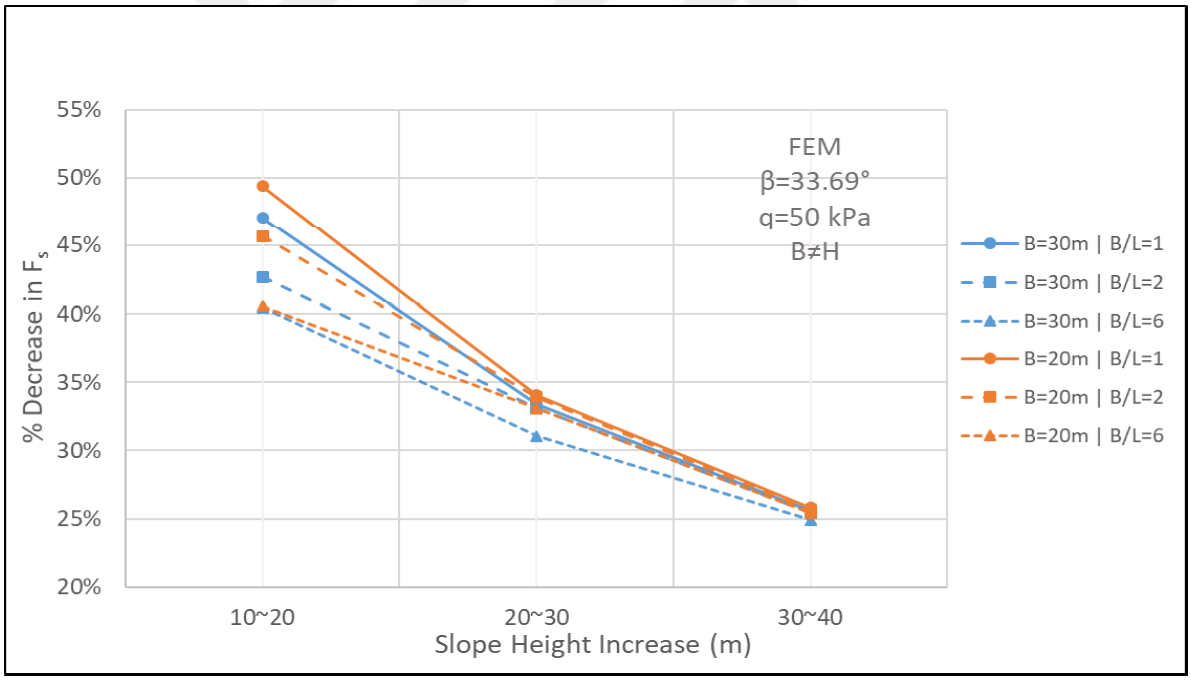
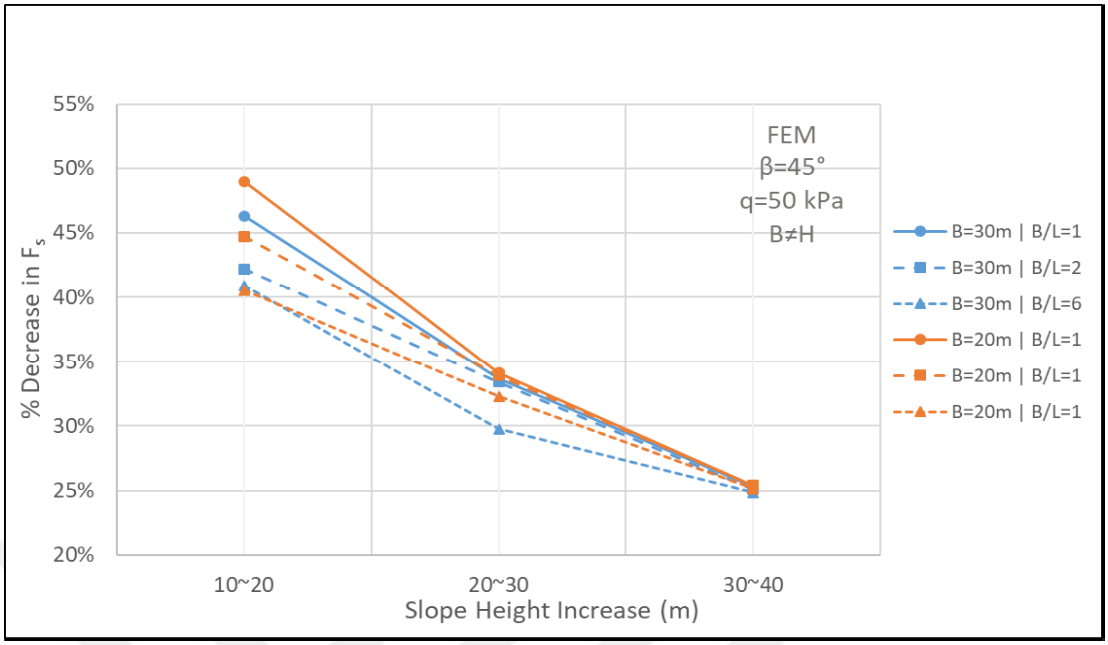
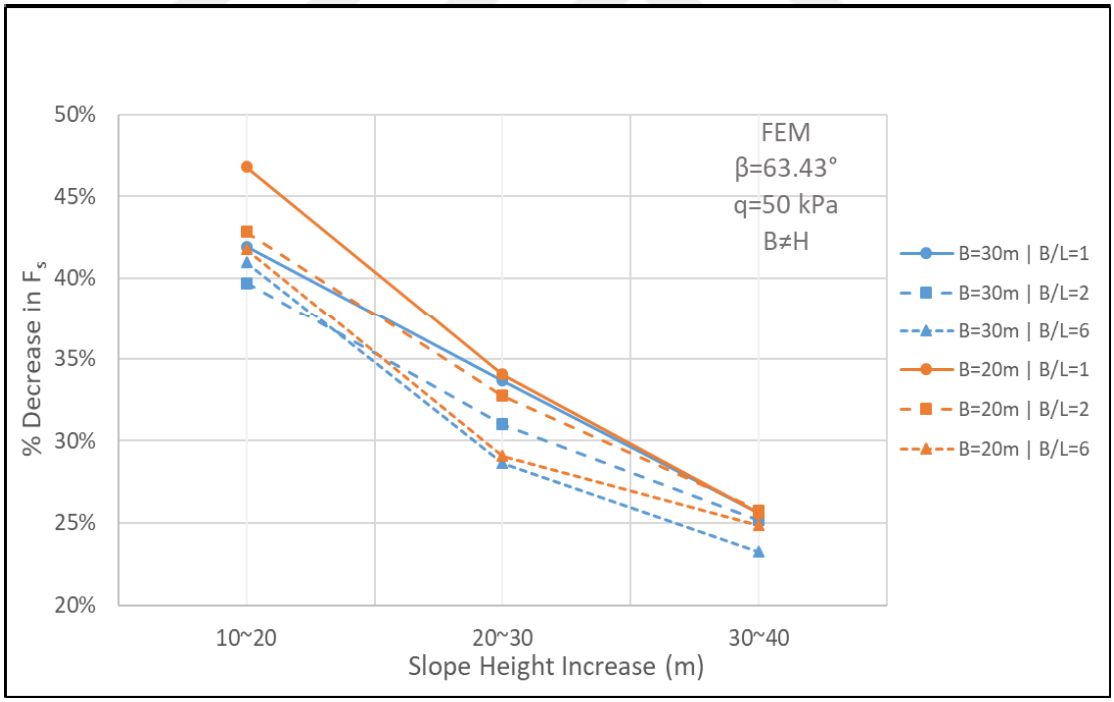


Figure 4.6. Decrease in factor of safety of different slope angles due to the change in H for q= 50 kPa in 3D FEM B≠H β= 33.69º.



(a) Slope angle (β) = 45°



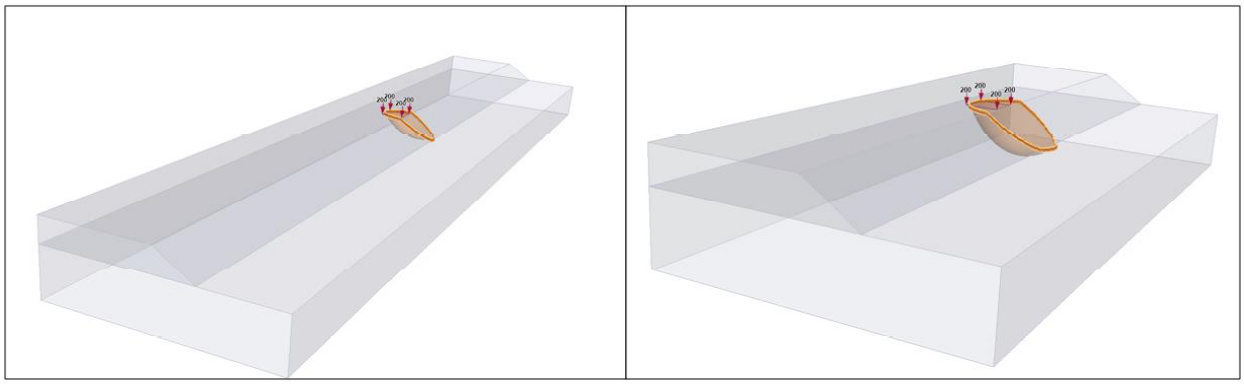
(b) Slope angle (β) = 63.43°

Figure 4.7. Decrease in factor of safety of different slope angles due to the change in H for q= 50 kPa in 3D FEM B≠H cases: (a) β= 45°; (b) β=63.43°.

4.2. Effect of Slope Geometry, Surcharge Magnitude and Shape on 3D Failure Surfaces

The weight of a potential sliding mass increases with depth, but strength does not, hence the critical slip surface for a homogenous clayey soil is likely to be deep. The only exception to this rule is steep clay slopes (such as those demonstrated by the study of Taylor in 1948) for slopes exceeding 53° degrees, in which case the critical slip surface would pass through the slope's toe (Salgado, 2022). In cases of $\beta > 53^{o}$ a toe circle failure surface is generally obtained. However, the failure shapes change with the presence of a surcharge load. In general, the slip surfaces obtained from FEM and LEM analyses of clayey slopes indicated deep-seated circular type failure surfaces in this study.

The failure surfaces obtained from LEM analysis for various slope heights (e.g., H= 10 m, 20 m, and 40 m) are shown in Figure 4.8 and Figure 4.9 for the following conditions: $\beta = 33.7^{o}$, q = 200 kPa, and L/B = 1. The results show that the failure surface is located just below the surcharge for H= 20 m and 30 m. It is important to note that the width of the failure surface widens as its slope height increases. For H=20 m and 30 m, toe failures were observed. For H= 40 meters, even for a high surcharge load of q = 200 kPa, it appears that the weight of the slope itself, rather than the surcharge, is dominant in the failure surface generated.



(a) H= 20 m (b) H= 30 m

Figure 4.8. Failure surfaces obtained from 3D LEM analysis of slopes of $\beta = 33.7^{o}$ slopes loaded with q=200 kPa and L/B = 1: (a) H=20 m (b) H=30 m.

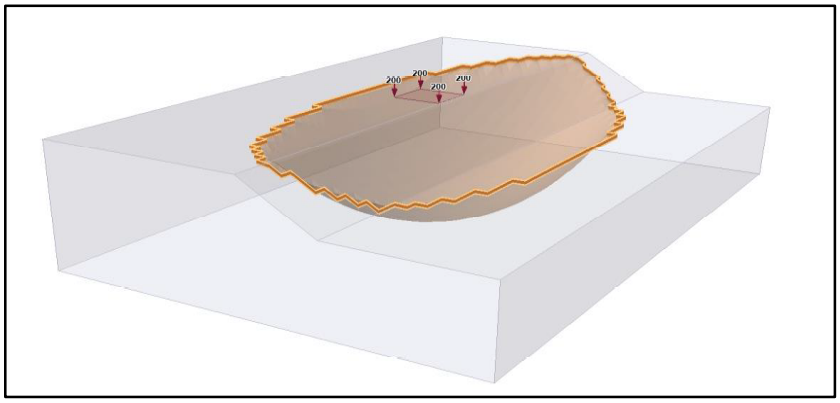
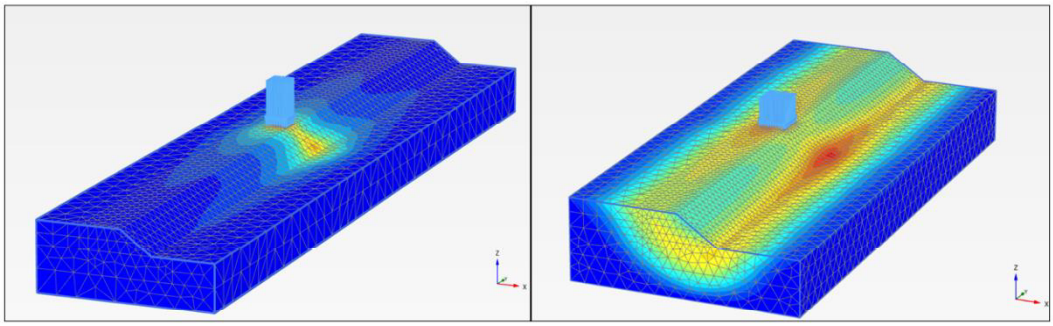


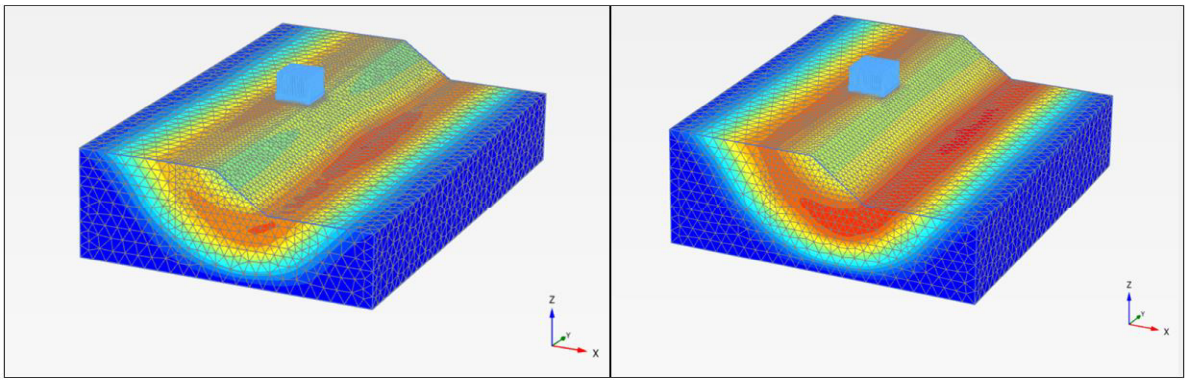
Figure 4.9. Failure surfaces obtained from 3D LEM analysis of slopes of β= 33.7° slopes loaded with q=200 kPa and L/B = 1 for H=40 m.

Figure 4.10 and Figure 4.11 displays the failure surfaces obtained from 3D FEM analysis of 33.7° slopes with heights ranging from 10 to 40 m, under a surcharge load of 100 kPa with an L/B=1. The shape an extend of failure surfaces support the F_s values calculated for these slopes. Figure 4.10a shows a localized failure surface below the surcharge load in the case with a slope height of 10 meters. The influence of the surcharge load on the failure shape gradually disappears with an increase in height as can be seen in the case of slopes with heights of 20 m, 30 m, and 40 m. This shows that rather than the surcharge load itself, the own weight of the higher slopes affects the failure surface. For this reason, the failure surface shape resembles the plane strain condition for these slopes, as such a 2D failure was observed.



(a) 10 m (b) 20 m

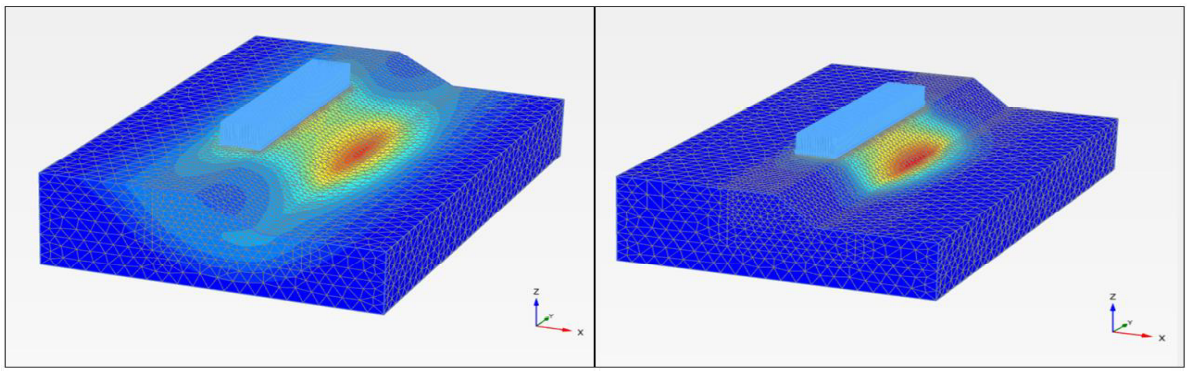
Figure 4.10. Failure surfaces obtained from 3D FEM analysis of slopes of β= 33.7°, loaded with q=100 kPa and L/B=1: (a) H=10 m; (b) H=20 m.



(a) 30 m (b) 40 m

Figure 4.11. Failure surfaces obtained from 3D FEM analysis of slopes of β= 33.7°, loaded with q=100 kPa and L/B=1: (a) H=30 m; (b) H=40 m.

The failure surfaces obtained from 3D FEM analysis of slopes with β= 33.7°, 45°, 63.4° under a surcharge load of 100 kPa with an L/B= 6 and a slope height of 30 meters are shown in Figure 4.12 and Figure 4.13. The observed failure surfaces vary with slope angle even though all are subjected to a surcharge load of same magnitude and area. For the case of a 33.7°, slope the surface is similar to those obtained in 2D analysis. On the other hand, a 3D failure surface, located under the surcharge load, is obtained when the slope angle is 63.4°. This shows that as the slope becomes steeper, the effect of surcharge becomes more dominant on the failure shape and the occurrence of 3D failure surfaces is likely. This result highlights that conducting a 3D analysis, becomes more important with increasing slope angle.



(a) β=33.7° (b) β=45°

Figure 4.12. Failure surfaces obtained from 3D FEM analysis of slopes of H=30 m loaded with q=100 kPa and L/B=6: (a) β=33.7°, (b) β=45°.

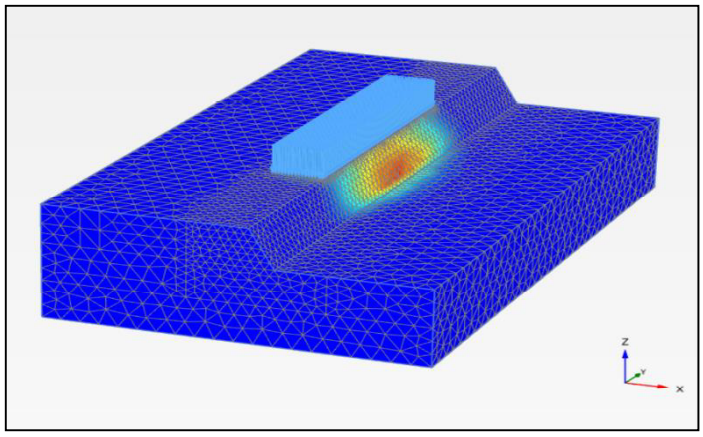
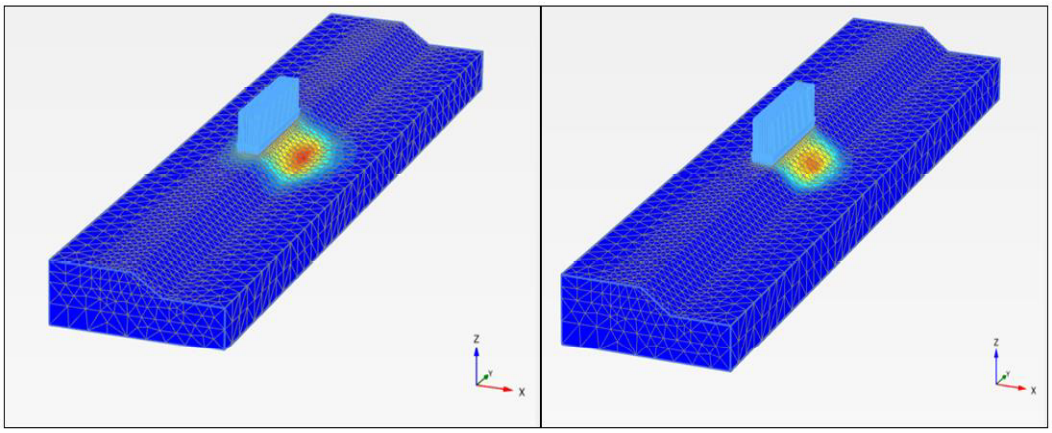


Figure 4.13. Failure surfaces obtained from 3D FEM analysis of slopes of H=30 m loaded with q=100 kPa and L/B=6 for β=63.4°.

Figure 4.14 and Figure 4.15 shows the failure surfaces obtained from 3D FEM analysis of 33.7° slopes of 10 m height loaded with a surcharge shape with L/B =6 and with magnitudes of 50, 100 and 200 kPa. In the case of 50 kPa surcharge load, the lowest surcharge case investigated, the origin of the failure surface extends beyond the toe and spreads out to be longer than the length of the surcharge load. However, when the surcharge load is 100 kPa, a clear toe failure is observed. When the surcharge load is further increased to 200 kPa, the failure type evolves to a bearing capacity failure.



(a) 50 kPa (b) 100 kPa

Figure 4.14. Failure surfaces obtained from 3D FEM analysis of 33.7° slopes with H=10 m, loaded with a surcharge L/B=6: (a) q=50 kPa, (b) q=100 kPa.

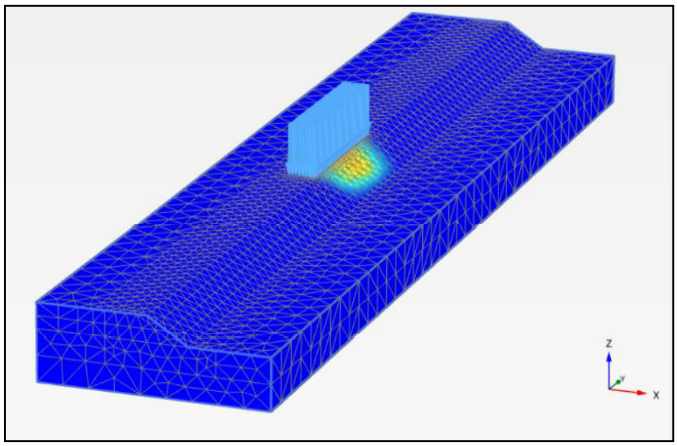
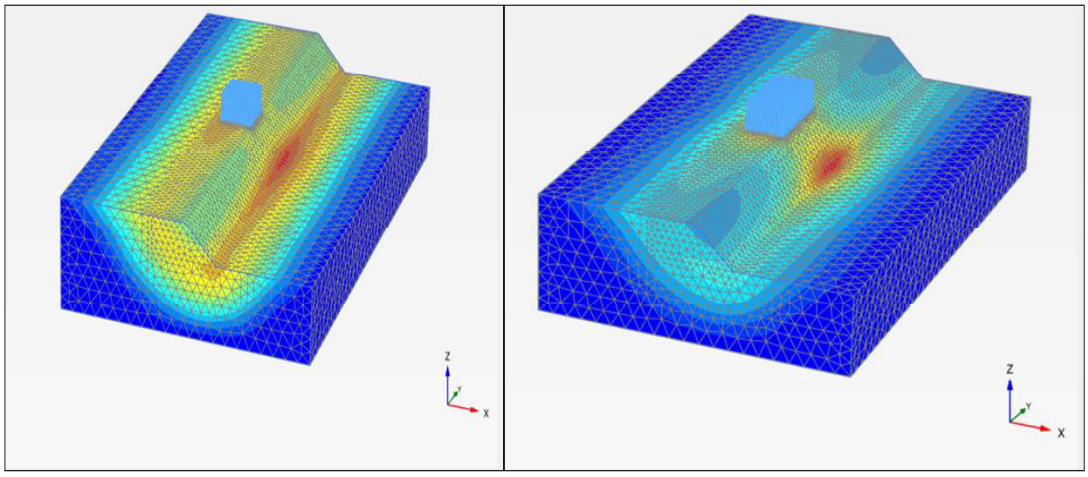


Figure 4.15. Failure surfaces obtained from 3D FEM analysis of 33.7^{o} slopes with H=10 m, loaded with a surcharge L/B=6 for q=200 kPa.

Figure 4.16 and Figure 4.17 shows the failure surfaces obtained from 3D FEM analysis of 33.7^{o} slopes with a height of 10 meters loaded with a surcharge load of 100 kPa with L/B = 1, 2, and 6. In the case of L/B=1, the 3D effects of surcharge load is not visible and a 2D failure mechanism is observed. With an increase in the L/B ratio, the failure shape becomes more localized and moves closer to the surcharge load. In the case of L/B ratio= 6, a clear 3D failure mechanism is observed.



(a) L/B=1 (b) L/B=2

Figure 4.16. Failure surfaces obtained from 3D FEM analysis with H=30 m, β=33.7^{o} and load with surcharge load of q=100 kPa cases: (a) L/B=1, (b) L/B=2.

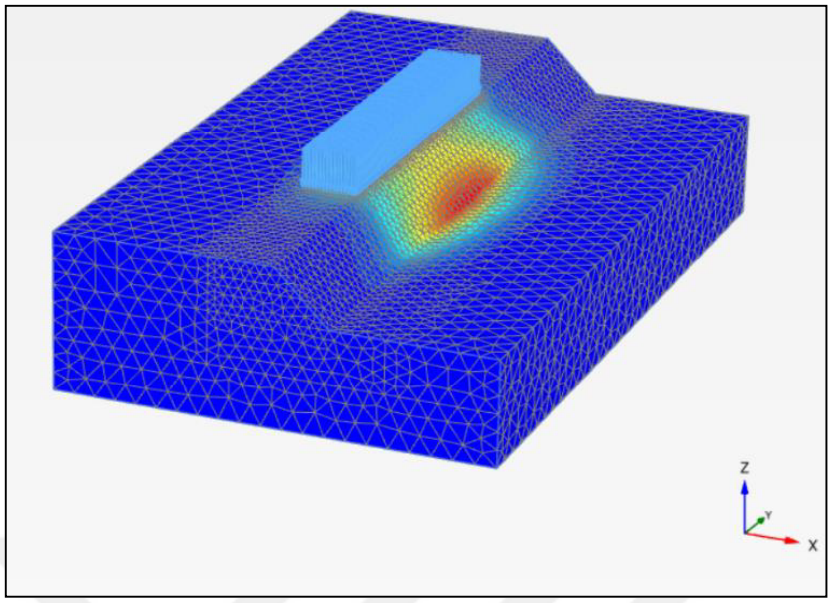
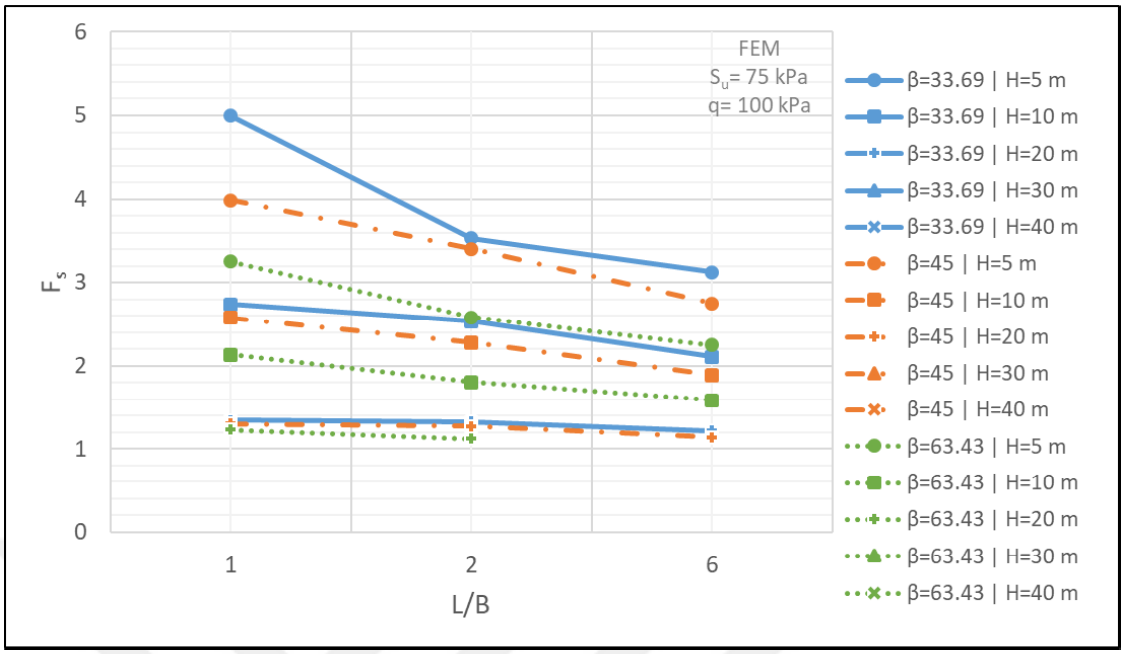


Figure 4.17. Failure surfaces obtained from 3D FEM analysis with H=30 m, β=33.7^{o} and load with surcharge load of q=100 kPa for L/B=6.

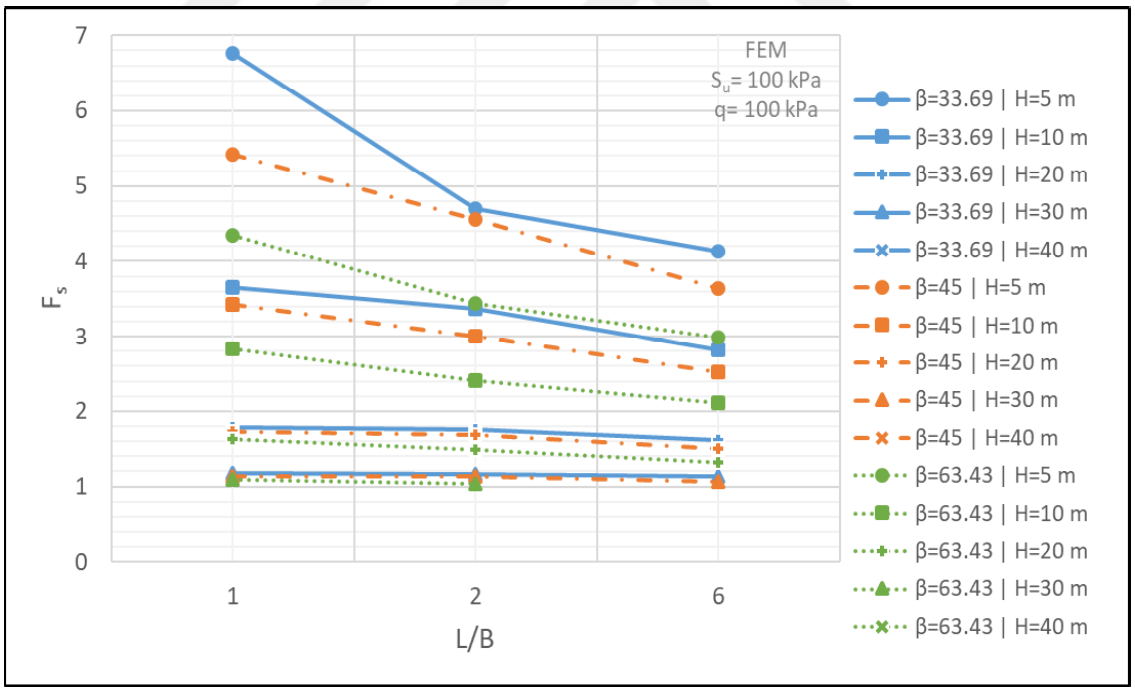
The failure shapes obtained from the 3D analysis of slopes also indicate that, 3D FEM analysis may provide more realistic failure mechanisms compared to those obtained from 3D LEM. This may be due to the shortcomings of the surface search techniques employed in 3D LEM software.

4.3. Effect of Surcharge Shape on 3D Slope Stability

The effect of soil parameters on F_s and critical failure surface are presented in this section for different slope geometries. Figure 4.18 and Figure 4.19 shows the results of F_s values obtained from the 3D FEM analysis of 33.69^{o}, 45^{o} and 63.43^{o} slope models with 5 m, 10 m, 20 m, 30 m and 40 m height, loaded with a surcharge load of 100 kPa with various L/B ratios. Figure 4.18 (a), (b) and Figure 4.19 (a) show L/B versus F_s values for S_u= 75 kPa, 100 kPa, 150 kPa and 200 kPa, respectively. With an increase in S_u of the clayey soil, F_s increases and the general trends of the series are similar to each other as expected. With an increase in L/B ratio, the F_s decreases. The decrease in F_s is more dominant for H = 5m and H = 10 m cases, as in these cases effects of surcharge is more dominant.

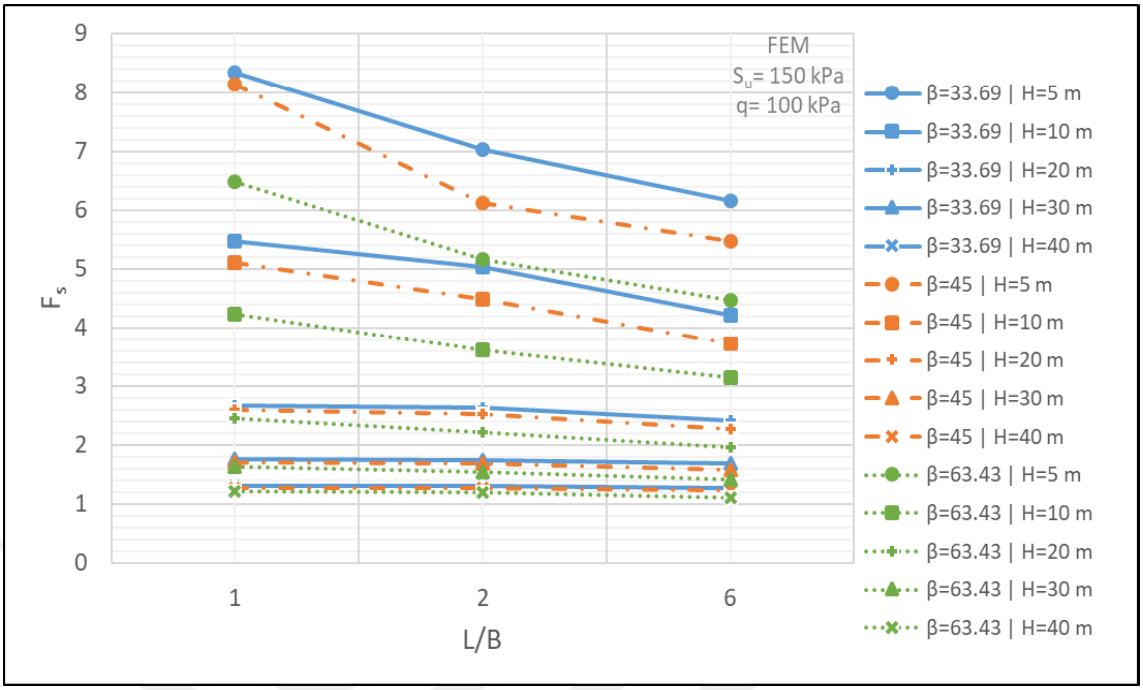


(a) S_u= 75 kPa

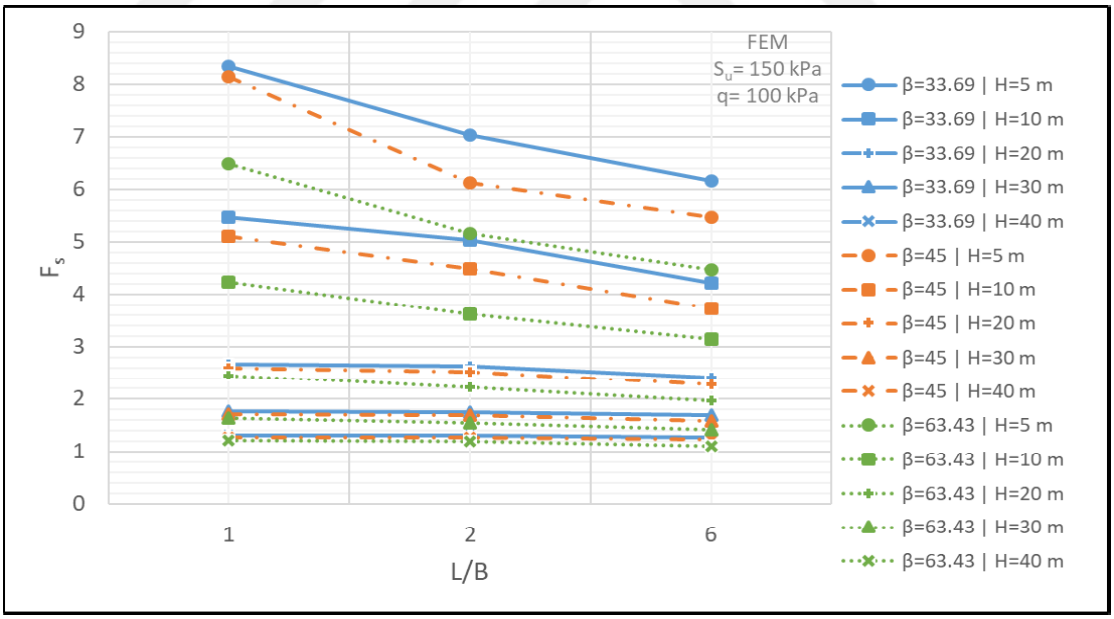


(b) S_u= 100 kPa

Figure 4.18. Surcharge load L/B ratio versus F_s obtained from 3D FEM analysis of slopes loaded with q=100 kPa: (a) S_u= 75 kPa; (b) S_u=100 kPa.



(a) S_u= 150 kPa

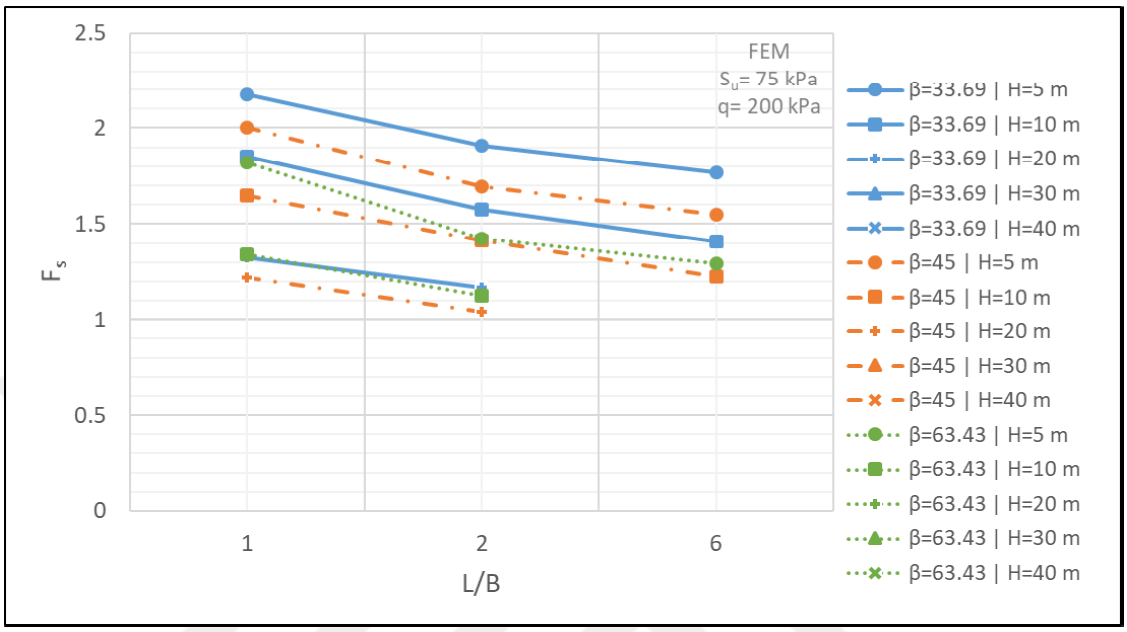


(b) S_u= 200kPa

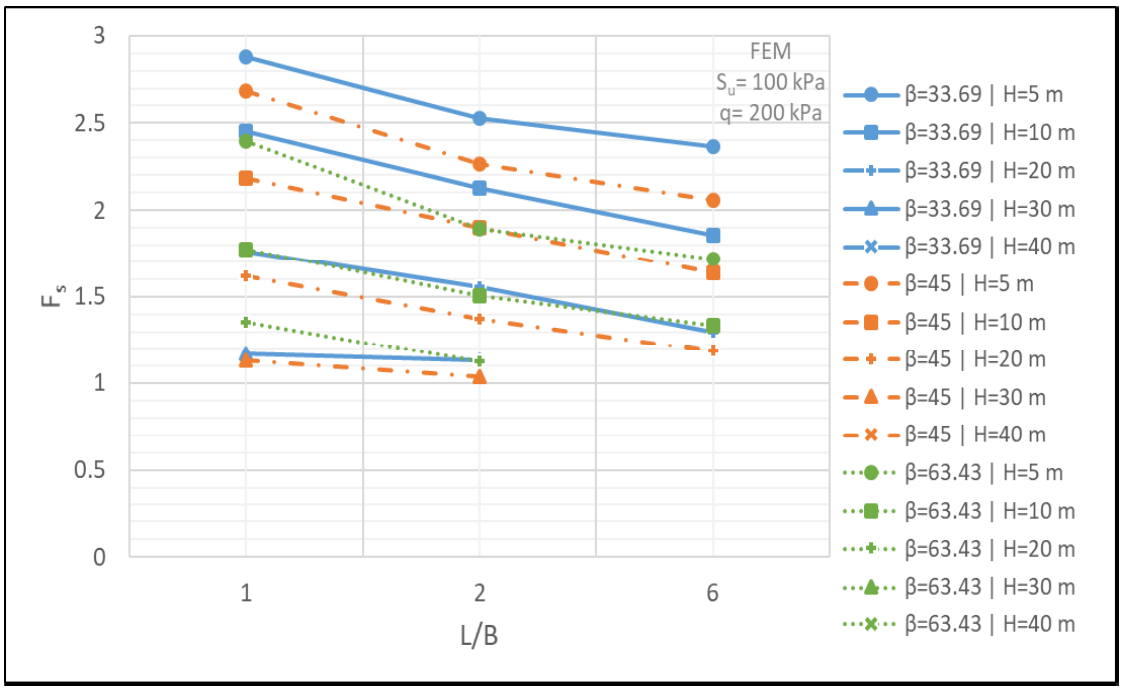
Figure 4.19. Surcharge load L/B ratio versus F_s obtained from 3D FEM analysis of slopes loaded with q=100 kPa: (a) S_u=150 kPa; (b) S_u =200 kPa.

Surcharge L/B ratio versus F_s obtained from 3D FEM analysis of slopes loaded with q=200 kPa, are shown in Figure 4.20 and Figure 4.21. In Figure 4.20 and Figure 4.21, a

similar trend was observed with the case of q=100 kPa; F_s values increase as S_u increases. However, with an increase in surcharge magnitude generally lower F_s values were obtained.

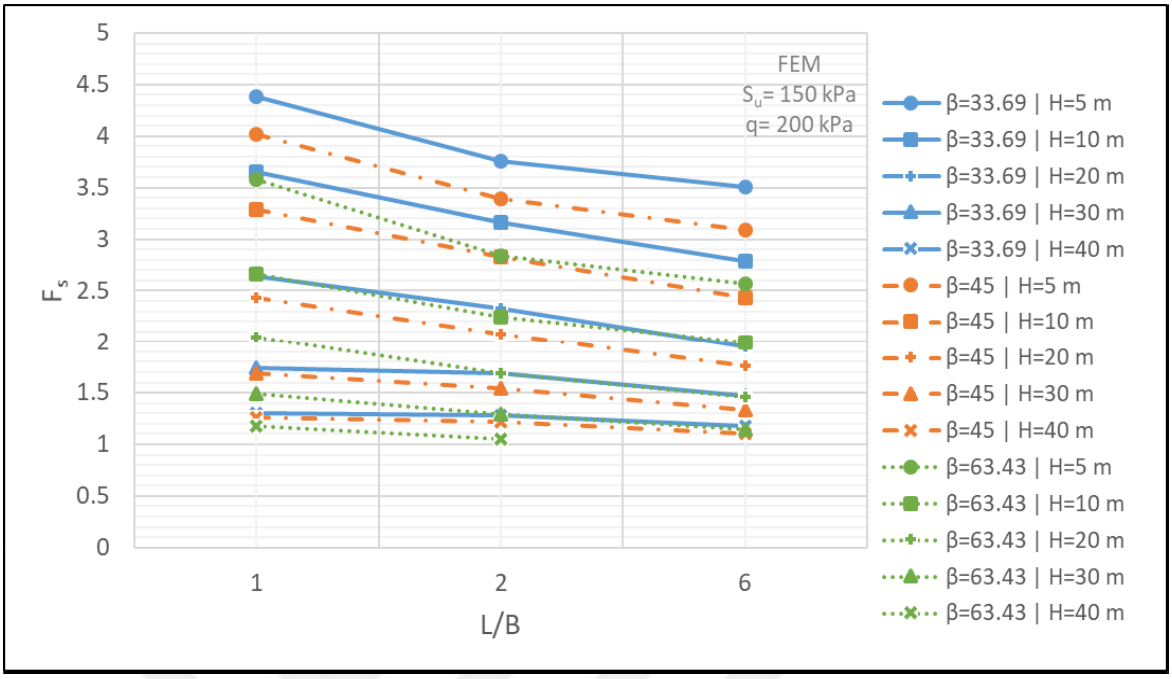


(a) S_u= 75 kPa

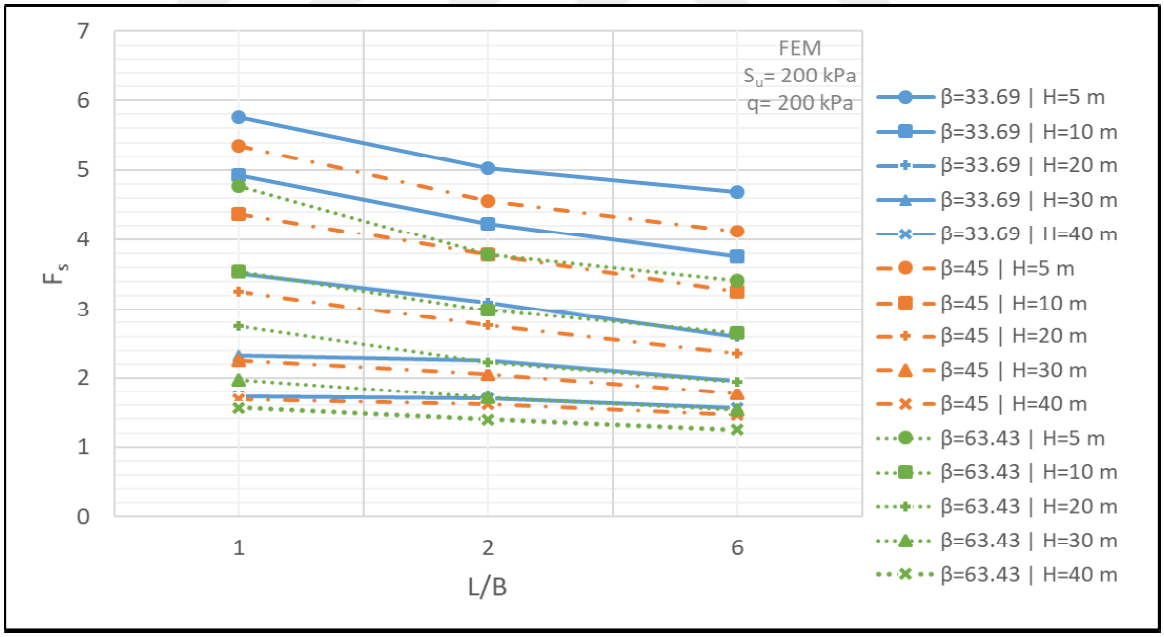


(b) S_u= 100 kPa

Figure 4.20. Surcharge load L/B ratio versus F_s obtained from 3D FEM analysis of slopes loaded with q=200 kPa: (a) S_u= 75 kPa; (b) S_u=100 kPa.



(a) S_u= 150 kPa



(b) S_u= 200 kPa

Figure 4.21. Surcharge load L/B ratio versus F_s obtained from 3D FEM analysis of slopes loaded with q=200 kPa: (a) S_u=150 kPa; (b) S_u =200 kPa.

The total displacements at the crest and the toe, obtained from the 3D FEM analysis of the slope model with a height of 30 m, with β=45°, S_u = 150 kPa, and loaded with q =100 kPa, and B=H are given in Table 4.1.

Table 4.1. Total Crest and Toe Displacements for S_u=150 kPa & q=100 kPa & β=45° in FEM.

	L/B	$U_{X\,CREST}$ (m)	$U_{X,TOE}$ (m)
B=H	1	$9.088*10^{-3}$	$6.007*10^{-3}$
B=H	2	$17.551*10^{-3}$	$14.882*10^{-3}$
B=H	6	$33.526*10^{-3}$	$38.827*10^{-3}$

The displacements obtained for the crest show that as the L/B ratio increases, the total displacements increase. In other words, as the surcharge effect increases, the deformations also increase. The toe displacements were also investigated. Just like the crest displacements, as the L/B ratio increases toe displacements also increase. While the toe displacement value in the X direction was $6.007x10^{-3}$ m (the lowest) for L/B = 1 case, for L/B =6 the toe displacement reached $38.827x10^{-3}$ m. In other words, when L/B increased by 6 times, the displacements also increased by approximately 6 folds. For the slope with a symmetrical loading and model, only the deformation value in the X direction was taken into account. Figure 4.22 shows the deformation contours for the slope model with a height of 30m, with β=45°, S_u=150 kPa and loaded with q=100 kPa, and B=H analyzed with 3D FEM.

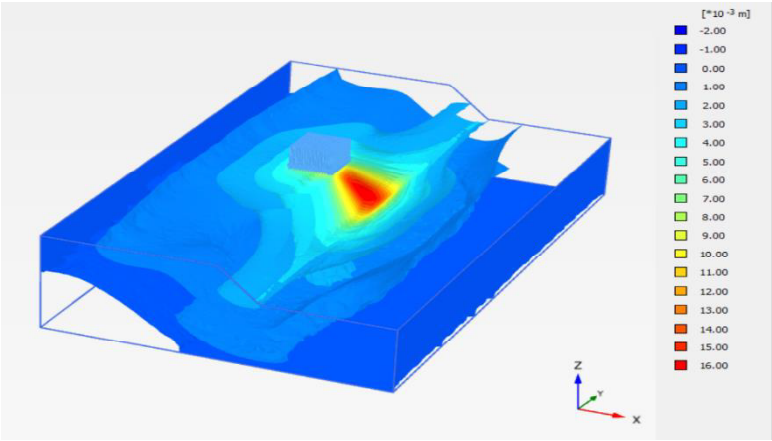


Figure 4.22. Deformation contours of slope with β=45° and q=100 kPa and S_u=150 kPa.

4.4.Comparison of the Results of the Analyses Performed Using 3D LEM and 3D FEM

In order to investigate the differences between the results obtained from the analyses performed using 3D FEM and 3D LEM, surcharge L/B versus the ratio of the F_s from 3D FEM to 3D LEM ($F_{s,3DFEM}/F_{s,3DLEM}$) are presented in this section. Figure 4.23 shows the ratio of the F_s obtained from the analysis performed using 3D FEM ($F_{s,3DFEM}$) compared with 3D LEM($F_{s,3DLEM}$) for the slope model with slope heights of 5 m, 10 m, 20 m, 30 m and 40 m, with S_u =75 kPa loaded with 100 kPa and 200 kPa surcharge loading for L/B =1, 2 and 6. The highest ratio obtained as 1.56 for a 5 m high slope loaded with 100 kPa with L/B = 1. The lowest ratio was obtained as 1.08 for a 20 m high slope loaded with 100 kPa with L/B ratio was 1. Generally, Figure 4.23 shows that largest percentage increases were observed for slope heights of 5 m and 10 m when the surcharge load is 100 kPa. However, for a 20 m slope, the ratios are greater for the surcharge 200 kPa.

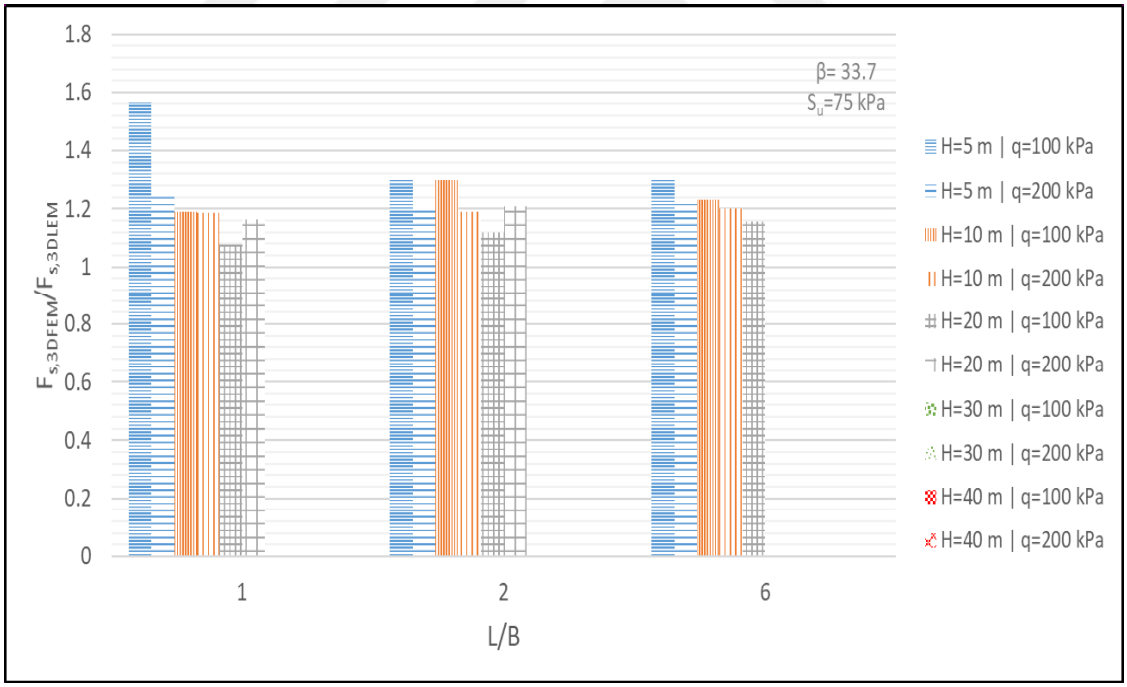


Figure 4.23. Surcharge L/B versus ratio of F_s obtained from the analyses performed using 3D FEM to 3D LEM for slopes with H =5 m, 10m, 20 m and 40m and β=33.7° and S_u =75 kPa.

Figure 4.24, shows the surcharge L/B versus ratio of F_s obtained from the analyses performed using 3D FEM to 3D LEM for slopes with H = 5 m, 10 m, 20 m and 40m and

β=33.7°, with S_u = 100 kPa. Similar to Figure 4.23, the largest ratio is attained as 1.56 for case with the L/B ratio is 1, the slope height is 5 m and the surcharge load is 100 kPa. The lowest ratio was obtained as 1.04 for the case of L/B = 1, the slope height = 30 m and q = 100 kPa. As a general trend, the ratio of F_s obtained from 3D FEM and 3D LEM ($F_{s,3DFEM}/F_{s,3DLEM}$) decreases as the L/B ratio increases. Similar to the trend seen in Figure 4.23, larger ratios were observed for the cases with the surcharge load of 200 kPa, for slope heights exceeding 20 m.

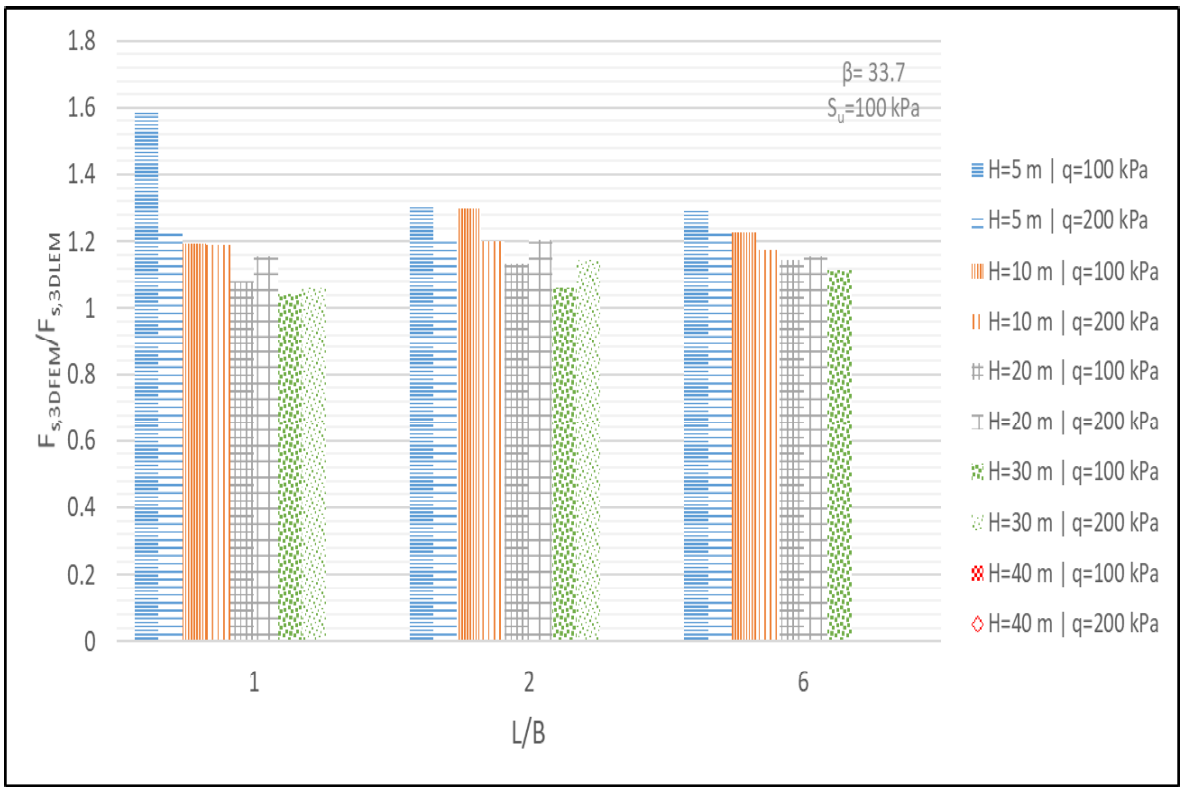


Figure 4.24. Surcharge L/B versus ratio of F_s obtained from the analyses performed using 3D FEM to 3D LEM for slopes with H =5 m, 10 m, 20 m and 40m and β=33.7° and S_u =100 kPa.

Figure 4.25 shows the surcharge L/B versus ratio of F_s obtained from the analyses performed using 3D FEM to 3D LEM for slopes with H =5 m, 10 m, 20 m and 40m and β=33.7° and S_u =200 kPa. Trends were similar to those obtained for S_u = 75 kPa and S_u = 100 kPa. Generally, the $F_{s,3DFEM}/F_{s,3DLEM}$ ratio decreases as the L/B value decreases. Similarly, $F_{s,3DFEM}/F_{s,3DLEM}$ ratio also decrease as slope height increases as the effect of surcharge decreases and self-weight starts dominating the results. However, the increase in

the surcharge load does not give similar results for each slope height. The $F_{s,3DFEM}/F_{s,3DLEM}$ are higher for 5m and 10m slope heights at 100 kPa for all shear strength values investigated. For higher slopes (i.e., h= 20 m, 30 m and 40 m) higher ratios were obtained for 200 kPa surcharge cases.

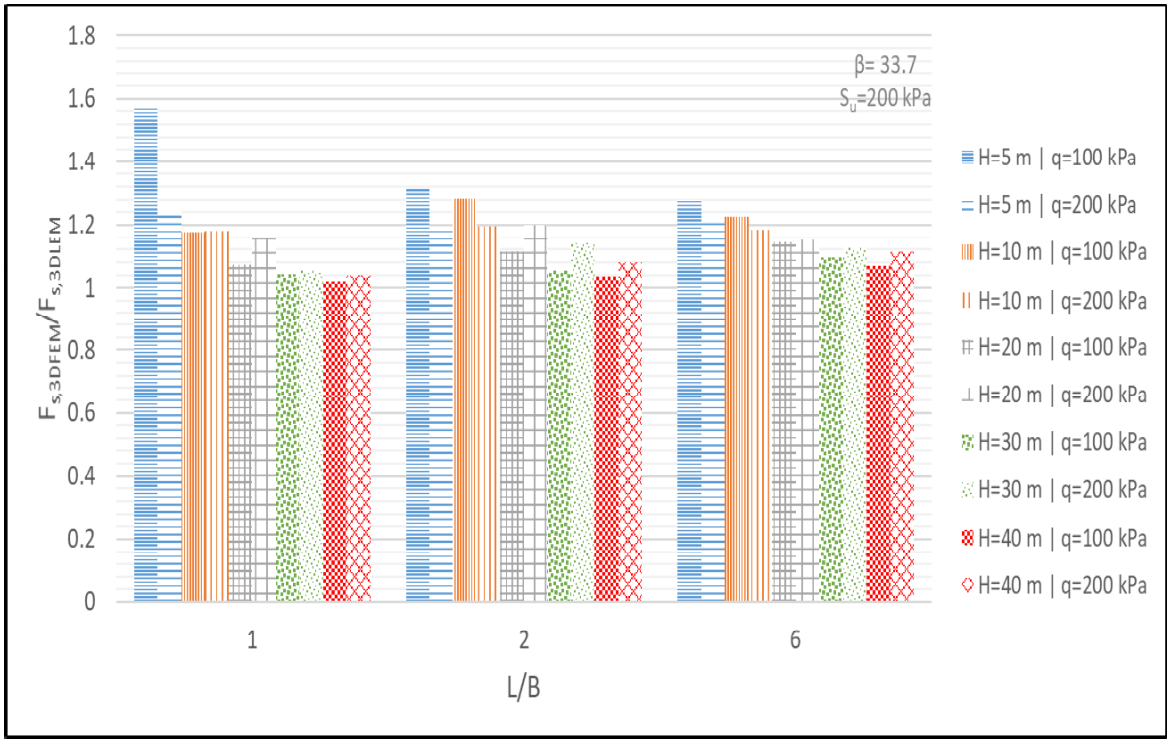


Figure 4.25. Surcharge L/B versus ratio of F_s obtained from the analyses performed using 3D FEM to 3D LEM for slopes with H =5 m, 10 m, 20 m and 40 m and β=33.7° and S_u =200 kPa.

The same studies were performed for the models with slope angles: 45° and 63.43°. Figure 4.26, Figure 4.27 and Figure 4.28 show the surcharge L/B versus ratio of F_s obtained from the analyses performed using 3D FEM to 3D LEM for slopes with H =5 m, 10 m, 20 m and 40m and β=45°, for S_u =75 kPa, 100 kPa and 200 kPa, respectively. Generally, the analysis performed on a 45° slope shows similar trends with those obtained for a 33.69° slope. The highest $F_{s,3DFEM}/F_{s,3DLEM}$ ratio was observed for the case of L/B=1, for the slope height of 5 m and for as surcharge of 100 kPa. However, for slopes with $H \geq 10\,m$ the $F_{s,3DFEM}/F_{s,3DLEM}$ ratios obtained for the 45° slope are higher than those obtained for the 33.69° slope.

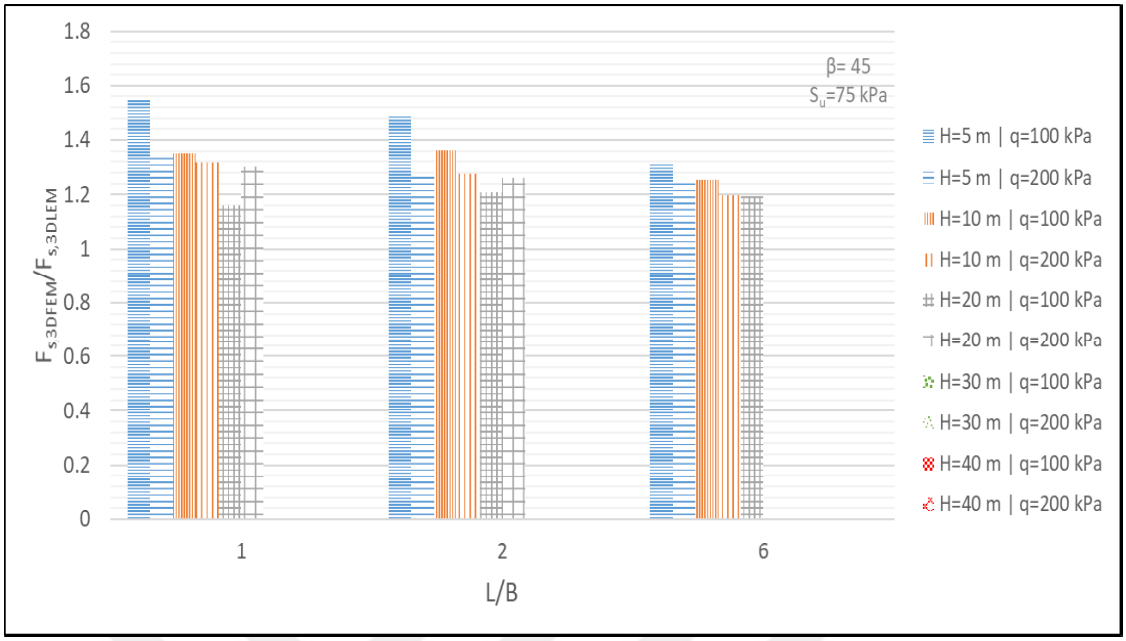


Figure 4.26. Surcharge L/B versus ratio of F_s obtained from the analyses performed using 3D FEM to 3D LEM for slopes with H =5 m, 10 m, 20 m, and 40 m and β=45° and S_u =75 kPa.

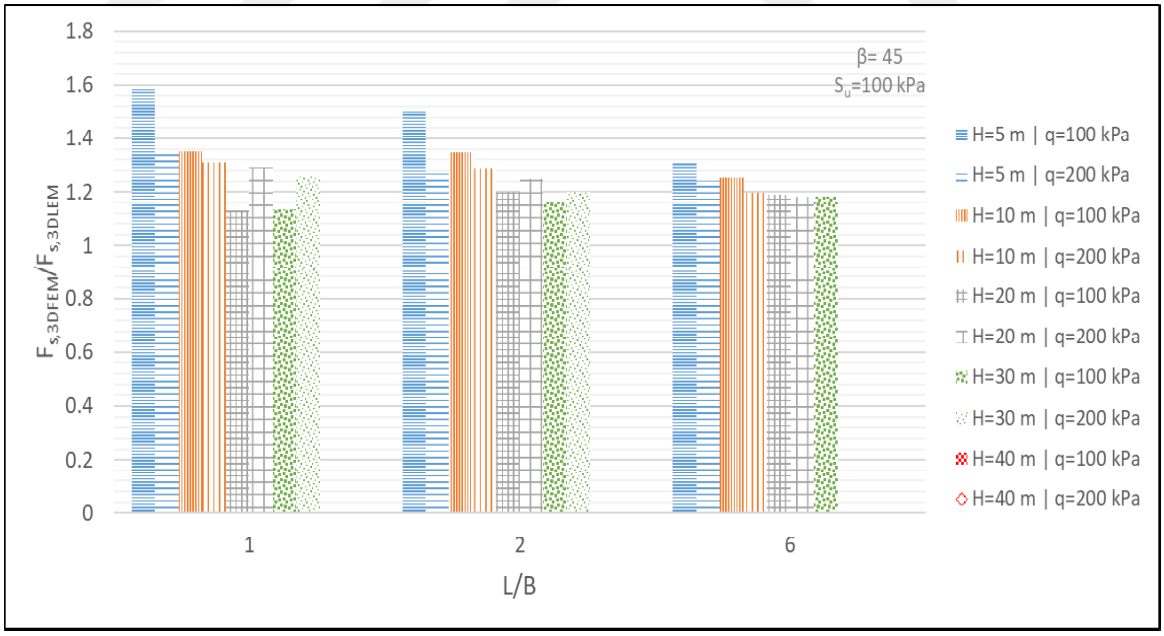


Figure 4.27. Surcharge L/B versus ratio of F_s obtained from the analyses performed using 3D FEM to 3D LEM for slopes with H =5 m, 10 m, 20 m, and 40 m and β=45° and S_u =100 kPa.

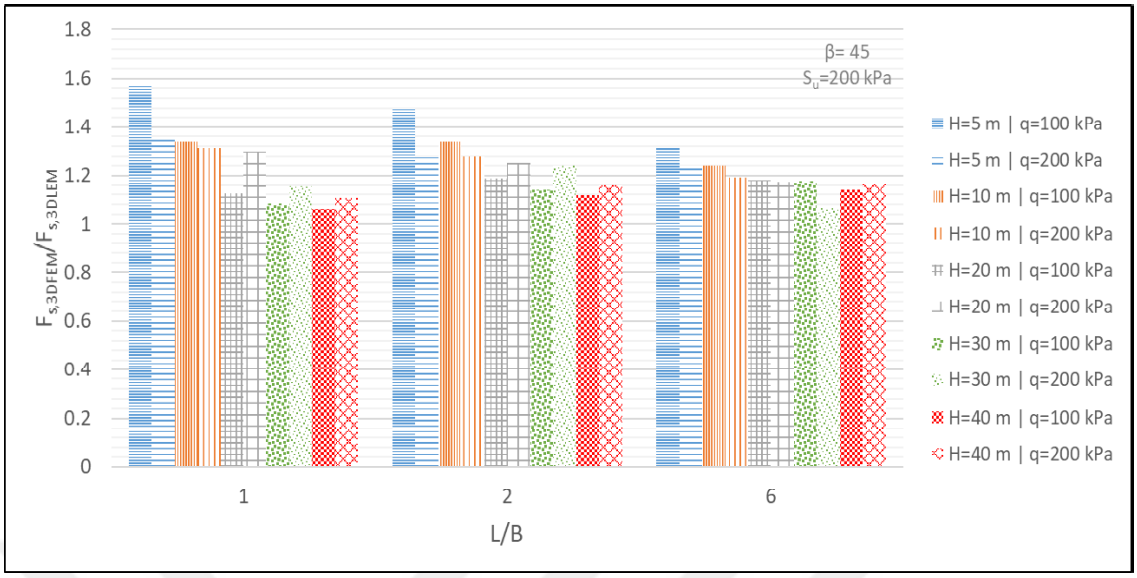


Figure 4.28. Surcharge L/B versus ratio of F_s obtained from the analyses performed using 3D FEM to 3D LEM for slopes with H =5 m, 10 m, 20 m and 40 m and β=45° and S_u =200 kPa.

Figure 4.29, Figure 4.30 and Figure 4.31 show the surcharge L/B versus ratio of F_s obtained from the analyses performed using 3D FEM to 3D LEM for slopes with H =5 m, 10 m, 20 m, and 40 m and β=63.43° for S_u =75 kPa, 100 kPa and 200 kPa, respectively. Similar trends are observed to the analyses performed on the 33.69° and 45° slopes.

When all graphs are evaluated together, it can be seen that highest ratios were examined together the highest $F_{s,3DFEM}/F_{s,3DLEM}$ ratio was observed for the case of a 63.4° slope angle and the lowest ratio $F_{s,3DFEM}/F_{s,3DLEM}$ ratio was observed for the case of a 33.7° slope. This indicates that conducting a 3D FEM analyses can be more effective leading to higher F_s values, and more economical designs in steeper slopes. Once the slope height is considered for all slope angles, the results indicate that the surcharge effect starts diminishing in slopes with H≥ 20 m for β=33.7° and 45°. Thus, in these cases the slope failure occurs due to its own weight and not due to the surcharge. However, this is not the case for the model with the slope with β=63.4°. As β increases, surcharge effects become predominant. Accordingly, for the slope with β=63.4°, even when the slope height reaches 40 meters, $F_{s,3DFEM}/F_{s,3DLEM}$ ratio is around 1.16.

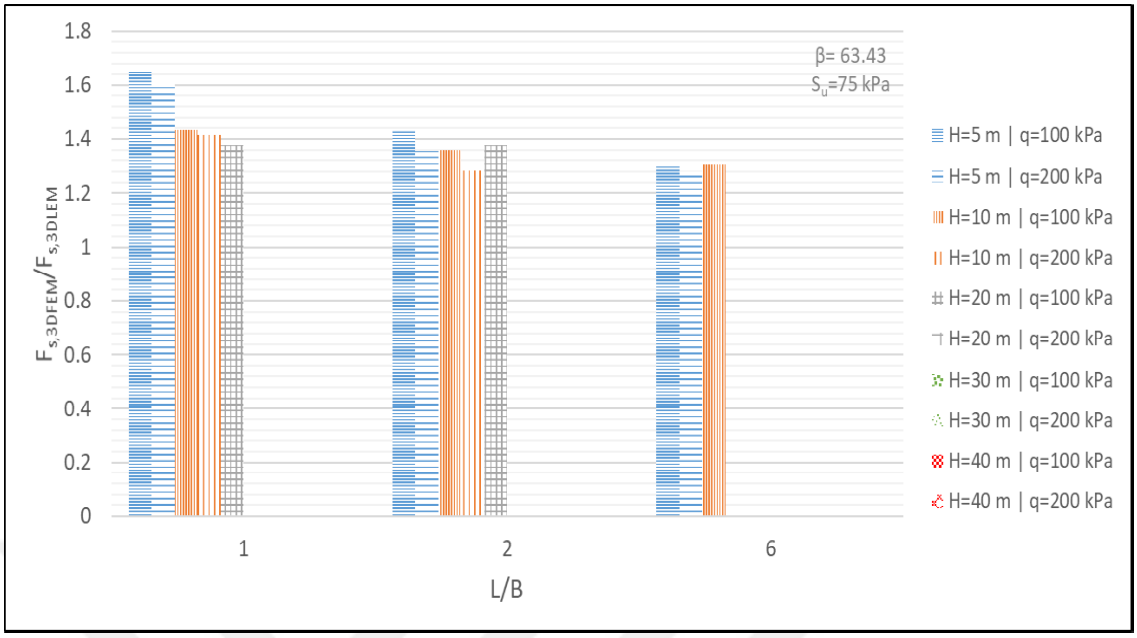


Figure 4.29. Surcharge L/B versus ratio of F_s obtained from the analyses performed using 3D FEM to 3D LEM for slopes H =5 m, 10 m, 20 m and 40 m and β=63.4° and S_u =75 kPa.

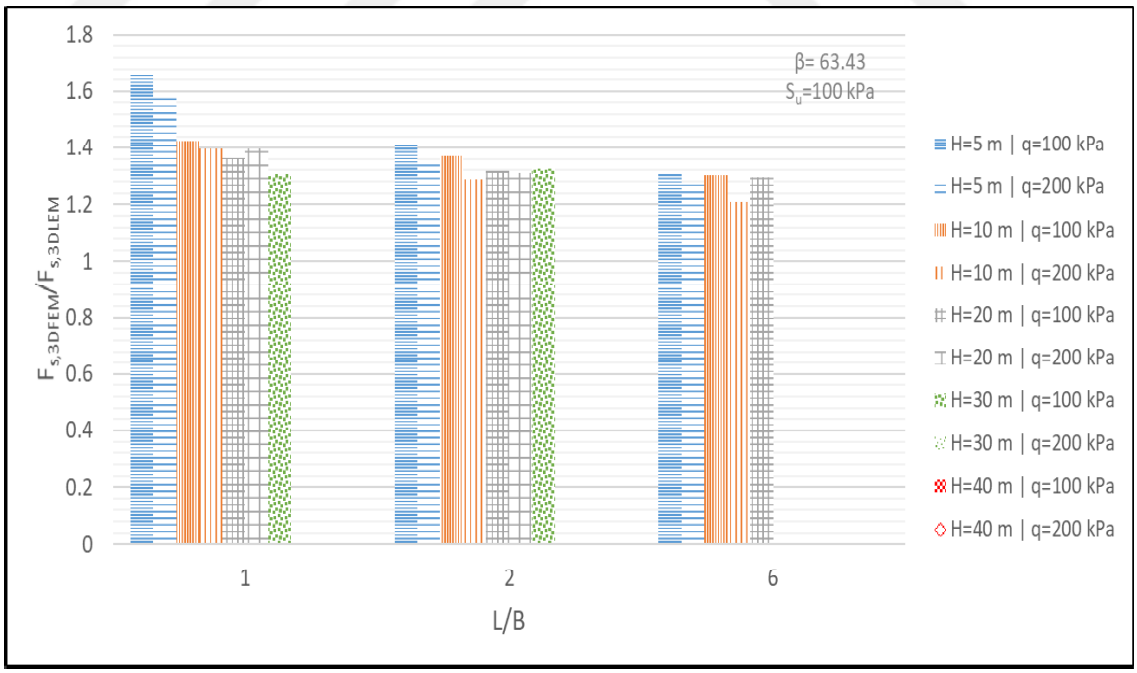


Figure 4.30. Surcharge L/B versus ratio of F_s obtained from the analyses performed using 3D FEM to 3D LEM for slopes with H =5 m, 10 m, 20 m and 40 m and β=63.4° and S_u =100 kPa.

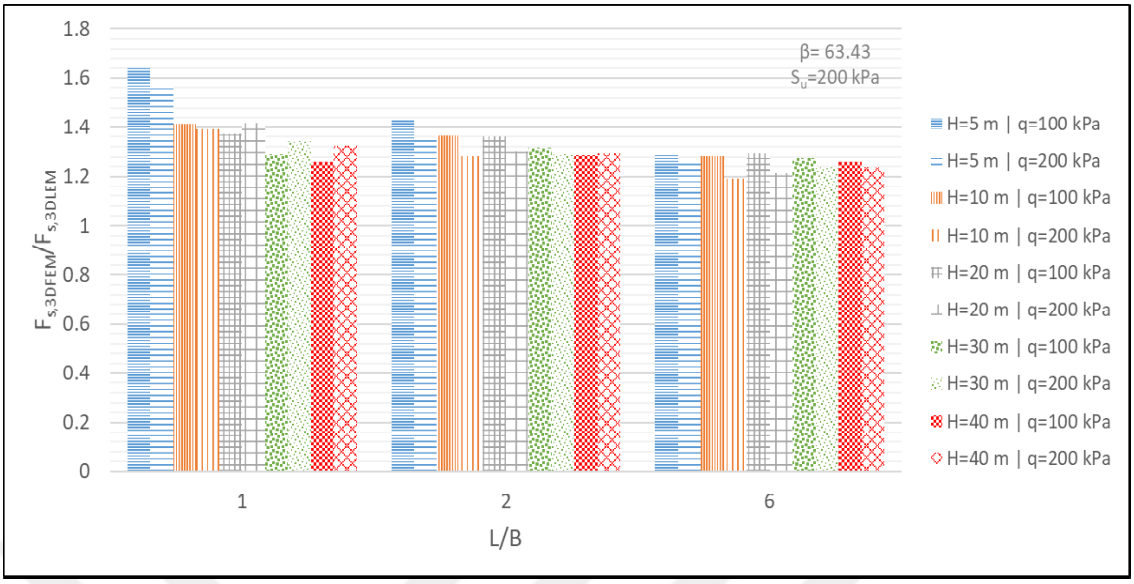
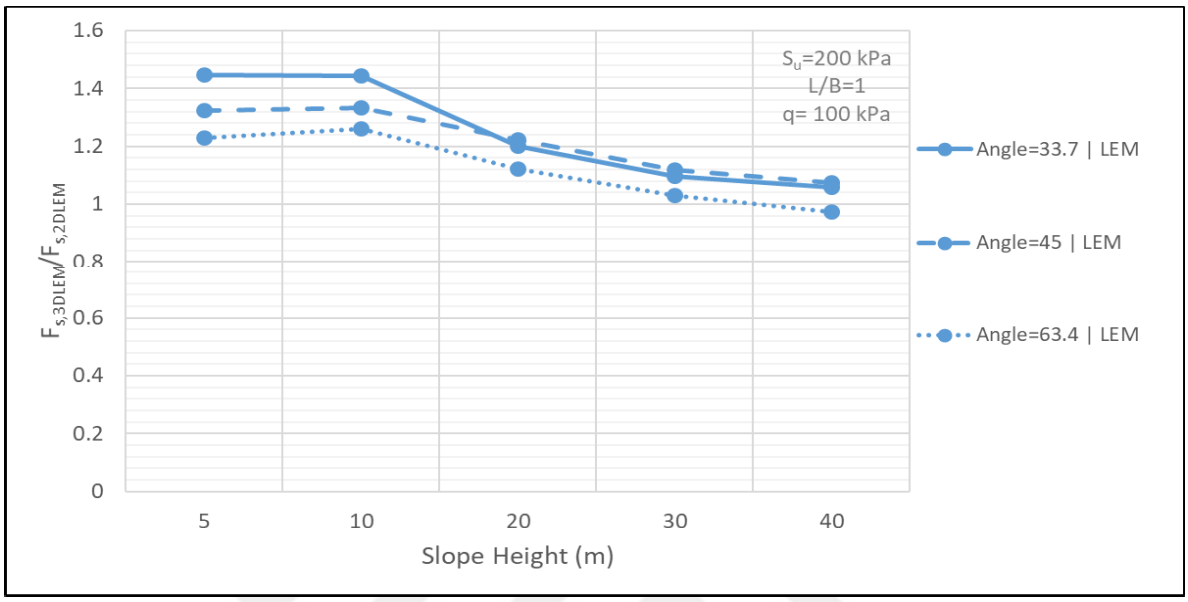


Figure 4.31. Surcharge L/B versus ratio of F_s obtained from the analyses performed using 3D FEM to 3D LEM for slopes with H =5 m, 10 m, 20 m and 40 m and β=63.4° and S_u =200 kPa.

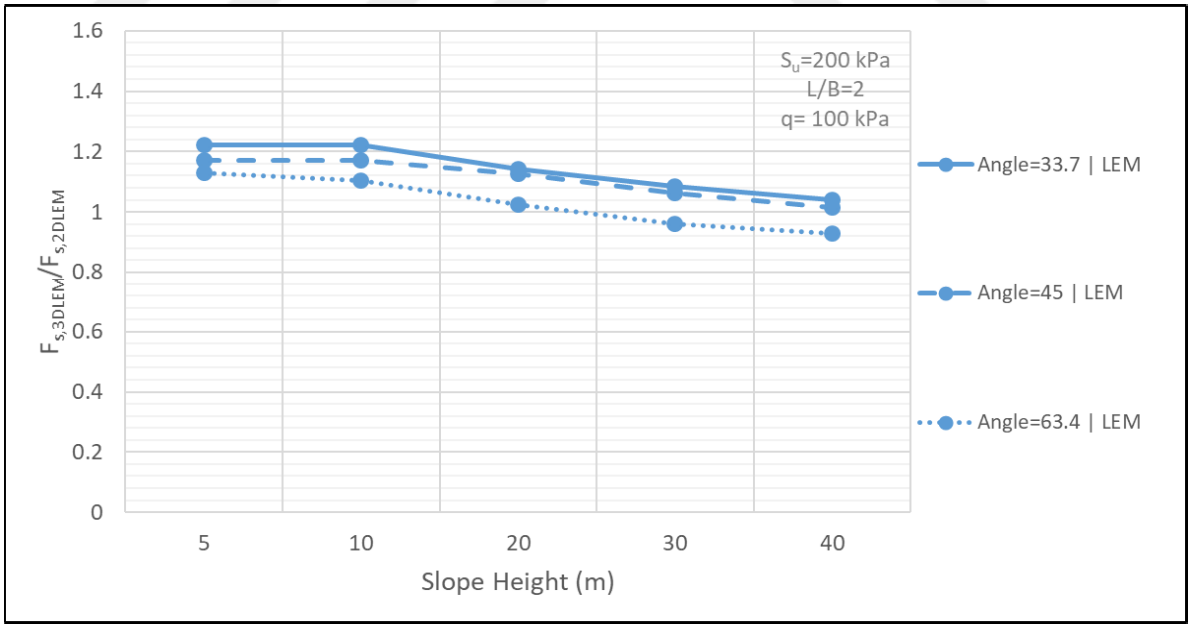
4.5.Comparison of 2D and 3D Analysis

Figure 4.32, Figure 4.33, Figure 4.34 and Figure 4.35 shows the ratio of the F_s values obtained from the analysis using 3D LEM ($F_{s,3DLEM}$) to the F_s results obtained from the analysis using 2D LEM ($F_{s,2DLEM}$) for q=100 kPa for L/B=1, 2 and 6, respectively. Figure 4.25 shows the ratio of the F_s values obtained from the analysis using 3D FEM ($F_{s,3DFEM}$) to the F_s results obtained from the analysis using 2F LEM ($F_{s,2DFEM}$) for q=100 kPa and for L/B=1, 2 and 6, respectively. The results indicate that generally the difference between 2D and 3D analysis is higher in the case of FEM compared with LEM. For a 5m slope, the $F_{s,3DFEM}$/ $F_{s,2DFEM}$ ratio is 2.26, that is quite high. $F_{s,3DFEM}$/$F_{s,2DFEM}$ is lowest at about 1.05 for a slope of 40 m. In the case of analysis performed using LEM, $F_{s,3DLEM}$/ $F_{s,2DLEM}$ ratio was 1.45, also the highest among all analysis for a slope of 5 m, similar to the results obtained from the analysis performed using FEM, and similarly, the lowest value was 0.93 observed at a slope height of 40 meters. The difference between the results of 2D and 3D analysis reduces as surcharge L/B ratio increases for both LEM and FEM cases. Since the length of the slope model is kept constant at 400 meters, as the L/B ratio increases, the Fs value obtained from 3D analyzes and the Fs values obtained from 2D analyzes approach each

other, as the L/B ratio approaches a surcharge loading extending along the slope, just like in the 2D models.



a) L/B=1



b) L/B=2

Figure 4.32. Slope height versus $F_{s,3DLEM}/F_{s,2DLEM}$ obtained from the analyses performed using 2D and 3D LEM for S_u=200 kPa, q=100 kPa: (a) L/B=1; (b) L/B=2.

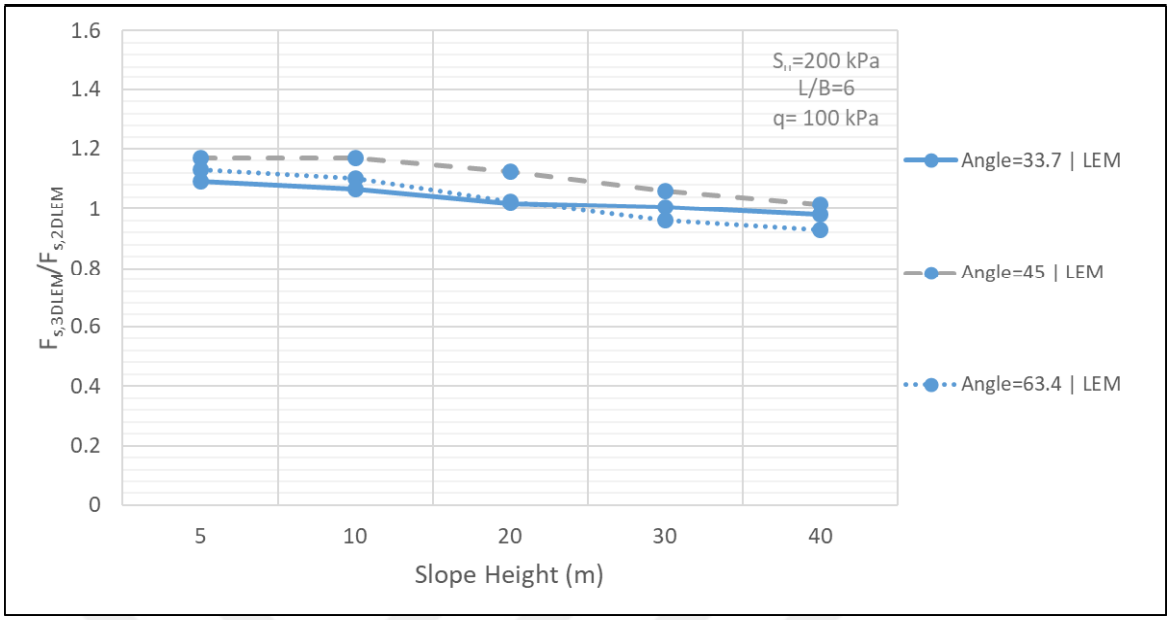


Figure 4.33. Slope height versus $F_{s,3DLEM}/F_{s,2DLEM}$ obtained from the analyses performed using 2D and 3D LEM for S_u=200 kPa, q=100 kPa and L/B=6.

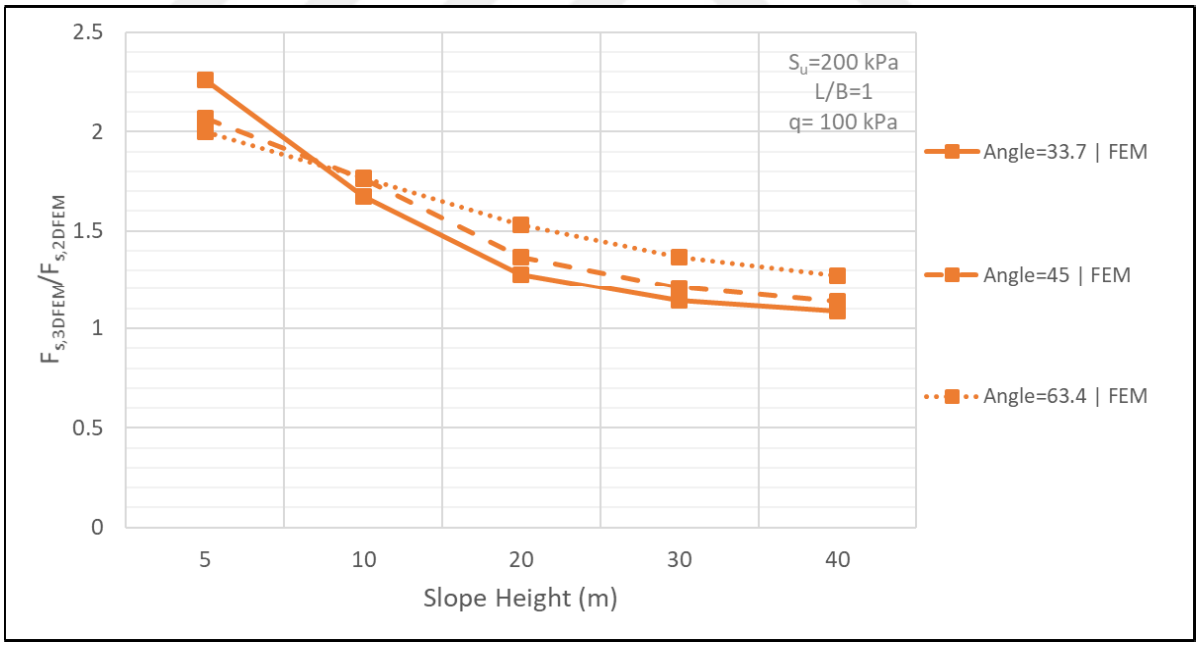
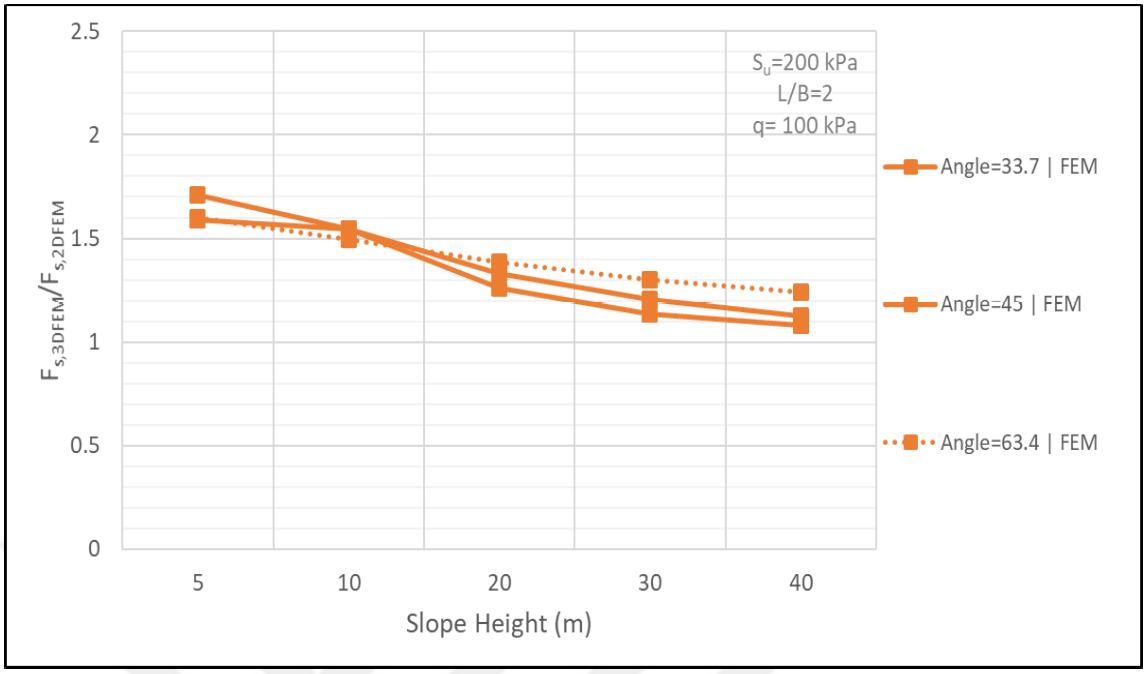
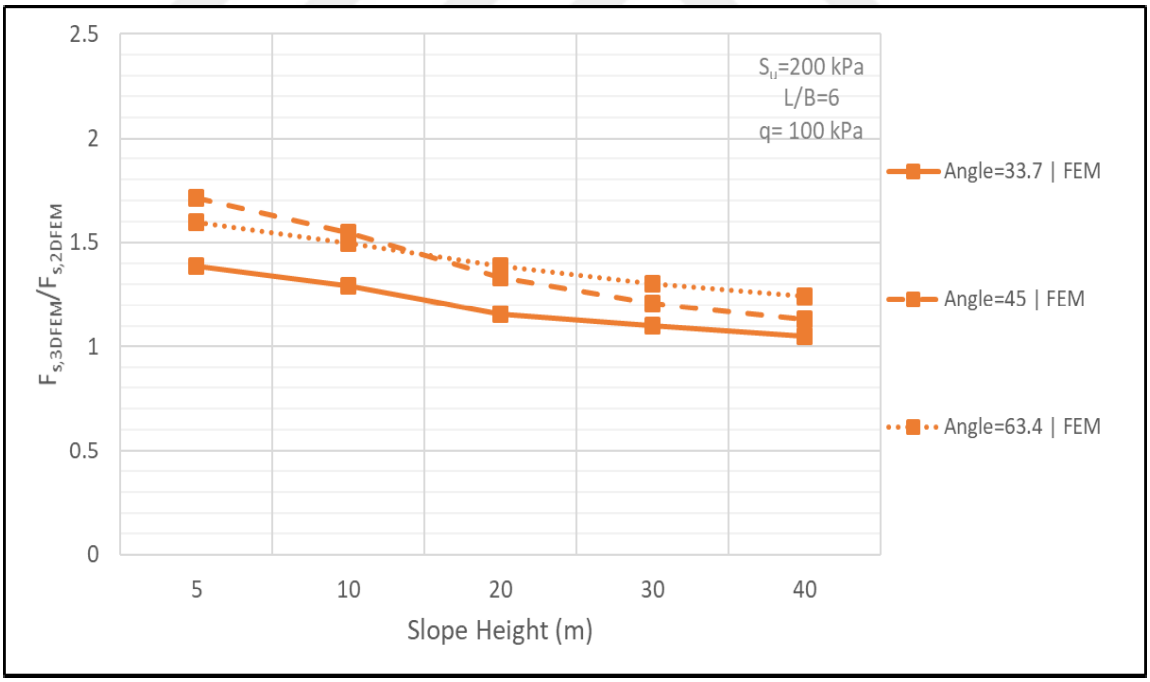


Figure 4.34. Slope height versus $F_{s,3DFEM}/F_{s,2DFEM}$ obtained from the analyses performed using 2D and 3D FEM for S_u=200 kPa, q=100 kPa and L/B=1.



a) L/B=2



b) L/B=6

Figure 4.35. Slope height versus $F_{s,3DFEM}/F_{s,2DFEM}$ obtained from the analyses performed using 2D and 3D FEM for S_u=200 kPa, q=100 kPa: (a) L/B=2; (b) L/B=6.

In Figure 4.36 and Figure 4.37, the $F_{s,3DFEM}/F_{s,2DFEM}$ ratio obtained from FEM analyses using surcharge dimensions of B=20 m and B=30 m cases, in essence the cases in which B≠H, are presented for slopes with β=33.69° and β=45°. For both β values $F_{s,3DFEM}/F_{s,2DFEM}$ ratio decreases as the slope height increases in the FEM analysis. This trend is valid for both surcharge width values (B=20 and B=30). For β=33.69°, the highest $F_{s,3DFEM}/F_{s,2DFEM}$ ratio observed was 1.49 for B=20 m and H=10 m. Additionally, for higher slopes the $F_{s,3DFEM}/F_{s,2DFEM}$ ratio obtained from the cases analyzed with B=30 m is generally higher than those obtained for the cases analyzed with B=20 m. A similar trend is also valid for β=45°.

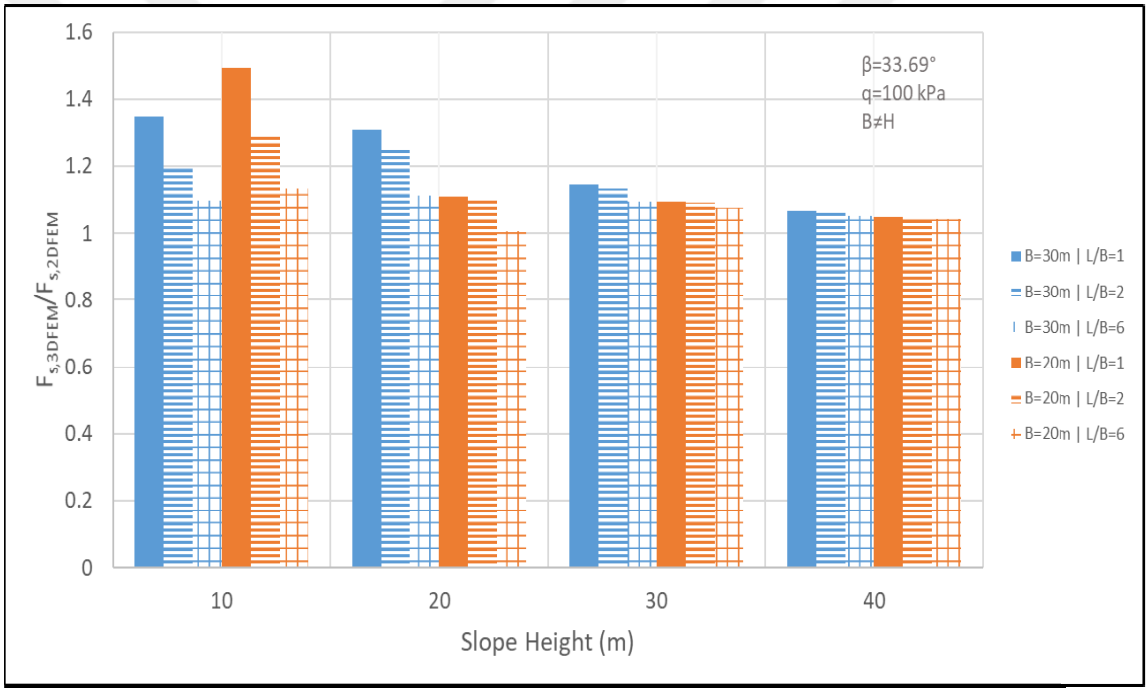


Figure 4.36. Slope height versus $F_{s,3DFEM}/F_{s,2DFEM}$ obtained from the analyses performed using 2D and 3D FEM for S_u=150 kPa, q =100 kPa, β=33.69° for surcharge widths B = 20 m & B = 30 m.

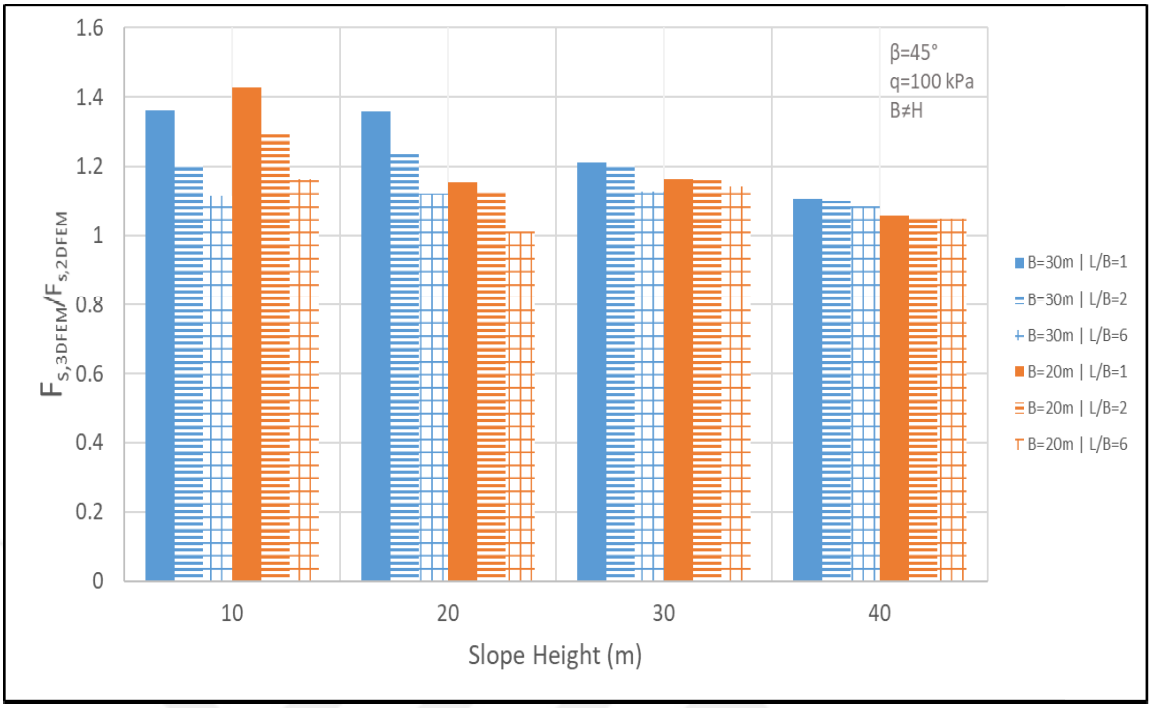


Figure 4.37. Slope height versus $F_{s,3DFEM}/F_{s,2DFEM}$ obtained from the analyses performed using 2D and 3D FEM for S_u=200 kPa, q =100 kPa, β=45º for surcharge widths B = 20 m & B = 30 m.

5. CONCLUSIONS

This study investigated the effects of surcharge shape and magnitude on the factor of safety (F_S) and the failure surfaces/shapes based on the three dimensional (3D) and two dimensional (2D) numerical analysis performed on a variety of slopes with varying slope angle (β) and slope height (H). Majority of the analyses were performed using 3D analysis using limit equilibrium method (LEM) and finite element method (FEM). 2D analyses using LEM and FEM were also performed to investigate the differences between 2D and 3D effects on the results. The following conclusions have been reached from the numerical analyses performed using 2D and 3D LEM and 2D and 3D FEM analysis of (un-stabilized) slopes:

- The results of the 3D numerical analyses performed on various show that failure shapes and F_S values depend on both surcharge geometry and magnitude. Generally, F_S decreases with an increase in length to width ratio (L/B) of the surcharge, as well as the surcharge magnitude.

- As the slope height increases from 5 m to 40 m, the effects of surcharge geometry and surcharge magnitude on the F_S and the failure surfaces progressively become less pronounced. Comparable trends were noted in the results of the analyses performed using both 3D FEM and 3D LEM for a variety of slope angles.

- When compared with the analyses performed using 3D LEM, the analyses performed using 3D FEM typically yields higher F_S values. The effect of the decrease in slope height, an increase in slope angle (β), and a decrease in the L/B ratio, all has a greater impact on the F_S obtained by using 3D FEM relative to those obtained by using 3D LEM.

- In the cases of the presence of a larger surcharge area or magnitude, the ratio between the FS values obtained from 3D FEM to 3D LEM ($F_{S,3DFEM}/F_{S,3DLEM}$) is the largest. This ratio, and hence the % difference in F_S obtained using these two methods decreases in scenarios with low surcharge impact. Therefore, for high slope angles and heights and low L/B ratios that lead to 3D failure surfaces, using 3D FEM provides a substantial benefit.

- It is significant to note that in every case investigated in this study that included surcharge loads, 2D analysis yielded more conservative F_S values. This clearly demonstrates that 3D slope stability analysis can lead to far more cost-effective design and increased efficiency compared with performing a 2D slope stability analysis.

- For all surcharge loaded slope cases analyzed, the ratio of the F_S obtained from 3D analysis to 2D analysis is grater using FEM compared with LEM. In essence, for the same cases analyzed, $F_{s,3DFEM}/F_{s,2DFEM}$ is greater than $F_{s,3DLEM}/F_{s,2DLEM}$.

- The difference between the results of the 2D and 3D analyses performed using LEM and FEM, decreased as the L/B value increased. Slope angle (β) has a greater impact on F_S when the L/B ratio is 1 compared with the cases with L/B> 1.

- In terms of failure shapes, increasing the slope height, decreasing the surcharge magnitude, and decreasing the L/B ratio all resulted in wider and deeper failure shapes. In these situations, it appears that the weight of the slope itself—rather than the surcharge—affects the failure shape. Consequently, rather than local failure shapes, failure shapes similar to those obtained in plane strain conditions were observed.

5.1.Recommendations for further research

Future studies on natural (un-stabilized) slopes can concentrate on examining the impact of various ground materials, such as slopes with rocks, sands, heterogeneous and layered soils on the slope failure shapes and F_S of slopes. Furthermore, the effects of different surcharge load geometries on the slope stability may also be investigated. Future research can also help to evaluate the effects of groundwater and seepage.

REFERENCES

Abramson, L. W., T. S. Lee, S. Sharma, And G.M. Boyce, 1996, *"Slope Stability and Stabilization Methods"*, John Wiley and Sons, New Jersey, USA.

Ahmed, Aly And Ugai, Keizo And Yang, Qing, 2012, "Assessment Of 3D Slope Stability Analysis Methods Based On 3D Simplified Janbu And Hovland Methods", *International Journal of Geomechanics*. Vol.12, Pp. 81-89.

Anagnosti P., 1969, "Three-Dimensional Stability of Fill Dams", *In Proceedings 7th International Conference Soil and Foundation Engineering*, Vol. 2, Pp. 275–280

Azizian, Ali & Popescu, Radu., 2006, "Three-Dimensional Seismic Analysis Of Submarine Slopes", *Soil Dynamics And Earthquake Engineering*. Vol. 26, Pp. 870-887.

Baker, R. And D. Leshchinsky, 1987, "Stability Analysis Of Conical Heaps", *Soils And Foundations*, Vol. 27, No. 4, Pp. 99-110.

Bishop, A.W., 1955, "The Use of The Slip Circle in The Stability Analysis of Slope", *Geotechnique*, Vol. 10, Pp. 129-150.

Brinkgreve, R. B. J., S. Kumarswamy, W. M. Swolfs, F. Fonseca, N. Ragi Manoj, L. Zampich, And N. Zalamea, 2021, *PLAXIS 3D 2021 Manual*. PLAXIS Bv, Delft, Netherlands.

Cavounidis, S., 1987, "On the Ratio of Factors of Safety in Slope Stability Analyses", *Geotechnique*, Vol. 37, No. 2, Pp. 207–210.

Chakraborty, Arunav & Goswami, Diganta, 2016, "State of The Art: Three-Dimensional (3D) Slope-Stability Analysis", *International Journal of Geotechnical Engineering*. Vol. 10, Pp. 1-6.

Chen, R. H., And Chameau, J. L., 1982, "Three-Dimensional Limit Equilibrium Analysis of Slopes", *Geotechnique*, Vol. 32, No. 1, Pp. 31–40

Chen, Z. Y., & Morgenstern, N. R., 1983, "Extensions to The Generalized Method of Slices for Stability Analysis", *Canadian Geotechnical Journal*, Vol. 20. No. 1, Pp. 104–119.

Cheng Y.M., Yip CJ., 2007, "Three-Dimensional Asymmetrical Slope Stability Analysis Extension of Bishop's, Janbu's, And Morgenstern–Price's Techniques", *Journal of Geotechnical and Geoenvironmental Engineering*, Vol. 133, No. 12, Pp. 1544–1555

Cheng, Y. M., And Liu, H. T., And Au, S. K., 2005, "Location of Critical Three-Dimensional Non-Spherical Failure Surface by NURBS Functions and Ellipsoid with Applications to Highway Slopes", *Computers and Geotechnics*, Vol. 32, Pp. 387–399

Cheng, Y.M., 2003, "Location of Critical Failure Surface and Some Further Studies on Slope Stability Analysis", *Computers and Geotechnics*, Vol. 30, No. 3, Pp. 255–267.

Cheng, Y.M. And Yip, C., 2007, "Three-Dimensional Asymmetrical Slope Stability Analysis Extension of Bishop's, Janbu's, And Morgenstern–Price's Techniques", *Journal of Geotechnical and Geoenvironmental Engineering*. Vol. 133.

Duncan, J. M., 1996, "State of The Art: Limit Equilibrium and Finite-Element Analysis of Slopes", *Journal of Geotechnical Engineering*, Vol. 122, No. 7, Pp. 577–596.

Duncan, J., Wright, S. And Brandon, T., 2014, "*Soil Strength and Slope Stability*", 2nd Edition, John Wiley and Sons, Inc., Hoboken.

E.C. Leong, H. Rahardjo, 2012, "Two and Three-Dimensional Slope Stability Reanalyses Of Bukit Batok Slope", *Computers and Geotechnics*, Vol. 42, Pp. 81-88,

Fredlund, D.G. And Krahn, J., 1977, "Comparison of Slope Stability Methods of Analysis", *Canadian Geotechnical Journal*, Vol. 14, Pp. 429-439.

Griffiths DV, Lane PA., 1999, "Slope Stability Analysis by Finite Elements", *Geotechnique*, Vol. 49, No. 3, Pp. 387–403.

Griffiths, D. V., And R. M. Marquez., 2007, "Three-Dimensional Slope Stability Analysis by Elasto-Plastic Finite Elements", *Géotechnique*, Vol. 57, No. 6, Pp. 537–546.

Ho, I-Hsuan., 2014, "Parametric Studies of Slope Stability Analyses Using Three-Dimensional Finite Element Technique: Geometric Effect", *Journal of Geoengineering*, Vol. 9, Pp. 33-43.

Hovland, H. J., 1977, "Three-Dimensional Slope Stability Analysis Method", *Journal of Geotechnical Engineering*, Vol. 103, No. 9, Pp. 971–986

Huang, C. C., And Tsai, C. C., 2000, "New Method For 3D And Asymmetrical Slope Stability Analysis", Journal Geotechnical and Geoenvironmental Engineering, Vol. 126, No. 10, Pp. 917–927.

Huang, C. C., Tsai, C. C., And Chen, Y. H., 2002, "Generalized Method for Three-Dimensional Slope Stability Analysis", *Journal of Geotechnical and Geoenvironmental Engineering*, Vol. 128, No. 10, Pp. 836–848.

Huang, Y.P.H., 2014, "*Slope Stability Analysis By The Limit Equilibrium Method: Fundamentals And Methods*", Asce Press

Hungr, O., 1987, "An Extension of Bishop's Simplified Method of Slope Stability Analysis to Three Dimensions", *Geotechnique*, Vol. 37, Pp. 113–117.

Hungr, O., Salgado, F. M., And Byrne, P. M., 1989, "Evaluation of A Three-Dimensional Method of Slope Stability Analysis", *Canadian Geotechnical Journal*, Vol. 26, Pp. 679–686

Janbu, N., 1957, "Earth Pressure and Bearing Capacity Calculations by Generalized Procedures of Slices", *In Proceedings 4th International Conference on Soil Mechanics and Foundation Engineering*, London.

Janbu, N., 1973, "Slope Stability Computation in Embankment Dam Engineering", *Casagrande Volume*, John Wiley & Sons, New York, Pp. 47–86.

Jiang, J. C. And T. Yamagami, 2004, "Three-Dimensional Slope Stability Analysis Using an Extended Spencer Method", *Journal of The Japanese Geotechnical Society of Soils and Foundations*, Vol. 44, No. 4, Pp. 127-135.

Jing-Cai Jiang, Takuo Yamagami, 2004, "Three-Dimensional Slope Stability Analysis Using an Extended Spencer Method", *Soils and Foundations*, Vol. 44, No. 4, Pp. 127-135,

Kelesoglu, Kubilay, 2015, "The Evaluation of Three-Dimensional Effects on Slope Stability by The Strength Reduction Method", *KSCE Journal of Civil Engineering*. Vol. 20.

Lam, L., And Fredlund, D. G., 1993, "A General Limit Equilibrium Model for Three-Dimensional Slope Stability Analysis", *Canadian Geotechnical Journal*, Vol. 30, Pp. 905–919

Leshchinsky, D., And Baker, R., 1986, "Three-Dimensional Analysis for Slope Stability Analysis", *International Journal Numerical and Analyical Methods Geomechanics*, Vol. 9, Pp. 199–223.

Leshchinsky, D., And Huang, C. C., 1992, "Generalized Three-Dimensional Slope Stability Analysis", *Journal of Geotechnical Engineering*, Vol. 118, No. 11, Pp. 1748–1764

Leshchinsky, D., Baker, R., And Silver, M. L., 1985, "Three-Dimensional Analysis of Slope Stability", *International Journal Numerical and Analyical Methods Geomechanics*, Vol. 9, Pp. 199–223.

Morgenstern, N.R., And Price, V.E., 1965, "The Analysis of The Stability of General Slip Surfaces", *Géotechnique*, Vol. 15, No. 1, Pp. 79–83

Niant. -K., Huang R.-Q., Wan S.-S., And Chen G.-Q., 2012, "Three-Dimensional Strength-Reduction Finite Element Analysis of Slopes: Geometric Effects." *Canadian Geotechnical Journal*, Vol. 49, No. 5, Pp. 574-588.

Rocscience Inc., 2023, "*Slide 9.02 2D Limit Equilibrium Slope Stability Analysis Program Manuel*", Toronto, Canada.

S.Y. Liu, L.T. Shao, H.J. Li, 2015, "Slope Stability Analysis Using the Limit Equilibrium Method and Two Finite Element Methods", *Computers and Geotechnics*, Vol. 63, Pp. 291-298,

Salgado, R., 2022, *"The Engineering of Foundations, Slopes and Retaining Structures (2nd Ed)."* CRC Press.

Spencer, E., 1967, "A Method of Analysis of Stability of Embankments Assuming Parallel Inter-Slice Forces.", *Géotechnique*, Vol. 17, No. 1, Pp. 11–26

Sun, G., Zheng, H., And Jiang, W., 2012, "A Global Procedure for Evaluating Stability of Three-Dimensional Slopes.", *Natural Hazards*, Vol. 61, No. 3, Pp. 1083-1098.

Takuo Yamagami, Jing-Cai Jiang, 1997, "A Search for The Critical Slip Surface in Three-Dimensional Slope Stability Analysis", *Soils and Foundations*, Vol. 37, No. 3, Pp. 1-16,

Ugai, K., 1988, "Three-Dimensional Slope Stability Analysis by Slice Methods", *In Proceeding of The International Conference on Numerical Methods in Geomechanics*, Innsbruck, Austria, Pp. 1369-1374.

Ugai, K., And D. Leshchinsky., 1995, "Three-Dimensional Limit Equilibrium and Finite Element Analyses: A Comparison of Results", *Soils and Foundations*, Vol. 35, No. 4, Pp. 1–7.

Wang, Z., Zhang, W., Gao, X., 2020, "Stability Analysis of Soil Slopes Based on Strain Information.", *Acta Geotechnica*, Vol. 15, Pp. 3121–3134.

Wei, W. B., Y. M. Cheng, And L. Li, 2009, "Three-Dimensional Slope Failure Analysis by The Strength Reduction and Limit Equilibrium Methods", *Computers and Geotechnics*, Vol. 36, No. 1–2, Pp. 70–80.

Yamagami, T., And Jiang, J. C., 1997, "A Search for The Critical Slip Surface in Three-Dimensional Slope Stability Analysis.", *Soils and Foundations*, Vol. 37, No. 3, Pp. 1–16

Yang, X. S. And Deb, S., 2009, "Cuckoo Search Via Levy Flights", *In Proceedings Of World Congress On Nature & Biologically Inspired Computing (Nabic,India)*, IEEE Publications, USA, Pp. 210-214.

Zhang, K., P. Cao, Z. Liu, H. Hu, And D. Gong, 2011, "Simulation Analysis on Three-Dimensional Slope Failure Under Different Conditions", *Transactions of Nonferrous Metals Society of China*, Vol. 21, No. 11, Pp. 2490–2502.

Zheng YR, Zhao SY, Kong WX, Deng CJ., 2005, "Geotechnical Engineering Limit Analysis Using Finite Element Method.", *Rock and Soil Mechanics*, Vol. 26, No. 1, Pp. 163–8.

Zheng, Hong & Liu, De & Li, Chunguang, 2005, "Slope Stability Analysis Based on Elasto-Plastic Finite Element Method.", *International Journal for Numerical Methods in Engineering*, Vol. 64, Pp. 1871 - 1888.

Zu-Yu Chen And N. R. Morgenstern., 1983, "Extensions to The Generalized Method of Slices for Stability Analysis.", *Canadian Geotechnical Journal*. Vol. 20, No. 1, Pp. 104-119.